Investigation and Modelling of Diesel Hydrotreating Reactions

Boesen, Rasmus Risum

Publication date:
2011

Document Version
Publisher's PDF, also known as Version of record

Investigation and Modelling of Diesel Hydrotreating Reactions

Ph.d. Thesis

By

Rasmus Risum Boesen

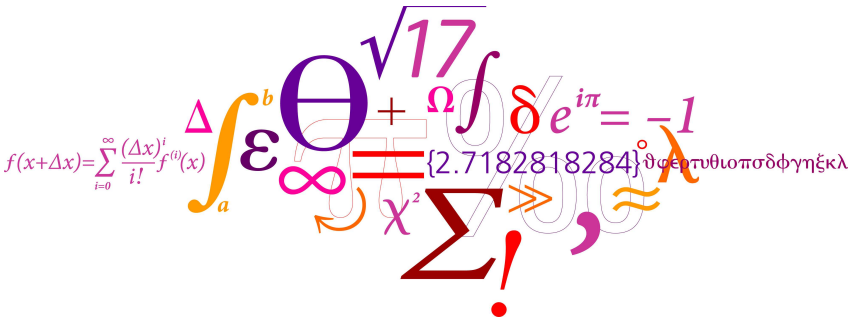

December 2010

Department of Chemical and Biochemical Engineering
Technical University of Denmark
DK-2800 Kgs. Lyngby
Denmark

Preface

This thesis is submitted as a partial fulfillment of the requirement for obtaining the Ph.d. degree at the Technical University of Denmark (DTU). The project has been a collaboration between Haldor Topsøe A/S (HTAS) and Center for Energy Resources Engineering (CERE) at the Department of Chemical and Biochemical engineering at DTU, and it has been carried out under the supervision of Kim G. Knudsen from HTAS and Nicolas S. von Solms and Michael L. Michelsen from DTU CERE. I would like to thank Haldor Topsøe A/S and the MP_2T Graduate School in Chemical Engineering for funding the project, and providing me the with the opportunity to carry out this Ph.D. Study.

I wish to thank all the people who have helped me during the course of this work. First of all I would like to thank Kim G. Knudsen, Nicolas S. von Solms and Michael L. Michelsen, for valuable help and guidance, and for being very supportive all the way through this project.

I wish to thank all the employees at Haldor Topsøe A/S who have helped me during this work. Everyone has been welcoming, helpful and willing to share their knowledge, and it has been a nice experience to be part of the research department. My thanks also goes to Rasmus G. Egeberg for following the project, and giving useful advice. I would like to give a special thanks to laboratory technician Peder Blom, who have been responsible for carrying out most of the experimental work and have always been willing to help me.

I would also like to thank everybody at CERE for creating a nice working environment. A special thanks should go to my friends and fellow Ph.d. students, for sharing both joys and frustrations with me.

During my study, I have had the opportunity to work at the Laboratory of Chemical Technology (LCT) at Ghent University for 5 months, and I wish to thank all the people I met there, who helped making it a pleasant stay. I wish to thank Guy B. Marin for allowing me to visit and Joris W. Thybaut for his guidance and for always taking the time to help.

Finally, I would like to thank my family and friends for always supporting me.

Kgs. Lyngby, December 2010

Rasmus Risum Boesen

Summary

This project consists of a series of studies, that are related to hydrotreating of diesel. Hydrotreating is an important refinery process, in which the oil stream is upgraded to meet the required environmental specifications and physical properties. Although hydrotreating is a mature technology it has received increased attention within the last decade due to tightened legislations regarding the sulfur content, e.g. the demand for Ultra Low Sulfur Diesel (ULSD) with a maximum sulfur content of as low as 10 ppm S has increased. The process is complex, as the performance of a hydrotreating reactor is governed by intrinsic kinetics, diffusion in the pores of the catalyst, mass transfer between the phases and the equilibrium between the gas and the liquid phase. In order to optimize the process and develop better simulation tools, a detailed understanding of the different processes and phenomena is needed.

The hydrogenation of aromatics during hydrotreating is important, as the aromatics content of the product influences the properties of the product, and since the conversion is important for the hydrogen consumption. It is well-known that saturation of fused aromatic rings can be limited by thermodynamic equilibrium at typical industrial hydrotreating conditions. Equilibrium constants have been calculated based on experimental measurements for the hydrogenation of naphthalene and phenanthrene.

The kinetics of hydrogenation of a model compound, naphthalene, has been studied on a commercial CoMo catalyst, and a simple kinetic model is presented. Hydrogenation of fused aromatic rings are known to be fast, and it is possible, that the reaction rates are limited by either internal or external mass transfer. An experiment conducted at industrial temperatures and pressure, using naphthalene as a model compound, have shown, that intra-particle diffusion resistance are likely to limit the reaction rate.

In order to produce ULSD it is necessary to remove sulfur from some of the most refractive sulfur compounds, such as sterically hindered dibenzothiophenes. Basic nitrogen compounds are known to inhibit certain hydrotreating reactions. Experimental results are presented, showing the effect of 3 different nitrogen compounds, acridine, 1,4-dimethylcarabazole and 3-methylindole, on the hydrodesulfurization of a real feed and of a model compound, 4,6-dimethyldibenzothiophene. It is shown, that a basic nitrogen compound is the strongest inhibitor, and that it not only inhibits the hydrodsulfurization reaction, but also the hydrodenitrogenation of other nitrogen compounds. The nitrogen compounds are shown to mainly inhibit the hydrogenation pathway rather than the direct desulfurization route due to a stronger adsorption on hydrogenation sites.

Since feeds used in the hydrotreating process, usually gas-oils, are complex mixtures with a large number of compounds, analysis of the reactions of individual compounds can be difficult. In this work a model-diesel feed consisting of 13 different compounds, representing the most important component classes, has been hydrotreated on a commercial NiMo catalyst. The difference of the reactivity and behavior of the different compounds in the mixture have been investigated.

A steady-state trickle-bed reactor model has been been set-up. The heterogeneous model considers co-current flow of two fluid phases, gas and liquid. The model takes internal and external mass transfer into account. It considers mass transfer between the 2 fluid phases (gas and liquid), and the equilibrium between them.

As reactor models is becoming an important tool to understand the process, detailed kinetics models are needed in order to simulate hydrotreating of complex mixtures. A Robinson-Mahoney reactor is a three-phase reactor that behaves as a continuous stirred tank reactor, and therefore allows for the direct measurement of reaction rates, which can be used to develop kinetic models. Hydrogenation reactions are quite fast, and in order to avoid mass transfer limitations, and only measure intrinsic rates, experiments are often conducted, at conditions that are milder than in industrial units. A reactor model for a Robinson-Mahoney reactor that takes mass transfer into account is presented, and it has been used to test a set of kinetic models at industrial conditions.

Resumé

Dette projekt består af en række undersøgelser relateret til hydrotreating af dieselolie. Hydrotreating er en vigtig process for moderne raffinaderier, hvor olien opgraderes således, at den lever op til de gældende miljøkrav, samtidig med at olien har de nødvendige fysiske egenskaber. Selvom processen har været benyttet siden midten af det 20. århundrede, men har de seneste år fået mere opmærksomhed, da grænserne for det maksimale svovlindhold i dieselolie er blevet strammet, og nu er så lavt som 10 ppm S. Selve processen er kompleks, da effektiviteten af reaktoren styres af kinetik, diffusion i katalystorpartiklernes porer, massetransport mellem faserne og gas-væske ligevægten mellem oliefasen og brintfasen. For at optimere processen og udvikle værktøjer til at simulere industrielle reaktorer, er det nødvendigt at have en indgående forståelse af de forskellige processer og fysiske fænomener.

Mætning af aromatiske forbindelser under afsvovlingsprocessen har betydning for det endelige produkts fysiske egenskaber og for det totale brintforbrug. Mætning af disse aromater kan være begrænset af termodynamisk ligevægt under typiske industrielle betingelser. Ligevægtskonstanter for naphthalene og phenanthrene er blevet beregnet på baggrund af eksperimentelle målinger.

Kinetikken for hydrogenering af naphthalene på en CoMo katalysator er blevet undersøgt, og en simpel model for reaktionshastigheden er blevet præsenteret. Ved mætning af den første ring i forbindelser med sammensatte aromatiske ring er reaktionshastigheden høj, og det er muligt at den begrænses af indre eller ydre massetransport. Forsøg der er blevet udført ved temperaturer og tryk som i industrielle reaktorer, med naphthalene som modelforbindelse, har vist, at det højst sandsynligt er diffusion i katalystorpillernes porer, der begrænser reaktionshastigheden.

For at producere diesel med et svovlindhold på under 10 ppm S, er det nødvendigt at fjerne svovl fra nogle af de mindst reaktive forbindelser, som for eksempel sterisk hindrede dibenzothiophener. Basiske nitrogenforbindelser har vist sig at kunne inhibere vigtige reaktioner under afsvovlingsprocessen. Effekten af tre forskellige nitrogenforbindelser på afsvovling af en rigtig olie og af 4,6-dimethyldibenzothiophene er blevet undersøgt. Den mest basiske forbindelse er den stærkeste inhibitor af de tre, og den inhiberer ikke kun afsvovlingen, men også fjernelsen af nitrogen fra de andre nitrogenforbindelser. Nitrogenforbindelser inhiberer primært hydrogeneringsreaktioner, da de binder sig stærkt til de steder på katalystoren hvor disse reaktioner foregår.

Eftersom oliefraktioner der bruges til processen, er blandinger af mange forskellige forbindelser kan analyse af enkelte reaktioner være vanskellig. I dette projekt er en blanding af 13

forskellige modelforbindelser, svarende til de vigtigste kemiske grupper, blevet brugt til forsøg med en kommerciel NiMo katalysator, og forskellen i reaktivitet og opførsel af de forskellige komponenter i blandingen er blevet undersøgt.

En steady-state model for en trickle-bed reaktor er blevet beskrevet. Modellen tager højde for intern og ekstern massetransport, og massetransport og ligevægt mellem gas- og væskefase.

Efterhånden som reaktormodeller bliver mere og mere vigtige værktøjer til at forstå processen, så er behovet for detaljerede kinetikmodeller til at beskrive komplekse blandinger stigende. En Robinson-Mahoney-reaktor er en tre-fasereaktor, der opfører sig som en ideel tankreaktor, hvori det derfor er muligt at måle reaktionshastigheder direkte. Denne type data er velegnet til udvikling af detaljerede modeller til beskrivelse af reaktionshastigheder, men for at undgå begrænsninger grundet massetransport udføres forsøgene ofte ved noget mildere betingelser end i industrielle reaktorer. En reaktormodel for en Robinson-Mahoney-reaktor, der tager højde for massetransport og diffusion er blevet udviklet, og den er blevet brugt til at teste hastighedsudtryk ved industrielle betingelser.

Notation

Abbreviations

Abbreviation	Explanation	Unit
$1,4$-$dmcbz$	1,4-dimethylcarbazole	-
$3me$-in	3-methylindole	-
$4,6$-$dmdbt$	4,6-dimethyldibenzothiophene	-
API	API gravity	-
BT	Benzothiophene	-
$CSTR$	Continuous Stirred Tank Reactor	-
DBT	Dibenzothiophene	-
DDS	Direct desulfurization route	-
DEC	Decalin	-
DFT	Density Functional Theory	-
dm-bp	3,3'-dimethylbiphenyl	-
$DMDS$	Dimethyldisulfide	-
FCC	Fluid Catalytic Cracking	-
GC	Gas Chromatography	-
HDA	Hydrodearomatization	-
HDM	Hydrodemetallization	-
HDN	Hydrodenitrogenation	-
HDO	Hydrodeoxygenation	-
HDS	Hydrodesulfurization	-
HYC	Hydrocracking	-
HYD	Hydrogenation route	-
LCO	Light Cycle Oil	-
$LHSV$	Liquid hourly space velocity	hr^{-1}
$mcht$	3-(3'-methylcyclohexyl)toluene	-
NAP	Naphthalene	-
PHE	Phenanthrene	-
SG	Specific gravity	-

Abbreviation	Explanation	Unit
$SRGO$	Straight Run Gas Oil	-
SRK	Soave-Redlich-Kwong equation of state	-
STM	Scanning Tunneling Microscopy	-
TET	Tetralin	-
$ULSD$	Ultra Low Sulfur Diesel	-
VLE	Vapor-Liquid Equilibrium	-
$WHSV$	Weight hourly space velocity	hr^{-1}

Symbols

Symbol	Explanation	
A_k	Peak area in gas chromatogram	m^2
$A_{reactor}$	Reactor cross section area	m^2
a_{LG}	Gas-liquid specific surface area	$m^2/m^3\ _{reactor}$
a_{LS}	Liquid-solid specific surface area	$m^2/m^3\ _{reactor}$
a_S	Liquid-solid specific surface area	$m^2/m^3\ _{reactor}$
c_k	Concentration	mol/m^3
$c_{k,0}$	Concentration on catalyst surface	mol/m^3
c_k^{eq}	Equilibrium liquid concentration	mol/m^3
c_k^L	Bulk liquid concentration	mol/m^3
c_k^S	Concentration on catalyst surfcace	mol/m^3
$\underline{c}$	Vector of concentrations	mol/m^3
$D_{e,k}$	Effective diffusion coefficient	m^2/s
D_k	Infinite dilution diffusion coefficient	m^2/s
d	Diameter	-
d_p	Diameter of catalyst particle	m
E_A	Activation energy	J/mol
f_k	Fugacity	Pa
F	Molar flow rate	mol/s
G_L	Superficial liquid mass velocity	$kg/m^2\ _{reactor \cdot s}$
$GOratio$	Gas-to-oil ratio	$Nm^3\ H_2/m^3\ _{liq.\ feed}$
H	Henrys law constant	mol/m^3
k	Rate constant	*Depends on the rate expression*
k_{ij}	Binary interaction coefficient	-
$k_{k,LG}$	Gas-liquid mass transfer coefficient	m/s
$k_{k,LS}$	Liquid-solid mass transfer coefficient	m/s
K	Adsorption constant	-

Symbol	Explanation	Unit
K_k	Gas-liquid K-factor	-
K_p	Gas phase equilibrium constant	*Depends on the reaction*
K_{ratio}	Equilibrium ratio between tetralin and naphthalene	-
L	Reactor height	m
M_k	Molecular weight	g/mol
M_w	Molecular weight	g/mol
L_0	Liquid feed flow rate	kg/h
l	Reactor position variable	m
$N_{k,LG}$	Flux at gas-liquid interface	$mol/m^2 \cdot s$
$N_{k,LS}$	Flux at liquid-solid interface	$mol/m^2 \cdot s$
P	Pressure	Pa
Q	Reaction quotient	*Depends on the reaction*
Q	Voumetric flow	ml/min
R	Ideal gas constant	$J/mol \cdot K$
R_k	Overall reaction rate	$mol/m^3 \cdot s$
$R_{k,app}$	Apparent reaction rate	$mol/m^3 \cdot s$
r	Distance from center of catalyst pellet	m
r'_m	Rate of reaction m	$mol/kg\ cat. \cdot s$
r_m	Rate of reaction m, $r_m = \rho_p \cdot r'_m$	$mol/m^3 \cdot s$
R_p	Radius of catalyst pellet	m
S	Selectivity	-
S_{ij}	Stoichiometric coefficient	-
T	Temperature	K / °C
u_G	Superficial gas velocity	m/s
u_L	Superficial liquid velocity	m/s
v_L	Liquid molar volume	m^3/mol
V_L	Liquid volume	m^3
V_m	Liquid molar volume	m^3/mol
V_R	Reactor volume	m^3
w	Concentration in % (w/w)	-
X	Conversion	-
x	Dimensionless distance from catalyst center	-
x	Liquid phase mole fraction	-
y	Gas phase mole fraction	-
y_k	Dimensionless concentration component k	-
$\underline{y}$	Vector of dimensionless concentrations	-
Y_i	Yield of component i	-

Symbol	Explanation	Unit
z	Dimension less reactor position	-
z	Overall mole fraction	-
Z	Compressibility factor	-
β	Relative temperature rise in catalyst pellet	-
ΔH_r	Reaction enthalpy	$^{J}/_{mol}$
ϵ_{bed}	Porosity of catalyst bed	-
ϵ_p	Porosity of the catalyst particles	-
ϵ_L	Liquid hold-up	-
γ_0	Specific gravity	-
η	Effectiveness factor	-
λ	Molecular diameter / catalyst pore diameter	-
λ	Heat conductivity	$^{J}/_{m \cdot s}$
μ_L	Liquid viscosity	$Pa \cdot s$
ν_{km}	Stoichiometric coefficient	-
ω	Acentric factor	-
ρ_{bed}	Density of catalyst bed	$^{kg\ cat.}/_{m^3\ reactor}$
ϕ_k	Thiele modulus	-
ϕ_k	Association factor	-
$\rho_k(\underline{y})$	Dimensionless reaction rate	-
ρ_L	Liquid density	$^{kg}/_{m^3}$
ρ_p	Density of catalyst pellet	$^{kg\ cat.}/_{m^3\ pellet}$
τ	WHSV^{-1}	hr
τ_p	Tortuosity of the catalyst particles	-
τ_L	Liquid residence time	min
ζ	Dimensionless distance from catalyst center	-

Sub- and superscripts

Symbol	Explanation
0	Initial / inlet
APP	Apparent
c	Critical
cD	Cis-decalin
comp	Composite
eq	Equilibrium
f	Feed
f	Forward reaction

Symbol	Explanation
G	Gas
int	Intrinsic
L	Liquid
LG	Gas-liquid
LS	Liquid-solid
N	Naphthalene
obs	Observed
p	Particle
r	Reduced
RA	Rackett
s	Surface
s	Solid
T	Tetralin
tD	Trans-decalin

Contents

Chapter 1

Introduction

Reducing pollution from the use of diesel oil as a tranportation fuel is an ongoing endeavour and important area of research. Concerns about the environment have resulted in tightened legislation regarding the sulfur content of diesel. Figure 1.1 shows how the sulfur limits in highway diesel fuel have changed since 1990 in Europe, the US, and Japan. As can be seen from the figure the maximum limits for the sulfur content are now as low as 10 ppm. Diesel that meet these specifications are often denoted as Ultra Low Sulfur Diesel (ULSD) or "sulfur-free" diesel.

The tightened legislations and the higher demand for transportation fuels has resulted in increased attention to refinery processes such as hydrotreating. In the hydrotreating process, the amounts of sulfur, nitrogen and aromatics are reduced, which limits the emissions of SO_x, NO_x and particles during combustion. Sulfur compounds act as poison for the catalysts used to limit the amount of particulates and NO_x released from the exhaust of diesel engines, and reducing the sulfur concentration in diesel is necessary in order to reduce the harmful emissions [1].

1.1 Oil refining

The purpose of an oil refinery is to turn crude oil into more valuable products that meet consumer demands and environmental specifications. Figure 1.2 shows a very simplified refinery. The first important process is the atmospheric distillation in which the crude oil is separated into more narrow boiling fractions. Diesel is produced from atmospheric or straight-run gas-oil (SRGO), which has boiling point range between that of kerosene and the atmospheric residue. Typically diesel has an initial boiling point of around 150-230 °C, and a 95 % (v/v) boiling point of 360 °C. The gas-oil is mainly hydrotreated in order to remove sulfur and to increase the cetane number.

Due to the high demand for transportation fuels such as diesel and gasoline, it is desired to convert the atmospheric residue into more valuable products. This is done by first performing a vacuum distillation and then converting the vacuum gas oil into a lighter fraction through either hydrocracking (HYC) for high-quality diesel production or fluid catalytic cracking (FCC)

for high-quality gasoline production. An important issue with using the heavier fractions of the crude oil for diesel production, is that the concentration of nitrogen and sulfur compounds is higher than in the atmospheric gas-oil making it necessary to have a pre-treatment of the oil in order to protect downstream HYC and FCC catalyst, and to limit SO_x emission from the FCC process.

1.2 Diesel oil

Diesel oil is a complex mixture consisting of different classes of hydrocarbons typically in the range C10 to C25. It consists of normal, branched and cyclic paraffins, and compounds containing single as well as fused aromatic rings. Aromatics are often classified as either mono-, di- or polyaromatics. Certain compounds contain heteroatoms, such as sulfur or nitrogen. The sulfur compounds are mainly thiophenic compounds or sulfides. The nitrogen compounds are classified as either basic or non-basic. The non-basic are mainly pyrrolic species, while the basic compounds are amines, anilines and pyridinic species in which the lone-pair on the nitrogen atom is available for donation.

An important property is the cetane number, which is a measure of the oil's ignition properties. For various refinery process streams used for diesel production, it can be between 20 and 60 [3]. In the EU a minimum cetane number of 51 (and a cetane index of minimum 46) is required for automotive diesel fuel [2]. Saturating aromatics can have a positive effect on the cetane number, and it is therefore an important way to control the fuel quality [4].

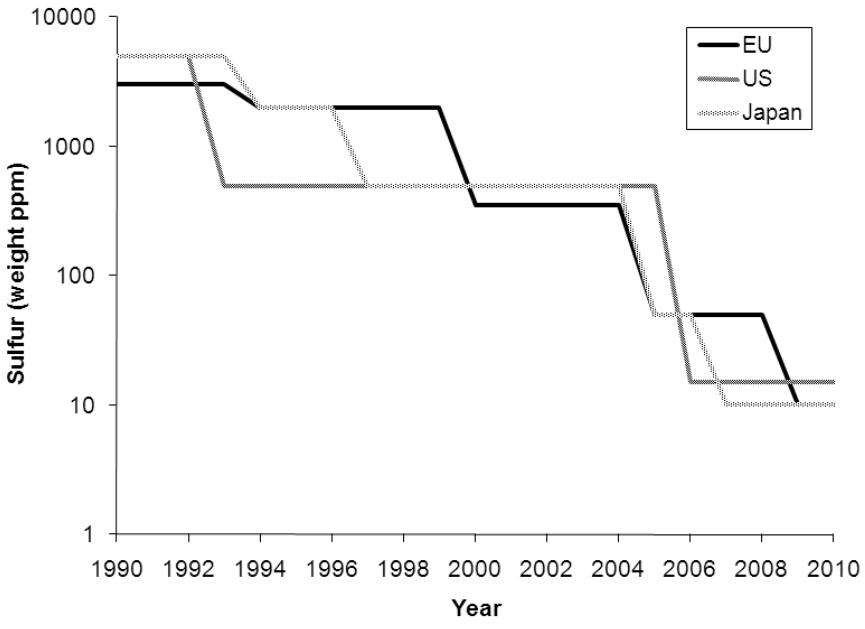

Figure 1.1: Sulfur limits in highway diesel fuel in the EU, US and Japan [2]

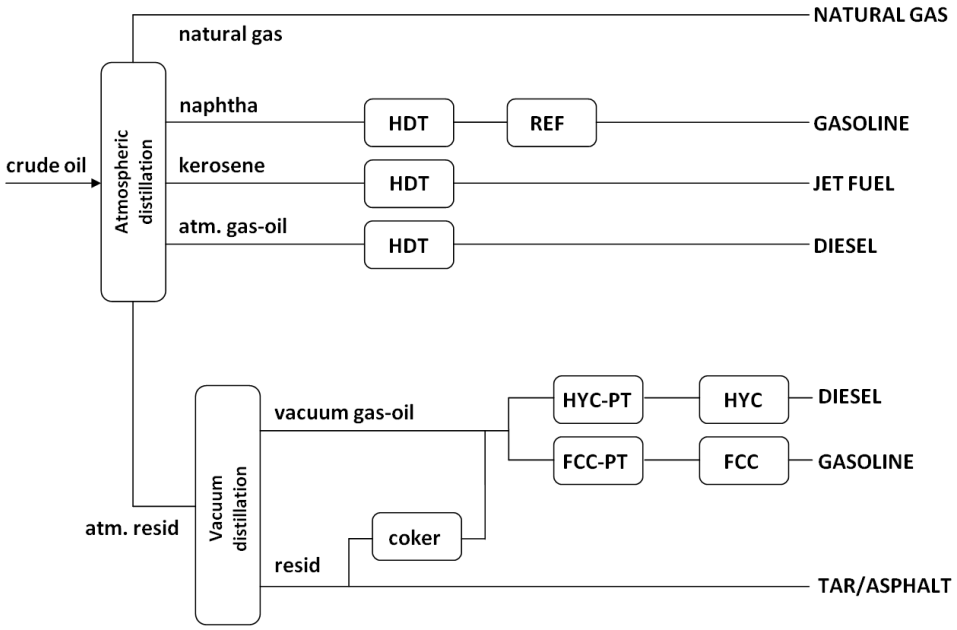

Figure 1.2: Illustration of a simple refinery. (HDT: Hydrotreater, REF: Reformer, HYC: Hydrocracker, FCC: Fluid Catalytic Cracker, PT: Pre-treatment)

1.3 Hydrotreating

The subject of this thesis is hydrotreating, which is a key process in the modern oil-refining industry. It is a catalytic process in which hydrogen reacts with oil in a trickle-bed reactor. A trickle-bed reactor is a fixed-bed reactor in which gaseous hydrogen and liquid oil is fed co-currently from the top. In the trickle-flow regime, the liquid trickles down over the catalyst pellets, while the gas forms a continuous phase [5]. Figure 1.3 shows a simple illustration of a trickle-bed hydrotreating reactor.

The hydrotreating process is essential in producing high quality diesel fuel with with low content of sulfur, nitrogen and aromatics. The typical catalysts used for the hydrotreating are sulfided $CoMo/Al_2O_3$ and $NiMo/Al_2O_3$. Hydrotreating of atmospheric gas oils has typically been carried out at temperatures between 315 and 400 °C, and pressures between 30 and 100 bar. The hydrogen flow is often set to be 3-4 times larger than the what is consumed in reaction [7]. The ratio of hydrogen to liquid feed can typically be in the range of 70-1000 Nm^3 hydrogen per m^3 liquid feed. Contact time between the reaction mixture and the catalyst is often expressed in terms of the Liquid Hourly Space Velocity (LHSV), which is defined as the ratio between the volumetric liquid feed flow, v_0, in m^3/hr divided by the volume of the catalyst in m^3:

$$LHSV = \frac{v_0}{V_{cat}} \tag{1.1}$$

Typical values of LHSV for ULSD lies between 0.5 and 3 hr^{-1} [8].

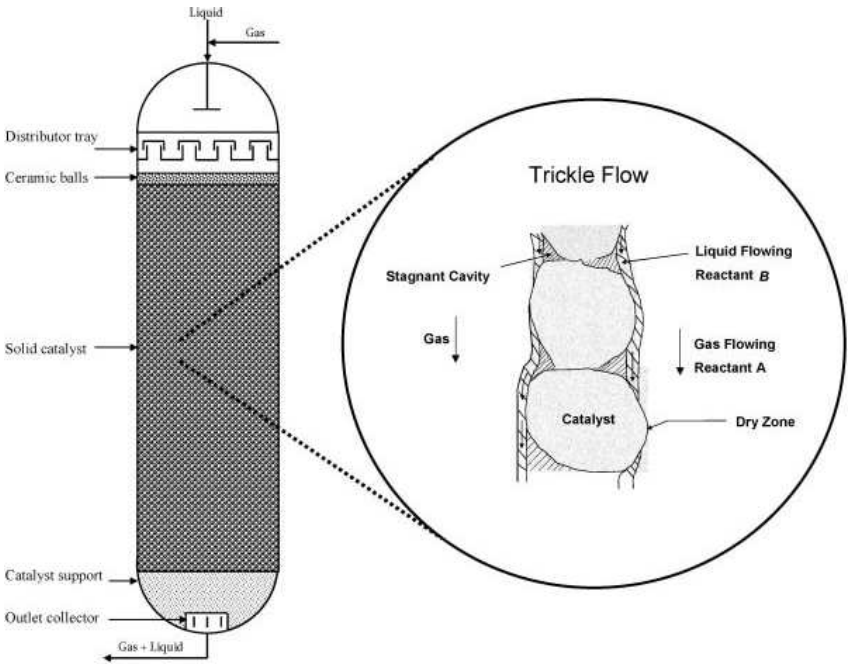

Figure 1.3: Illustration of the trickle-flow regime in trickle-bed reactor [6]

1.3.1 Hydrotreating reactions

The three main types of reactions taking place during the hydrotreating process are hydrodesulfurization (HDS), hydrodearomatization (HDA) and hydrodenitrogenation (HDN).

1.3.1.1 Hydrodesulfurization

The sulfur compounds present in gas oil covers a large range of reactivity. In order to produce ULSD it necessary to remove sulfur from the most refractive compounds, such as higher molecular weight dibenzothiophenes with side substituents at positions adjacent to the sulphur atom as illustrated in figure 1.4. Typical model molecules representing the most refractive sulfur compounds are 4-methyldibenzothiophene and 4,6-dimethyldibenzothiophene.

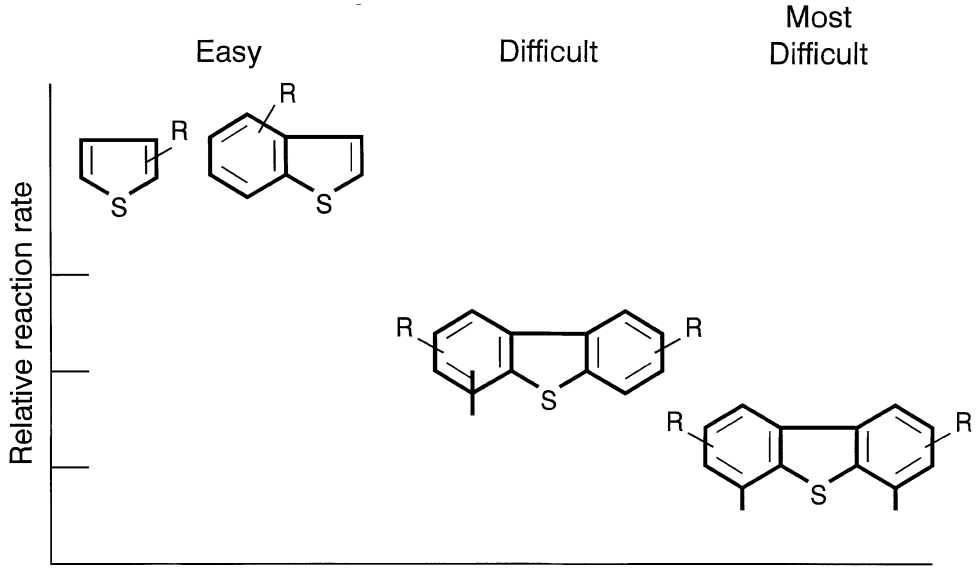

Figure 1.4: Illustration of the difference in reactivity for typical sulfur compounds in gas oils [9]

An important reaction is the hydrodesulfurization of benzothiophene. Benzothiophene is relative easy to desulfurize as illustrated in figure 1.4. A possible reaction scheme is illustrated in figure 1.5.

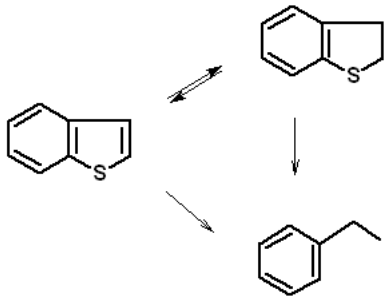

Figure 1.5: Reaction pathways for benzothiophene hydrodesulfurization [10]

Desulfurization of dibenzothiophenes can occur through two different paths, a direct desulfurization (DDS) route and a pre-hydrogenation (HYD) route as is illustrated in figure 1.6.

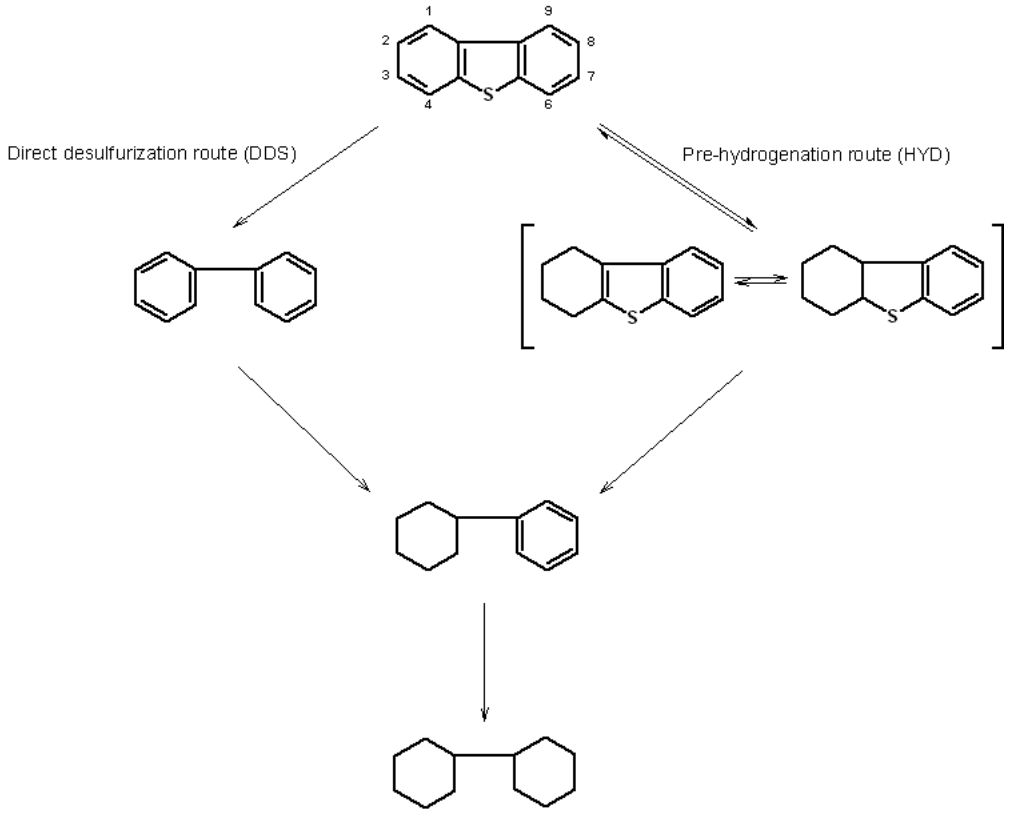

Figure 1.6: Reaction pathways for dibenzothiophene hydrodesulfurization [11]

1.3.1.2 Hydrodearomatization

Hydrodearomatization reactions are reactions in which aromatic rings are saturated with hydrogen. For polycondensed aromatic hydrocarbons the hydrogenation of the first ring is in general the fastest, and the rate of hydrogenation for subsequent rings tend to be lower with the last ring being the least reactive [12]. The reaction pathway for a typical diaromatic compound, naphthalene, is shown in figure 1.7. The rate of hydrogenation of the last ring is significantly lower than of the first one.

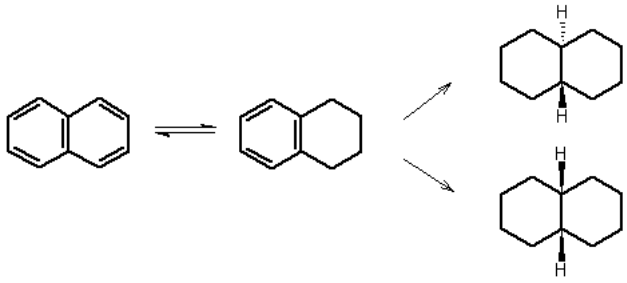

Figure 1.7: Reaction pathway for naphthalene hydrogenation [13]

Phenanthrene is a good model compound to represent polyaromatics. A detailed reaction network has been proposed by Korre et al. [14], and is shown in figure 1.8.

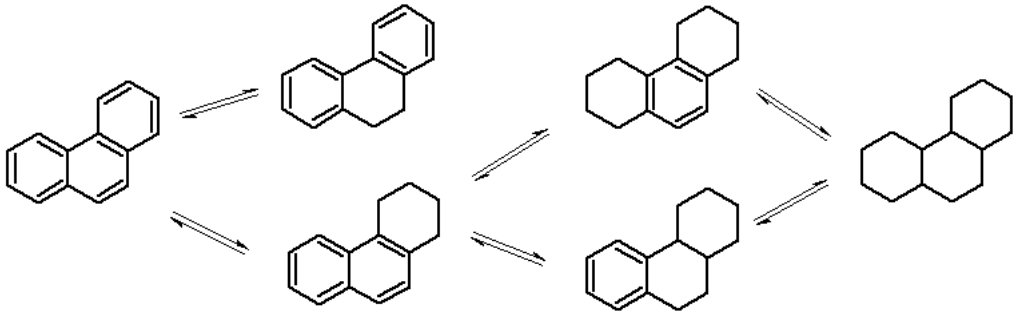

Figure 1.8: Reaction network for phenanthrene hydrogenation [14]

An important aspect of the hydrodearomatization reactions is that at typical hydrotreating conditions, the conversion can be limited by thermodynamic equilibrium. A general aromatics saturation reaction of the compound A is as follows:

$$A + nH_2 \rightleftharpoons AH \tag{1.2}$$

AH is the hydrogenated species, and the equilibrium mole fractions, y_A and y_{AH}, are given by the following expression:

$$\frac{y_A}{y_A + y_{AH}} = \frac{1}{1 + K_a \cdot (P_{H_2})^n} \tag{1.3}$$

Here P_{H_2} is the hydrogen partial pressure and K_a is the equilibrium constant for the overall reaction equation 1.2. The expression shows, that increasing the hydrogen partial pressure will move the equilibrium towards the saturated species AH. Since hydrogenation reactions are exothermic, increasing the temperature results in a decrease in the equilibrium constant [15], meaning that high temperatures do not favor high equilibrium conversions of aromatics.

1.3.1.3 Hydrodenitrogenation

Hydrodenitrogenation reactions are important, not only for their own sake, but also because nitrogen compounds can act as inhibitors for hydrogenation reactions. Nitrogen compounds are grouped into 2 different classes: Basic and non-basic. The non-basic species are compounds such as indoles and carbazoles, while the basic are compounds such as aliphatic amines, anilines, pyridines, quinolines and acridines[16]. A common feature of HDN of aromatic nitrogen compounds, is that they are relatively slow reacting, and that hydrogenation of the aromatic ring has to happen prior to hydrogenolysis of the carbon-nitrogen bond [17]. A possible reaction pathway for acridine, a basic nitrogen compound, is shown in figure 1.9.

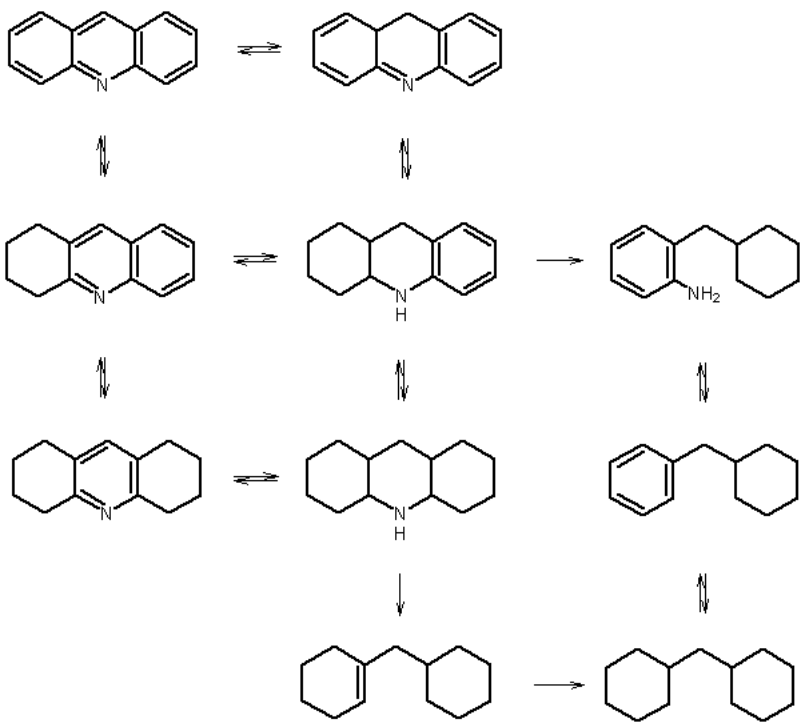

Figure 1.9: Reaction network for acridine hydrodenitrogenation [18]

1.3.1.4 More reactions

Furthermore reactions such as hydrocracking (HYC) and hydrodemetallization (HDM) take place especially during hydroprocessing of heavy oils. The oxygen content of petroleum is considerably smaller than the sulfur and nitrogen content, so hydrodeoxygenation (HDO), removal of oxygen, can also occur during hydrotreating [17]. HYC, HDM and HDO reactions will not be considered in this work.

1.3.2 Catalysts

The typical catalysts used for hydrotreating are sulfided CoMo and NiMo supported on alumina (Al_2O_3). A lot of research over the years has been dedicated to understanding the nature of the active sites, the reason for the catalytic activity and the role of the promoters Co and Ni. Experimental studies have suggested that hydrogenation reactions (saturation of aromatic rings) and hydrogenolysis reactions (removal of heteroatoms), does not occur on the same active site [19].

Topsøe and co-workers identified Co-Mo-S (or Ni-Mo-S) structures, that were found to be responsible for the increase in activity when adding the promoters. In these Co-Mo-S structures, the promoter atoms, Co or Ni, are located at the edges of MoS_2-like stuctures in the same plane as the Mo atom structures [20, 21]. It is believed that the promoter atoms enhance the formation of sulfur vacancies and facilitate the creation of new and more active sites [22]. Direct sulfur removal is believed to occur on these sulfur vacancies located at the edge of Co(Ni)-Mo-S

crystals. Hydrogen sulfide can bind to these sites, which can explain why H_2S is and inhibitor for hydrogenolysis reactions. Substituents in the 4 and 6 position on a DBT molecule will result in the molecule being more likely to react through the pre-hydrogenation route due to the S-atom being sterically hindered [23].

The active Co(Ni)-Mo-S phase exists as small layered crystals on the alumina support. The bottom layer that is in contact with Al_2O_3 is difficult to sulfide into an active form, and multi-layered stacks are likely to result in more active catalysts [24]. One can distinguish between two types of sites, Type I that has a strong interaction with the support and Type II sites which have weaker interaction and a larger intrinsic activity [21].

A combination of Density Functional Theory (DFT) calculations and Scanning Tunneling Microscopy (STM) studies have led to the discovery of the so-called brim sites which are located next to the edge of the crystals [22] as illustrated in figure 1.10. The figure shows the hexagonal Co-Mo-S crystal, and the brim sites appear as bright regions in the STM image.

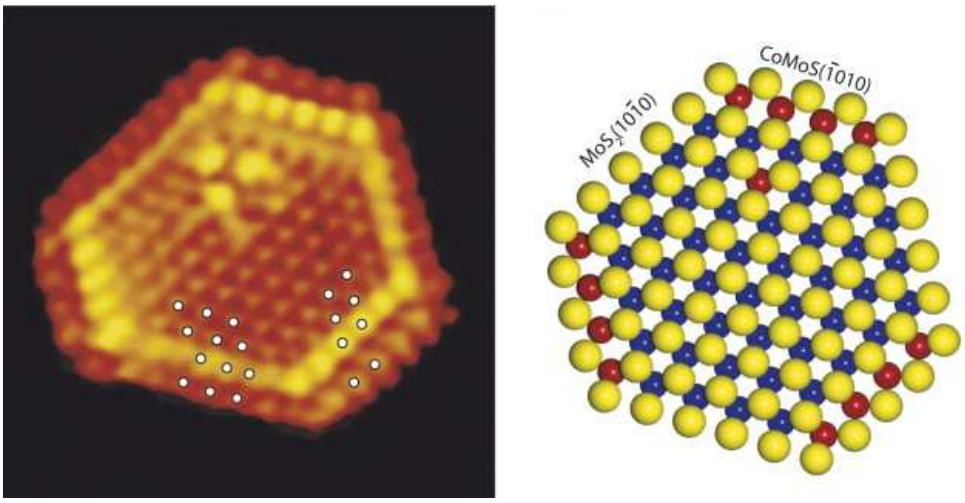

Figure 1.10: Left: Atom-resolved STM image of Co-Mo-S nanocluster (51×52 Å^2). Right: Ball-model of the Co-Mo-S nanocluster (S: yellow, Mo: blue, Co: red) [25]

The brim is a region which has a high electron density which facilitates π-bonding. These sites have been shown to be active in hydrogenation reactions, and since these sites does not interact strongly with H_2S, there is practically no inhibiting effect on these types of reactions. The STM studies have shown that the promoter atoms are preferably located at a specific type of edge sites, the so-called S edges [21].

In general NiMo based catalysts have a higher activity in hydrogenation reactions, while CoMo catalysts show a higher activity for hydrogenolysis reactions. The choice of catalyst will in general depend on the purpose of the hydrotreatment and the composition and properties of the feed.

1.4 Purpose of this work

The purpose of this Ph.D. project has been to investigate several aspects of the hydrotreating process through a combination of experimental and modelling work, particularly related to diesel oil. Better understanding of the process and the reactions will be helpful in optimizing hydrotreaters and predicting the reactivity of different feedstocks.

All experiments were performed using fixed-bed lab-scale reactors, and most of the kinetics studies have been done using model compounds. Knowledge of the kinetics and reactivity of individual compounds was the basis of a component-based reactor model for a trickle-bed hydrotreater. The experimental results presented in this thesis is the result of work done during this project, and as part of the ongoing research at Haldor Topsøe A/S.

The main parts of this work are the following:

- Investigation of internal mass transfer limitations using naphthalene as model compound
- Investigation of the effect of nitrogen compounds on sulfur removal from 4,6-dimethyldibenzothiophene
- Hydrotreating of a model diesel mixture of 13 compounds
- Description of a model of an isothermal trickle-bed reactor
- Modeling of a Robinson-Mahoney reactor (Work carried out during an external stay at Ghent University)

Hydrogenation of poly- and di-aromatics are very fast reactions, and part of this work has been to investigate and understand to what extent the reactions are limited by internal mass transfer. This is a phenomenon, that has an influence on the performance in the top of a hydrotreater. The effect of particle size has been investigated and values of the effectiveness factors have been determined.

In order to reach ULSD specifications it is necessary to remove some of the most refractive sulfur compounds such as sterically hindered dibenzothiophenes. Certain nitrogen compounds act as inhibitors mainly for the hydrogenation pathway, and knowledge of the nature of the inhibition is important in order to understand the kinetics of HDS of diesel. The effect of different nitrogen compounds, basic and non-basic, on the HDS of 4,6-dimethyldibenzothiophene and on the HDS of a real feed mixture has been investigated.

Real feed diesel mixtures are complex mixtures of a lot of different compounds. In this work a simplified model feed with 13 compounds representative of the different component classes in diesel oil, has been hydrotreated. The effects of temperature, pressure, hydrogen to oil ratio and space velocity have been investigated.

Detailed models of hydrotreating reactors, that take the different transport processes, phase equilibrium and reaction kinetics into account, are needed in order to develop improved simulation tools. A steady-state model for an isothermal trickle-bed hydrotreater is described in detail.

The model takes internal and external mass transfer into account, as well as the equilibrium between the liquid phase and the gas phase.

A Robinson-Mahoney reactor is a three-phase catalytic reactor, that behaves as a CSTR. As part of a research visit to the Laboratory of Chemical Technology (LCT) at Ghent University, Belgium, a model has been build for this type of reactor. The model was used to test existing kinetic models at industrial conditions where mass transfer limitations could be expected.

Chapter 2

Experimental Set-up and Methods

This chapter contains a description of the experimental set-up that has been used for most of the experimental work in chapter 3, 4, 6 and 7. Furthermore, characteristics of the catalysts that have been used are given. The analytical methods that have been to used analyze products are also listed.

2.1 Catalyst

Two different types of catalysts have been used in this work. The first one is a CoMo catalyst, while the second one, is a NiMo catalyst. Properties of the two catalysts are listed in table 2.1.

Catalyst	CoMo	NiMo
ϵ_p (porosity)	0.58	0.54
ρ_p (density) [kg/m^3]	1470	1560

Table 2.1: Characteristics of the hydrotreating catalysts used for experiments

Both catalysts was available as extrudates in the form of 1/20" trilobes. The catalysts were crushed down before use. A standard size fraction, 600-850 μm, is normally used for this particular set-up, but in this work, several other size fractions have also been tested.

2.2 Liquid feeds

The majority of experiments in this work were done using model feeds rather than real diesel feeds. The feeds consisted of an organic solvent, which has been either n-heptane, n-dodecane, n-tetradecane or n-hexadecane, in which the reactant(s) were either dissolved or mixed. For GC analysis of the product, an internal standard was also added.

2.3 Experimental setup

Most of the experiments for this work were carried out using a small scale laboratory reactor as illustrated in figure 2.1.

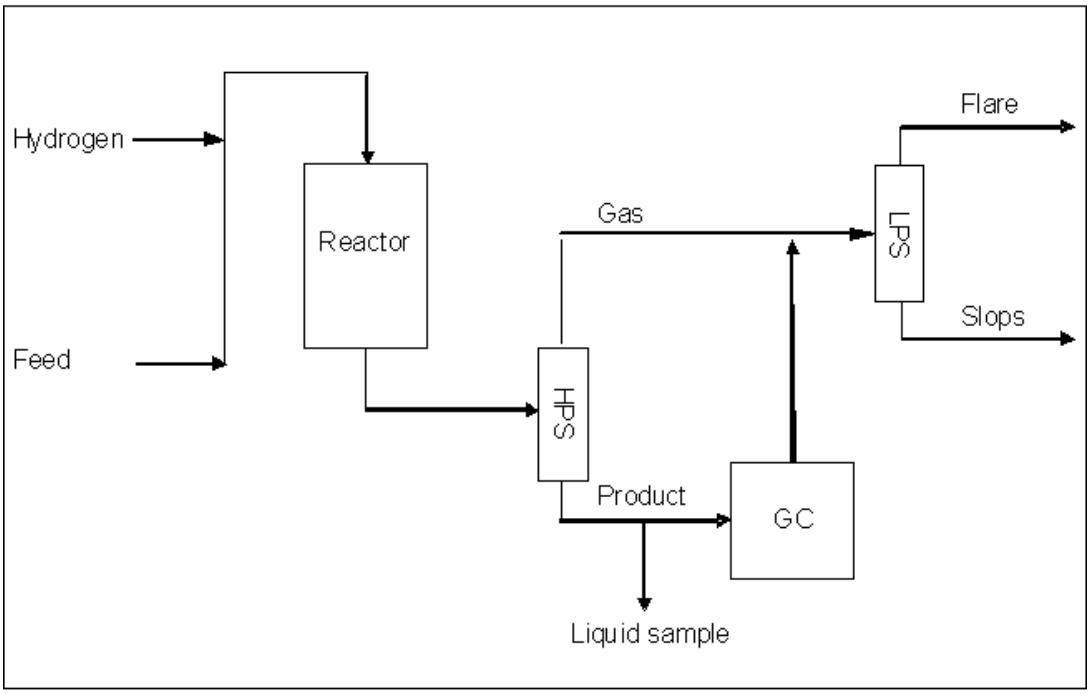

Figure 2.1: A schematic representation of the set-up used for kinetic experiments. (HPS = High Pressure Separator and LPS = Low Pressure Separator, GC = Gas Chromatograph)

The reactor tube has an internal diameter of 7.5 mm, and it is placed in a heater. Figure 2.2 shows how the reactor is loaded. The temperature is measured on the middle of the catalyst bed using a Pt-100 thermo couple, but the effect of the heater is controlled using a set-point of the temperature in the heater, outside the reactor. When loading the reactor, the position of the bed is adjusted by placing 4 ml of ballotini, 150-250 μm, above and below the catalyst bed. The catalyst is diluted with ballotini to give a total volume of 1 ml. Catalyst amounts between 25 mg and 2 g have been used in experiments, and in some cases the total amount of catalyst had a volume larger than 1 ml. In this case the amount of ballotini was adjusted to make sure, that the temperature measurement was in the middle of the bed. On the top layer of ballotini 4 ml of 3 mm glass beads was added.

The liquid feed and hydrogen is mixed before the reactor, and the layer of glass beads and ballotini is assumed to give a good distribution of gas and liquid. After the reactor gas and liquid is separated at high pressure and low temperature, and the liquid product was analyzed online on a GC. n-nonane, which was assumed not to undergo any reaction was used as internal standard in the GC, and the reactant and product concentrations were calculated by normalizing to the internal standard. In this way variations in the performance of the GC is taken into account.

In some cases liquid samples were collected from the high pressure separator for further

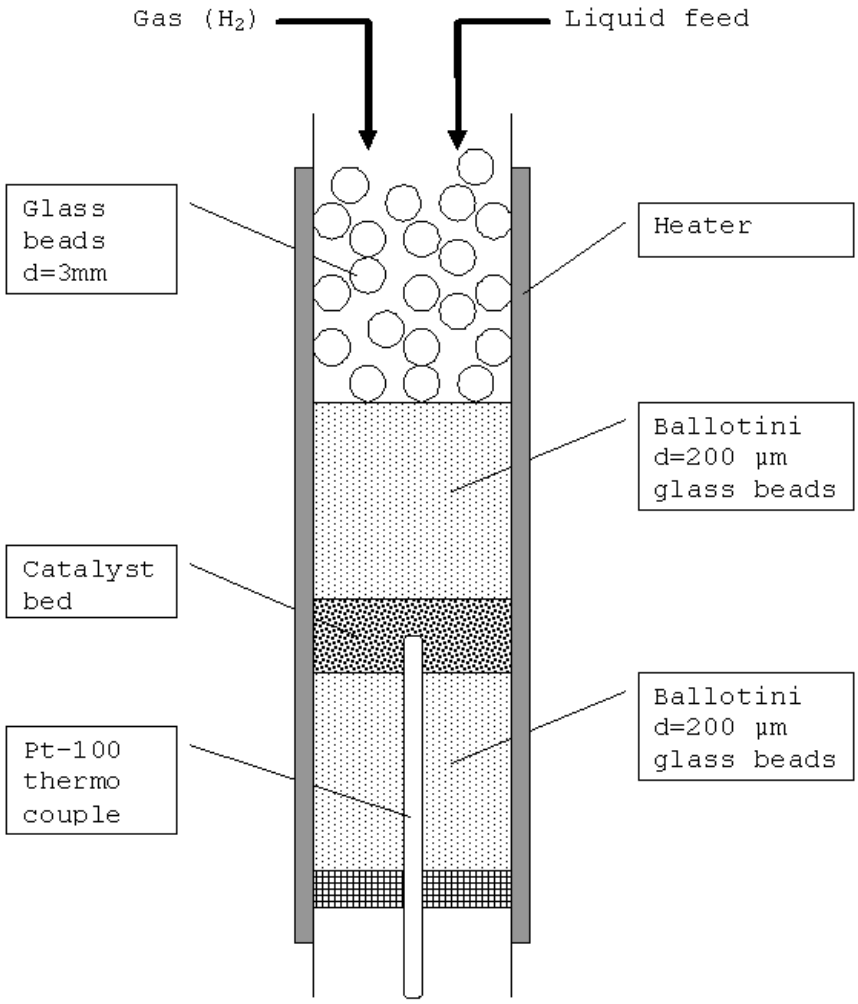

Figure 2.2: An illustration of the loading of the reactor

analysis. For samples that contained sulfur species, any dissolved hydrogen sulfide in the sample was removed, by exposing the sample to ultrasound for 1-2 hours, at ambient conditions. This is done to avoid the formation of elementary sulfur from the reaction between H_2S and O_2:

$$8H_2S \ + \ 4O_2 \ \rightarrow \ 8H_2O \ + \ S_8 \tag{2.1}$$

Before weighing the catalyst and loading it into the reactor, the catalyst is dried for 2 hours at 250 °C. This is done to remove water, thereby limiting uncertainties when measuring the catalyst mass.

When the reactor has been loaded, it is heated to 150 °C at a rate of 5 °C/ min. When the temperature is reached, a sulfiding feed consisting of 2.5 % DMDS in n-heptane is fed to the reactor. The reactor is then heated 2 °C/ min to 350 °C and held there for 4 hours. When the catalyst is 100 % sulfided, the feed is changed to the test feed, and liquid flow, hydrogen flow,

temperature and pressure are changed to test conditions. When sulfiding, the liquid feed flow is 0.3 ml/min, the hydrogen flow rate is 15 Nl/hr and the pressure is 50 barg.

The contact time between the reaction mixture and the catalyst is given in terms of the Weight Hourly Space Velocity (WHSV), which is defined in the following way:

$$WHSV = \frac{mass\ flow\ of\ liquid\ feed\ [kg/hr]}{mass\ catalyst\ [kg]} \tag{2.2}$$

The space velocity is a useful parameter when scaling up a reaction. If the reaction is not limited by external mass transfer, the conversion will not change with the liquid mass flow rate, if the weight hourly space velocity (WHSV) is kept at the same value.

2.4 Product analysis

In all experiments the liquid product was analyzed on a Gas-chromatograph and normalized according to an internal standard. In situations where peaks in the gas chromatogram were not known, they could be identified by the use of GC-MS. In some experiments the liquid product was analyzed for the total amount of sulfur using either ASTM D7212 or ASTM D4294. Similarly the nitrogen concentration has been determined using ASTM D4629. The total amount of aromatics as either mono-, di- or poly-aromatics was determined using ASTM D6591.

Chapter 3

Thermodynamic Equilibrium of Hydrogenation Reactions

Hydrogenation reactions are known to be limited by thermodynamic equilibrium at typical hydrotreating conditions, and in order to model the kinetics of the reactions, values of the equilibrium constants should be known. The thermodynamic data available in literature for naphthalene and phenanthrene hydrogenation is very scarce. Frye [26] and Frye and Weitkamp [27] performed experiments to determine gas phase equilibrium constants for these and several other compounds. The equilibrium constants are functions of the absolute temperature, and are described by an expression as follows:

$$\log(K_p) = \frac{A}{T} + B \tag{3.1}$$

The parameters A and B depend on the reaction.

In this section some experimental results obtained as part of a master project within Haldor Topsøe A/S are presented to test the validity of the existing equilibrium data. The experiments were performed in the set-up described in section 2. Feed mixtures consisted of solutions of reactants and products in n-heptane. The temperature was kept constant at 350 °C, and the pressure was 30 bar. The hydrogen to oil ratio varied between 250 and 4000 Nm^3/m^3. Phase equilibrium calculations using the Soave-Redlich-Kwong equation of state as described in section 8.4, have shown that with the temperature and pressure used for the experiments all liquid will evaporate, and only a gas phase will be present in the reactor. Since the experimental temperature is above the highest possible dew point temperature, capillary condensation in the catalyst pores is not taking place. A commercial PtPd catalyst was used to make sure that equilibrium was reached.

3.1 Equilibrium of naphthalene hydrogenation

It is desired to determine the equilibrium constants for the following two reactions:

$$naphthalene + 2H_2 \overset{K_{P1}}{\rightleftharpoons} tetralin \tag{3.2}$$

$$naphthalene + 5H_2 \overset{K_{P2}}{\rightleftharpoons} decalin \tag{3.3}$$

The two isomers, cis- and trans-decalin, are treated as one compound. It is assumed that the mixture behaves ideally, and the equilibrium constants can be calculated as follows:

$$K_{P1} = \frac{[TET]}{[NAP] \cdot P_{H_2}^2} \tag{3.4}$$

$$K_{P2} = \frac{[DEC]}{[NAP] \cdot P_{H_2}^5} \tag{3.5}$$

The ratio between the molar concentrations of tetralin and naphthalene and of decalin and naphthalene has been obtained from the GC analysis of the liquid product. It is assumed that the hydrogen partial pressure is constant down through the reactor, and is not changed by the reactions. The results are presented in table 3.1. There is good agreement between the values obtained in different experimental runs. The values at the highest gas to oil ratios, 2000 and 4000 Nm^3/m^3, appear to be slightly higher than at 250 Nm^3/m^3. The reason might be, that the change in hydrogen partial pressure is not negligible at the lowest gas to oil ratio.

Table 3.1: Experimental equilibrium constants for hydrogenation of naphthalene (NAP) to tetralin (TET) and decalin (DEC) from different experimental runs at 350 °C

H_2/oil [Nm^3/m^3]	P_{H_2} [atm]	[TET]/[NAP]	[DEC]/[NAP]	K_{P1} [atm^{-2}]	K_{P2} [atm^{-5}]
250	19.1	4.3	14.6	$1.16 \cdot 10^{-2}$	$5.70 \cdot 10^{-6}$
250	19.2	4.5	15.6	$1.21 \cdot 10^{-2}$	$5.93 \cdot 10^{-6}$
250	19.2	4.5	15.7	$1.23 \cdot 10^{-2}$	$5.99 \cdot 10^{-6}$
2000	28.8	11.2	131.7	$1.36 \cdot 10^{-2}$	$6.67 \cdot 10^{-6}$
2000	28.8	11.8	139.6	$1.43 \cdot 10^{-2}$	$7.07 \cdot 10^{-6}$
4000	29.8	11.5	147.1	$1.29 \cdot 10^{-2}$	$6.21 \cdot 10^{-6}$
4000	29.8	12.6	161.2	$1.42 \cdot 10^{-2}$	$6.81 \cdot 10^{-6}$

The corresponding values of the equilibrium constant at the experimental temperature calculated from the expressions given by Frye and Weitkamp [27] are $9.8 \cdot 10^{-3}$ atm^{-2} for K_{P1} and $3.5 \cdot 10^{-6}$ atm^{-5} for K_{P2}. Thus the experimental values in table 3.1 are higher than the expressions predict.

The data presented here only provides knowledge of the equilibrium constant at a single temperature. Assuming that the A parameters, and therefore the hydrogenation enthalpy, given by Frye and Weitkamp [27] are correct, the B values in equation 3.1 can be modified, such that the experimental values can be reproduced. The values are given in table 3.2:

Table 3.2: Parameters to calculate equilibrium constants for naphthalene hydrogenation from equation 3.1

Equilibrium constant	A	B
K_{P1}	6460	-12.28
K_{P2}	17103	-32.71

3.2 Equilibrium of phenanthrene hydrogenation

It is also desired to test the equilibrium constants for the hydrogenation of phenanthrene. As in the case of naphthalene, there is no distinction between the stereo isomers of the products. The difference between the symmetric, and the asymmetric octahydro-phenenthrene is not considered. Equilibrium constants for the following 4 reactions have been measured experimentally:

$$phenanthrene + \ H_2 \overset{K'_{P1}}{\rightleftharpoons} dihydro - phenanthrene \tag{3.6}$$

$$phenanthrene + 2H_2 \overset{K'_{P2}}{\rightleftharpoons} tetrahydro - phenanthrene \tag{3.7}$$

$$phenanthrene + 4H_2 \overset{K'_{P3}}{\rightleftharpoons} octahydro - phenanthrene \tag{3.8}$$

$$phenanthrene + 7H_2 \overset{K'_{P4}}{\rightleftharpoons} perhydro - phenanthrene \tag{3.9}$$

$$\tag{3.10}$$

The equilibrium constants can be calculated from the following expressions:

$$K'_{P1} = \frac{[DHP]}{[PHE] \cdot P_{H_2}} \tag{3.11}$$

$$K'_{P2} = \frac{[THP]}{[PHE] \cdot P^2_{H_2}} \tag{3.12}$$

$$K'_{P3} = \frac{[OHP]}{[PHE] \cdot P^4_{H_2}} \tag{3.13}$$

$$K'_{P4} = \frac{[PHP]}{[PHE] \cdot P^7_{H_2}} \tag{3.14}$$

$$\tag{3.15}$$

For these experiments the liquid feed only contained phenanthrene, but none of the products. The results from the experiments are summarized in table 3.3 and 3.4. As was the case in the naphthalene equilibrium experiments, the constants are slightly lower when the hydrogen to oil ratio is at its lowest (250 Nm^3/m^3) than with the larger ratios. Using the expressions from Frye [26] the following values for the equilibrium constants have been calculated: K'$_{P1}$ has a value of $1.18 \cdot 10^{-2}$ [atm^{-1}], K'$_{P2}$ has a value of $2.04 \cdot 10^{-3}$ [atm^{-2}], K'$_{P3}$ has a value of $3.80 \cdot 10^{-6}$ [atm^{-4}] and K'$_{P4}$ has a value of $6.52 \cdot 10^{-10}$ [atm^{-7}]. In general there is good agreement between these

values and the experimental results, although it appears that most of the experimental values are larger than the predictions, except for K'$_{P1}$. A reason might be that in this work, the gas phase has been considered ideal, whereas Frye [26] used an empirical expression to calculate the fugacity of hydrogen.

Table 3.3: Experimental equilibrium constants for hydrogenation of phenanthrene (PHE) to dihydro-phenanthrene (DHP) and tetrahydro-phenanthrene (THP) from different experimental runs at 350 °C

H_2/oil [Nm^3/m^3]	P_{H_2} [atm]	[DHP]/[PHE]	[THP]/[PHE]	K'$_{P1}$ [atm^{-1}]	K'$_{P2}$ [atm^{-2}]
250	18.9	0.183	0.800	$9.69 \cdot 10^{-3}$	$2.23 \cdot 10^{-3}$
250	19.1	0.192	1.01	$1.00 \cdot 10^{-2}$	$2.78 \cdot 10^{-3}$
2000	28.6	0.263	2.64	$9.18 \cdot 10^{-3}$	$3.21 \cdot 10^{-3}$
4000	29.7	0	2.84	-	$3.22 \cdot 10^{-3}$

Table 3.4: Experimental equilibrium constants for hydrogenation of phenanthrene (PHE) to octahydro-phenanthrene (OHP) and perhydro-phenanthrene (PHP) from different experimental runs at 350 °C

H_2/oil [Nm^3/m^3]	P_{H_2} [atm]	[OHP]/[PHE]	[PHP]/[PHE]	K'$_{P3}$ [atm^{-4}]	K'$_{P4}$ [atm^{-7}]
250	18.9	0.681	0.450	$5.3 \cdot 10^{-6}$	$5.16 \cdot 10^{-10}$
250	19.1	1.01	0.971	$7.58 \cdot 10^{-6}$	$1.04 \cdot 10^{-9}$
2000	28.6	6.79	24.726	$1.01 \cdot 10^{-5}$	$1.56 \cdot 10^{-9}$
4000	29.7	8.66	31.831	$1.11 \cdot 10^{-5}$	$1.56 \cdot 10^{-9}$

Just as for the naphthalene data, the parameters for equation 3.1 for phenanthrene hydrogenation from Frye [26] have been modified in order to match the measured equilibrium constants, and the results are presented in table 3.5.

Table 3.5: Parameters to calculate equilibrium constants for phenanthrene hydrogenation from equation 3.1

Equilibrium constant	A	B
K'$_{P1}$	2600	-6.32
K'$_{P2}$	6565	-13.10
K'$_{P3}$	13030	-26.03
K'$_{P4}$	23190	-46.24

3.3 Conclusion

In this chapter a set of measured equilibrium constants for naphthalene and phenanthrene hydrogenation have been presented by Frye [26] and Frye and Weitkamp [27]. Comparing the constants with with values shows a good agreement, and the same order of magnitude is found. In most cases the measured equilibrium constants were higher than the predictions, and therefore a set of new parameter values for equation 3.1 was presented, that give equilibrium constants in better agreement with the experimental results.

Chapter 4

Experimental Investigation of Naphthalene Hydrogenation

The hydrogenation of naphthalene has been investigated using the experimental set-up described in section 2. The catalyst was a commercial CoMo catalyst with properties as shown in table 2.1. Naphthalene reacts with hydrogen to form tetralin. Further reaction to cis- or trans-decalin is possible, but was tested and shown to be negligible at the applied conditions. The results presented in this chapter are a continuation of a previous master project. The main purpose has been to investigate whether internal diffusion resistance had an influence on the observed reaction rate. This was done by investigating the effect of the size of the catalyst particle. Furthermore the effect of the temperature, feed concentration and hydrogen partial pressure on the naphthalene conversion has been investigated.

Assuming that the density of the liquid did not change during the reaction, the naphthalene conversion, X, can be calculated from the weight fraction of naphthalene in the feed, w_0, and the weight fraction of naphthalene in the product, w_p, as:

$$X = 1 - \frac{w_p}{w_0} \tag{4.1}$$

Pseudo first order rate constants have been calculated from the conversion as follows:

$$k = -\ln(1 - X) \cdot WHSV \tag{4.2}$$

4.1 Catalyst and chemicals

For the experiments in this chapter the CoMo catalyst with properties given in table 2.1 has been used. A solution of naphthalene in either n-heptane or n-hexadecane has been used as liquid feed. In most of the experiments, the feed concentration of naphthalene was kept relatively low, around 2% w/w, in order to avoid a temperature rise in the reactor, due to the heat evolved by

the reaction.

4.2 Effect of WHSV

The set-up described in chapter 2, was used to investigate the hydrogenation of naphthalene using a solution in n-heptane as liquid feed. Since saturation of the first ring in naphthalene is a fast reaction at typical hydrotreating conditions, the experiments have been carried out at relatively high space velocities, i.e. WHSV values from 25 hr^{-1} and as high as 1500 hr^{-1}, which would correspond to the top of an industrial reactor. Figure 4.1 shows a first order kinetic plot of the measured naphthalene conversions. The figure shows, that especially at high space velocities, the conversion follows a first order rate expression well. At lower space velocities (WHSV $< 100\ hr^{-1}$), the measured conversion is lower, than a first order rate law predicts. This is because the reaction is limited by thermodynamic equilibrium.

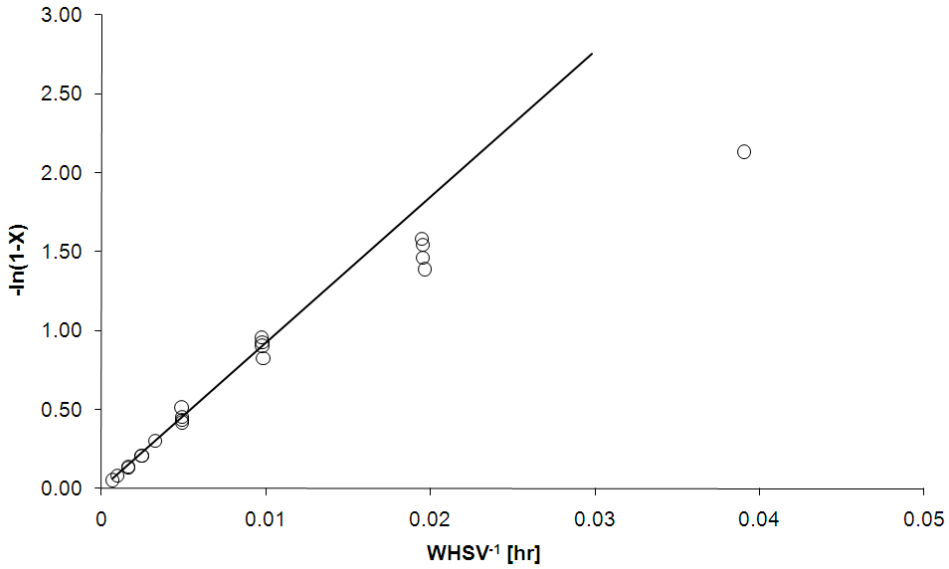

Figure 4.1: 1. order kinetic plot of the naphthalene conversion obtained using the standard 600-850 μm particle size fraction. The liquid feed is a solution of 2 % w/w naphthalene in n-heptane. ($T = 344\ ^{\circ}C$, $P = 30\ barg$ and $H_2/oil = 250\ Nl/l$)

Although the first order rate expression is certainly a simplified way of describing the kinetics, the first order rate constant is a useful measure of the reactivity, and can be used when comparing the different catalyst particle size fractions.

4.3 Particle size

4 different particle size fractions have been tested: 63-105 μm, 300-425 μm, 600-850 μm and 850-1000 μm. The catalyst mass was varied between 40 and 200 mg. Figure 4.2 shows a plot of the pseudo first order rate constant as a function of the inverse space velocity. It is clear from the figure, that there is a difference in the observed reaction rate between the two fractions 300-425

μm and 600-850 μm. The smallest fraction, 300-425 μm, results in first order rate constants, that are up to 40 % larger than for the 600-850 μm. This suggests, that either internal or external mass transfer resistance is limiting the reaction. The observed rate constants for the 63-105 μm and 850-1000 μm fraction, are however not in agreement with this trend. At the high space velocities, i.e. low reaction times, the rate constants are in between the rate constants for the 300-425 μm and 600-850 μm fractions, but it appears that as the reaction time increases, they approach the value of the 600-850 μm fraction. From these results, it is very difficult to make any conclusions regarding whether or not mass transfer has an effect on the observed reaction rate. Some conditions have been repeated, and show, a rather large experimental uncertainty.

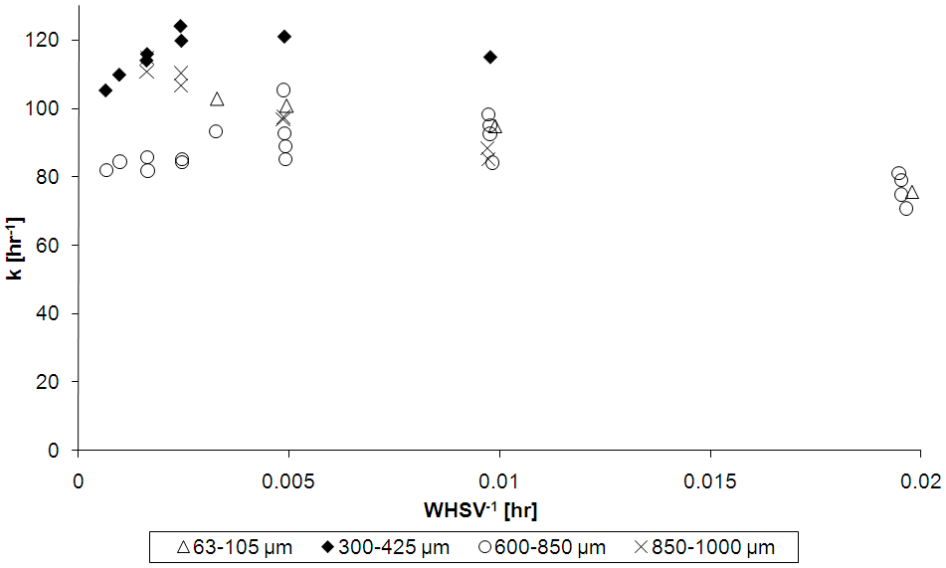

Figure 4.2: Effect of particle size on the first order rate constant. The liquid feed is a solution of 2 % w/w naphthalene in n-heptane. It was expected that the observed rate constant would increase with decreasing particle size. But the 300-425 μm fraction, which is not the smallest fraction show the highest rate constant at all space velocities. At long reaction times, there is very little difference between the 63-105 μm, μm, 600-850 μm and 850-1000 μm, but at the shorter reaction times the 850-1000 μm fraction has a higher rate constant than the 600-850 μm fraction, which is not the expected trend. ($T = 344\ ^{\circ}C$, $P = 30\ barg$ and $H_2/oil = 250\ Nl/l$)

4.3.1 Effect of particle size in n-hexadecane

The results shown in figure 4.2 were obtained using a liquid feed of 2 % naphthalene in n-heptane. The effect of the particle size was also tested using a heavier solvent, n-hexadecane. This was done to ensure that a liquid phase was present in the reactor, at the experimental conditions, and therefore would be similar to the situation in industrial hydrotreaters. To eleminate some of the uncertainty, that was observed in the experiments using n-heptane, the catalyst mass was kept constant at 200 mg. Figure 4.3 shows the pseudo first order rate constants for the 4 different particle size fractions. The results from the 63-105 μm show that there is still some variation in the observed rate constants, and the values for this fraction are not considerably different from the 300-425 μm and 600-850 μm fractions. If the smallest fraction is not considered, the

expected trend is found, in that the observed rate constant decreases with increasing particle size. In this case the largest particles results in a significantly lower rate constant, than the other fractions. This was not seen in the n-heptane experiments, but the reason for the difference is not fully understood.

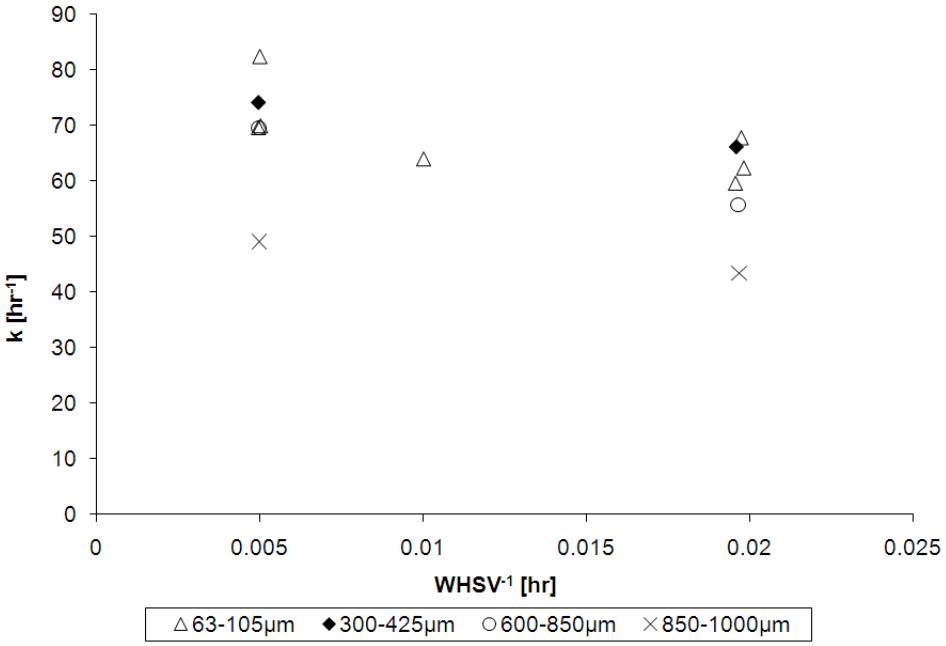

Figure 4.3: Effect of particle size on the first order rate constant. The liquid feed is a solution of 2 % w/w naphthalene in n-hexadecane. ($T = 340\ ^{\circ}C$, $P = 30\ barg$ and $H_2/oil = 250\ Nl/l$)

4.4 Effect of temperature

An apparent activation energy has been determined by estimating the first order rate constant at 3 different temperatures: 270, 300 and 340 °C using the standard size fraction of 600-850 μm. At the highest temperature, the reaction becomes limited by thermodynamic equilibrium at high conversions, therefore the rate constant used in the Arrhenius plot in figure 4.4, has been obtained, at rather high space velocities (100-200 hr^{-1}) where the conversion was less than 0.4, and the rate should thus not be limited by equilibrium. Figure 4.4 show an Arrhenius plot with a slope of -3524 K, which corresponds to an activation energy of 29.3 kJ/mol. This is a rather low value for an activation energy, which could be an indication that the reaction is limited by diffusion resistance. Since a pseudo first order rate constant is used, the apparent activation energy might be a combination of the activation energy of the rate determining step and adsorption enthalpies for products and reactants, rather than a true activation energy.

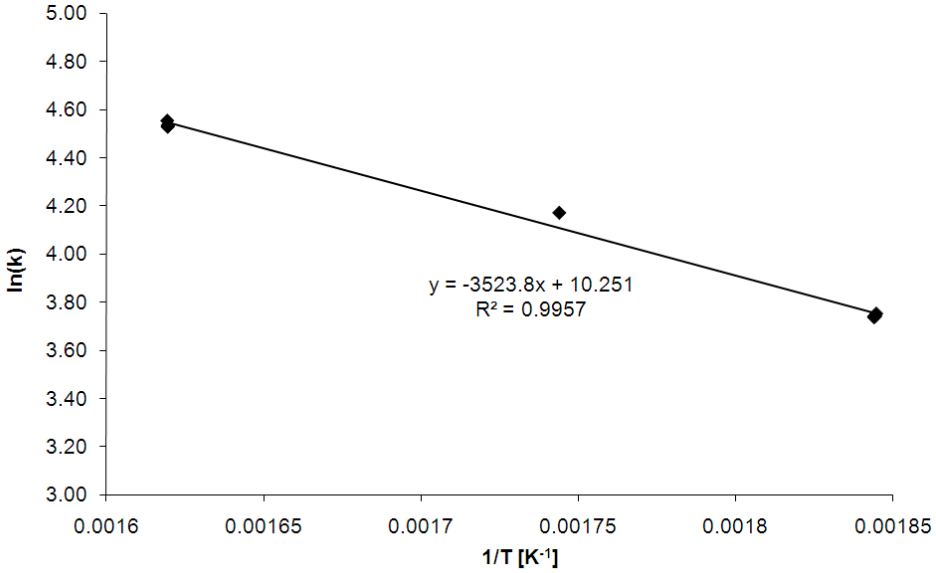

Figure 4.4: Arrhenius plot of the pseudo first order rate constant obtained using a 600-850 μm particle size fraction. ($WHSV = 100 - 200\ hr^{-1}$, $P = 30\ barg$ and $H_2/oil = 250\ Nl/l$)

4.5 Effect of feed concentration

In the previous experiments the naphthalene feed concentration was kept constant at 2 % w/w. Since the conversion fitted relatively well with a first order rate expression it was assumed that the reaction was first order with respect to naphthalene. To see if this was actually a reasonable assumption experiments have been conducted with different concentrations of naphthalene in the feed. Previous experiments showed, that the observed rate constant was largest for the 300-425 μm fraction, suggesting, that the effectiveness factor of the pellet in this case was closest to 1.

Plotting the conversions in a first order kinetic plot shows that the initial concentration has an effect on the rate constant as illustrated in figure 4.5. This is not in agreement with a first order rate expression, which is therefore obviously a simplified rate expression. It is observed that the first order rate constant decreases with increasing initial concentration which in catalytic reactions would often correspond to increased coverage of the surface of the catalyst. It is possible to describe this kind of trend using a Langmuir-Hinshelwood Hougen-Watson (LHHW) type of rate expression. If it is assumed that the hydrogen concentration can be considered constant, the hydrogen concentration can be incorporated in the rate constant. If it is furthermore assumed that adsorption of the product, tetralin, is very weak and can be ignored, one will get a rate expression that only depends on the naphthalene concentration. At the lower temperature, the reaction is not limited by equilibrium. The concentrations of naphthalene have been calculated using the ideal gas law. Any change in volumetric flow rate due to the reaction is so small, that it can be neglected.

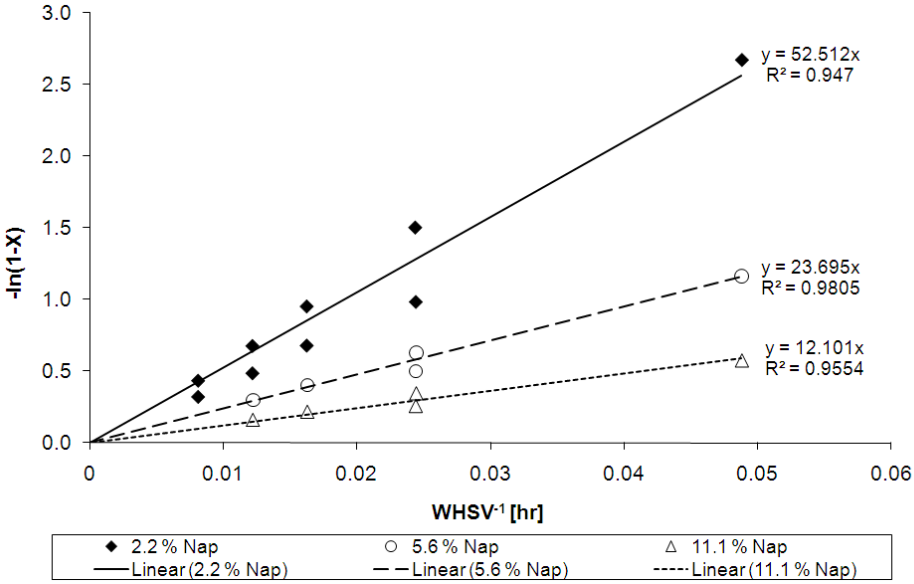

Figure 4.5: Effect of naphthalene feed concentration on a first order kinetic plot. Since the slope, i.e. the first order rate constant, depends on the initial concentration, first order kinetics are too simple to fully describe the behavior. ($T = 270\ ^{\circ}C$, $P = 30\ barg$ and $H_2/oil = 250\ Nl/l$)

The simplest possible form of a Langmuir-Hinshelwood type rate equation is the following:

$$-\frac{dC_{Nap}}{d\tau} = C_{Nap0}\frac{X}{d\tau} = \frac{kC_{Nap}}{1 + KC_{Nap}} = \frac{kC_{Nap0}(1-X)}{1 + KC_{Nap0}(1-X)} \tag{4.3}$$

Here $WHSV^{-1}$ is denoted as τ. Integrating the expression gives the following relation between the conversion and the space velocity:

$$\tau = -\frac{\ln(1-X)}{k} + \frac{K}{k}C_{Nap0}X \tag{4.4}$$

Two unknown parameters exist in the equation, the rate constant k, and the adsorption constant K. Optimal values can be found by defining the following objective function and minimizing:

$$obj. = \sum_{i=1}^{N}(\tau_{exp,i} - \tau_{calc,i})^2 \tag{4.5}$$

Other rate expressions are certainly possible, but this one is able to describe the observed conversion adequately within the investigated conversion and space velocity range. The parameters, that give the best fit are listed in table 4.1. Figure 4.6 shows the experimental conversions compared with the model. The model captures the trends when varying the feed concentration, and is able to describe the experimental results quite well, although the conversion is over-predicted at large reaction times. This might be because the adsorption of the product tetralin has been neglected. If the product is blocking some of the active sites, the actual reaction rate will be lower than what is predicted, and the observed conversion will be lower.

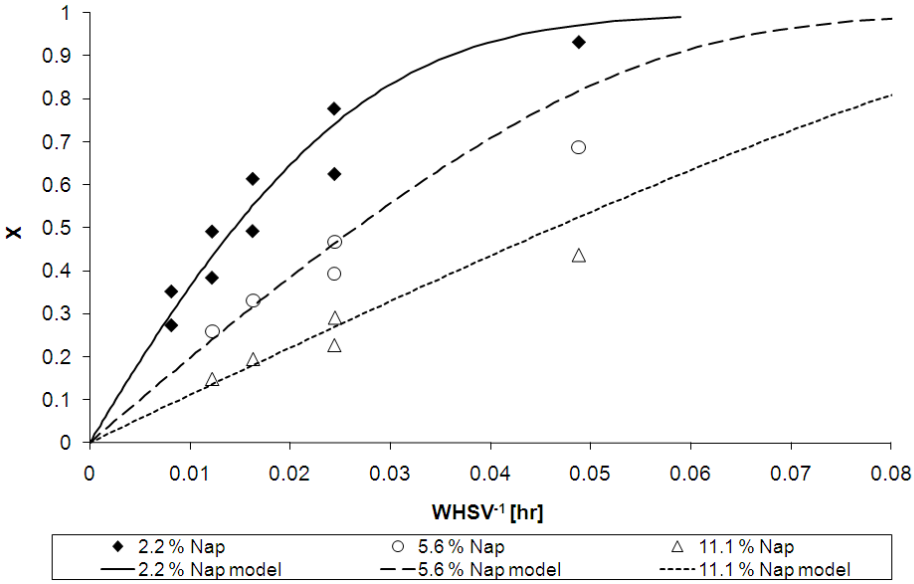

Figure 4.6: Experimental results and model predictions using a simple Langmuir-Hinshelwood Hougen-Watson rate expression. ($T = 270\ ^{\circ}C$, $P = 30\ barg$ and $H_2/oil = 250\ Nl/l$)

k $[hr^{-1}]$	K $[m^3/mol]$
106.2	0.38

Table 4.1: Parameters for the rate expression in equation 4.3

4.6 Hydrogen dependency

All the previous experiments have been carried out at the same hydrogen to oil ratio in the feed. Since hydrogen is present in great surplus, it is a good approximation that the hydrogen concentration (or partial pressure) is more or less constant down through the reactor. Since this is the case, any hydrogen dependency has been incorporated in the calculated rate constants. To estimate how the rate depends on the hydrogen concentration a series of experiments have been performed with varying hydrogen partial pressure, but constant partial pressure of naphthalene. The conditions and partial pressure of hydrogen and naphthalene are given in table 4.2.

GOratio [Nm^3/m^3]	P_{total} [bar]	P_{H_2} [bar]	$P_{naphthalene}$ [bar]
125	21.00	9.47	0.199
250	30.02	18.66	0.196
500	51.79	39.71	0.209

Table 4.2: Conditions (gas-to-oil-ratio and pressure) used to determine H_2 dependency

Figure 4.7 shows the effect of the hydrogen partial pressure on the first order kinetic plot. The slopes, and therefore the pseudo first order rate constant, clearly increases with increasing hydrogen pressure. Assuming that the observed first order rate constant is proportional to the

partial pressure of hydrogen to the power of n gives:

$$k = k' \cdot P_{H_2}^n \tag{4.6}$$

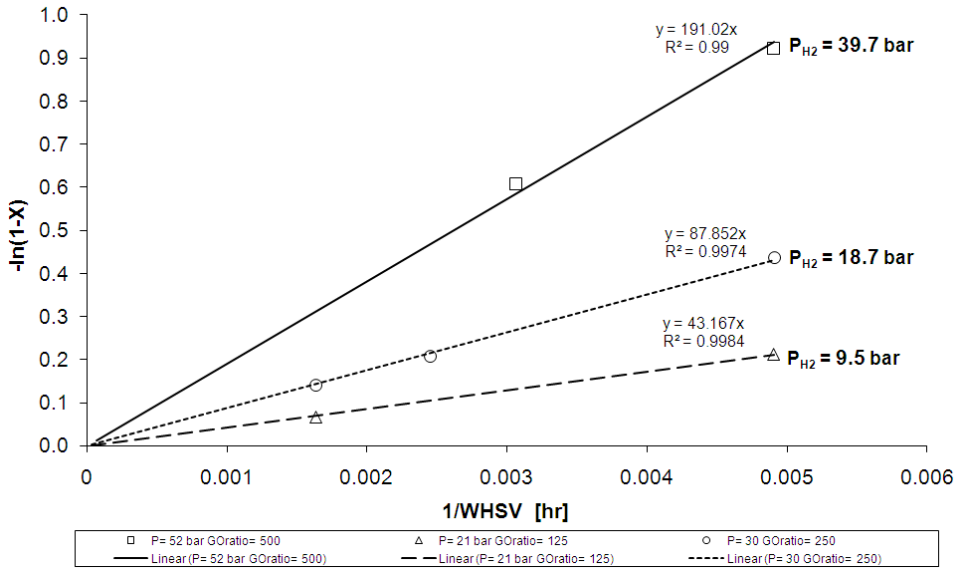

Figure 4.7: First order kinetic plot at various hydrogen partial pressures obtained using the standard 600-850 μm particle size fraction. ($WHSV \sim 200 - 600\ hr^{-1}$, $T = 344°C$, $P_{naphthalene} = 0.2\ bar$)

The hydrogen reaction order, n, can be determined as the slope of a logarithmic plot of the observed rate constant as a function of the hydrogen partial pressure. Figure 4.8 shows that such a plot yields a straight line, with a slope of 1.0, and therefore the reaction rate is first order in the hydrogen concentration.

4.7 Experimental uncertainty

Since previous experiments have shown unexpected behavior, meaning no clear trend, when changing the size of catalyst particles, further experiments have been conducted to see if the reason for this could be clarified. A possible explanation for the observed behavior could be that very small amounts of catalyst were used in the experiments, and this might result in significant uncertainties in the observed reaction rate from experiment to experiment. This would be the case if for example, some of the particles were flushed out of the reaction zone or were completely removed from the reactor.

In order to avoid this, experiments were conducted using a larger amount of catalyst. To ensure that the conversion was in the same range as in the previous experiments, it was necessary to conduct the experiments at a lower temperature. This results in a lower rate constant and a decrease in the possibility for pellet diffusion playing a role, but on the other hand it should improve the chances of getting more consistent experimental results.

The temperature was lowered to 270 °C, compared to 340 °C in the previous experiments,

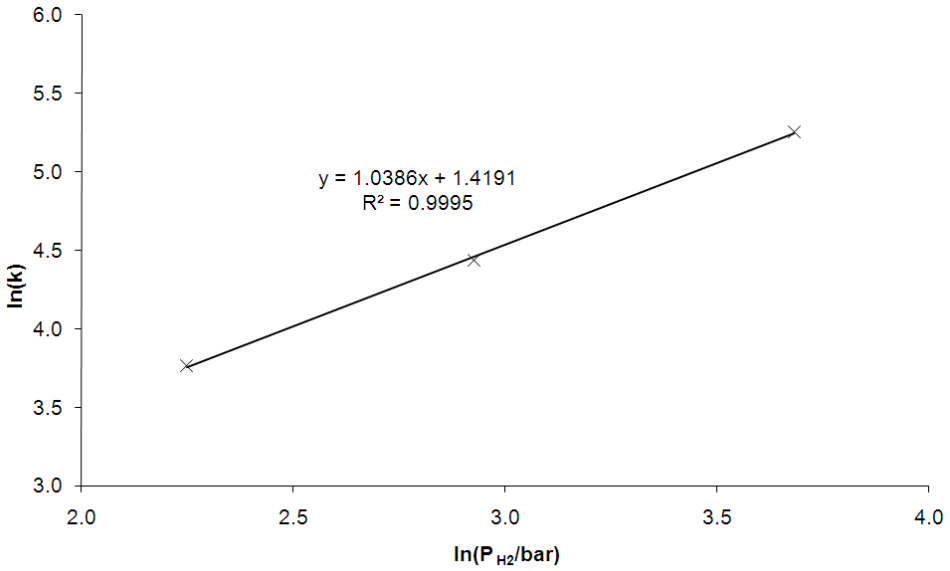

Figure 4.8: Pseudo first order rate constant as function of the hydrogen partial pressure. The slope of the straight line is equal to the reaction order of hydrogen. ($T = 344°C$ and $P_{naphthalene} = 0.2\ bar$)

which meant that the amount of catalyst could be increased to 0.5 g. In the previous experiments it was observed that the conversion could be described reasonably well with a first order rate expression. This is also observed at the lower temperature. Four different particle size fractions have been used: 63-105 μm, 300-425 μm, 600-850 μm and 850-1000 μm, and in some cases different amounts of the same fraction were used. If the observed first order rate constant is plotted as a function of the inverse space velocity, as is done in figure 4.9, it can be seen that all but two of the experimental runs give the same rate constant within $\pm$ less than 10 %. On the other hand two of the experimental series give rate constants that are significantly different from the rest. The experimental run using the particle size fraction 63-105 μm and 0.5 g catalyst gives an average rate constant around 32 hr^{-1} while a run using the fraction 300-425 μm gives an average rate constant around 57 hr^{-1}. It seems obvious that something went wrong in these two experiments. Two experiments using the 63-105 μm fraction and a catalyst mass of 0.25 g and 1.0 g respectively both yield rate constants around 43 hr^{-1}. And a repetition of the experiment using the 300-425 μm fraction and 0.5 g of catalyst gave a rate constant of around 49 hr^{-1}.

Based on this experiment it can be concluded that at 270 °C no diffusion limitations exist within the catalyst pellets. Also there appear to be systematic errors in some of the experimental runs, such that all of the experimental points are wrong, and not only a single point. This suggests, that the error or difference is related to the loading of the catalyst. A result of this could be that part of the catalyst mass is not available for reaction. This would result in the actual space velocity being different from what is expected, and this would shift the rate constant down. Another reason for these systematic errors could be control of the flow rate, which if lower than the set-point would results in a larger rate constant than expected.

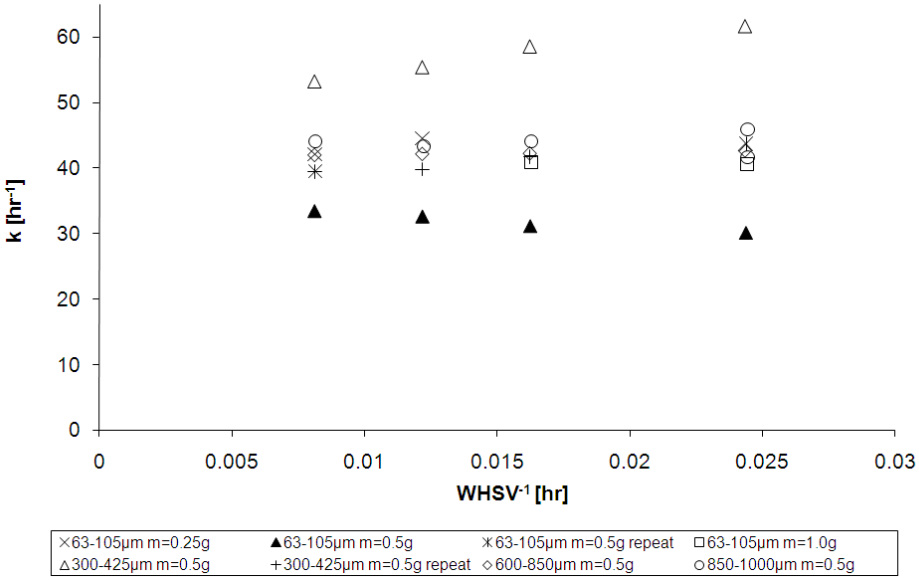

Figure 4.9: First order rate constant for different particle size fractions and amounts of catalyst. ($T = 270\ °C$, $P = 30\ barg$ and $H_2/oil = 250\ Nl/l$)

4.8 Conclusion

From the experimental results presented in this chapter several conclusions can be made. Pseudo first order rate constants have been used to analyse the results, and it appears to be a good measure of the observed reactivity. Changing the size of the catalyst particles has an effect on the observed rate constants, but the trends are not clear, and might be influenced by unknown factors. Furthermore experiments at a low temperature, 270 °C, where internal mass transfer does not limit the rate have shown differences between each loading which can result in large uncertainties.

Varying the feed concentration of naphthalene has shown, that the first order rate expression is an approximation, as the pseudo first order rate constant decreases with increasing naphthalene concentration. A simple LHHW expression captures this trend, and describes the experimental data rather well.

Varying the hydrogen partial pressure has shown, that the reaction rate is described well as being first order in hydrogen. This suggests that a rate expression of the following type is suited to describe the hydrogenation of naphthalene:

$$-r_{nap\ f} = \frac{k \cdot [nap] \cdot [H_2]}{1 + K_{nap} \cdot [nap]} \tag{4.7}$$

In order to get more consistent experimental data with respect to changing the particle size, experiments have been performed in another experimental set-up allowing for several fractions to be tested simultaneously. These results are presented in chapter 5

Chapter 5

Experimental Investigation of Diffusion Limitations in Naphthalene Hydrogenation on a CoMo Catalyst

In this chapter results from an investigation of the effect of the catalyst particle on the rate of hydrogenation of naphthalene is presented. The experiments have been carried out in a set-up consisting of 16 parallel reactors. It is shown, that the reaction is limited by intra-particle diffusion, and estimated values of the effectiveness factors are presented.

5.1 Introduction

It is well-known, that hydrogenation of fused aromatic rings is very fast at typical hydrotreating conditions. Furthermore, saturation of aromatics is limited by thermodynamic equilibrium at typical hydrotreating temperatures and pressures.

Because of the very fast reaction rate, it is likely, that the observed reaction rate is limited by mass transfer or internal diffusion in the catalyst pellets. In this work an experimental investigation has been made, of the effect of catalyst particle size on the hydrogenation of naphthalene at industrial hydrotreating conditions, temperatures between 300 and 360 °C and a pressure of 30 barg. This is done in order to determine whether internal diffusion resistance or mass transfer has an influence on the reaction rate, and to provide some data, that can be used to estimate values of effectiveness factors.

5.2 Catalyst and chemicals

The catalyst in these experiments was a CoMo catalyst, and different size fractions were prepared by crushing the particles and separating them using sieves with different mesh sizes. The size and short name for the different fractions are shown in table 5.1.

The fraction denoted as F in table 5.1 was prepared by crushing the catalyst several times through a sieve with a mesh size corresponding to 1.4 mm. Particles which had approximately

Table 5.1: Different size fractions of the CoMo catalyst used in the experiments

Fraction name	*Fraction size*
A	63-105 μm
B	150-212 μm
C	300-425 μm
D	600-850 μm
E	850-1000 μm
F	$\sim$ 1450 μm

the same length and width were chosen to be used for the experiments.

Experience has shown that the set-up is sensitive to dust on the surface of the catalyst particles which can clog the pipes. To avoid this, dust was removed from the fractions A and B, by using a vacuum on the back side of the sieve. Before use, the catalyst was kept for 2 hours at 250 °C in order to remove moisture from the catalyst.

The liquid feed was a solution of 2 % (w/w) naphthalene in n-tetradecane. For the subsequent GC analysis 0.5 % n-nonane was added to be used as internal standard. 100 ppm S as DMDS was added in order to keep the catalyst in a sulfided state. During the start-up the catalyst was sulfided using a liquid feed consisting of 2 % S as DMDS in n-tetradecane.

5.3 Experimental set-up and procedures

The set-up used to test the different size fractions is shown in figure 5.1. It consists of 16 parallel reactors placed in two different furnaces 8 in each. In this way it is possible to carry out multiple experiments at 2 different temperatures simultaneously. All the reactors are fed with liquid from the same feed pump, which means that the liquid flow cannot be changed independently in the 16 reactors.

In order to make sure that the flow is distributed evenly between the reactors, the pressure drop during flow of N_2 through each reactor is measured before use. When the set-up is in use the flow in each reactor is determined by weighing the amount of liquid recovered from each reactor within a certain time span, which for this experiment was between 3 and 22 hours.

Each reactor tube is approximately 30 cm long and has an internal diameter of 4 mm. In the bottom of each reactor is a filter. When loading the reactors they were first filled with a layer of ballotini, 150-212 μm, up to a height of approximately 12 cm. The reactors were shaken in order to make the ballotini settle. The height was measured and extra ballotini were added to ensure that the layer of ballotini was the correct height. After this, the catalyst particles were mixed with ballotini and added above the bottom layer of ballotini. The amount of ballotini was chosen such that the diluted catalyst beds had a height of approximately 7.5 cm. On top of the catalyst layer another 10 cm of ballotini were added. Again the reactors were shaken to ensure a good packing of the particles and the height in each reactor was adjusted to the same value with ballotini. The top layer of ballotini helps to get a good distribution of gas and liquid

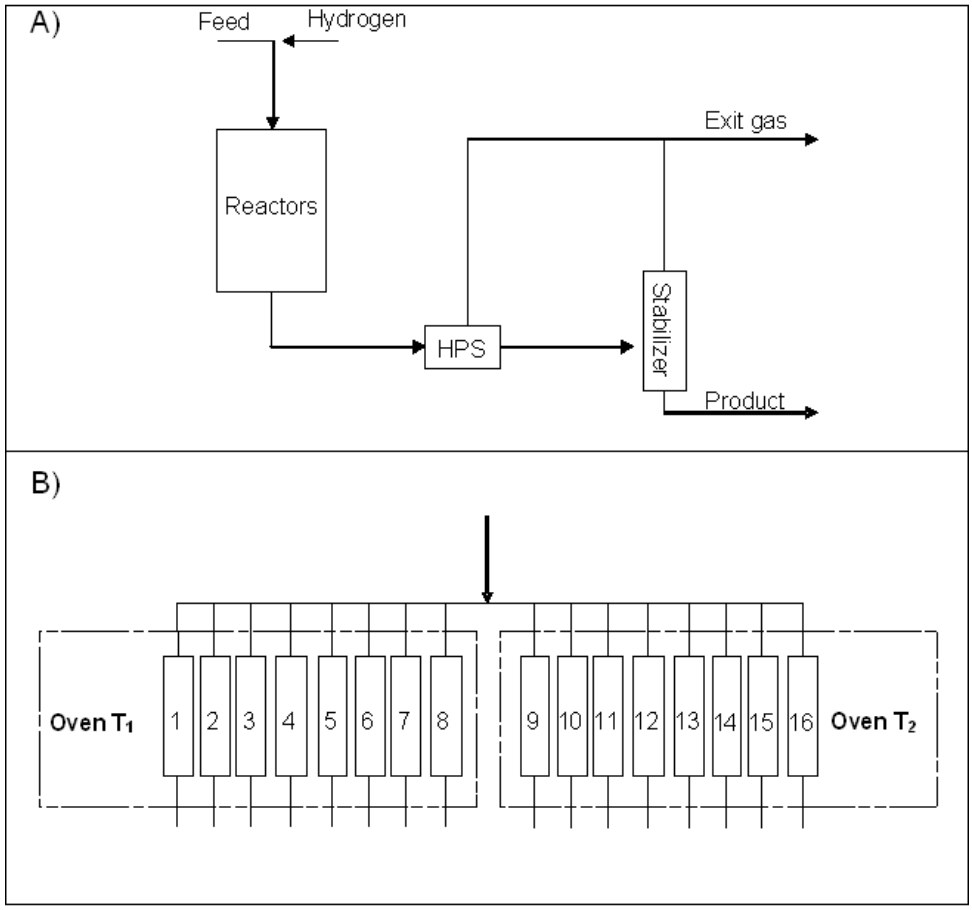

Figure 5.1: A) Schematic overview of the set-up used for testing the effect of particle size on naphthalene hydrogenation. B) Illustration of the 16 parallel reactors in the set-up. (HPS = High Pressure Separator)

flow in the reactor. After this the pressure drop in each reactor was measured. It was found to be between 220 and 280 mbar for the 16 reactors which is an acceptable variation.

Table 5.2 shows the loading of the 16 reactors. In order to make sure, that there was no reaction taking place without a catalyst present, one reactor tube in each oven (8 and 16) was loaded only with ballotini. To get an idea of the experimental uncertainty 2 of the reactor tubes in each oven had the same loading.

After the loaded reactor tubes had been installed in the set-up, the catalyst was dried for an hour with nitrogen at 2 bar. During the sulfiding of the catalyst the hydrogen to oil ratio was 500 Nl/l and the pressure was 30 barg. The reactors were heated 0.4 °C/min up to 350 °C, where they were held for 9 hours. After that the feed was changed to the test feed, and temperature, pressure and flow were set to test conditions.

5.3.1 Product analysis

The hydrogenation reaction was investigated at 4 different conditions as shown in table 5.3. For conditions 1-3 liquid samples were collected after 20, 21 and 22 hours, where it was assumed that steady-state had been reached. For condition 4, samples were collected after 17, 18 and 19

Table 5.2: Loading of the reactors

Reactor no.	1	2	3	4	5	6	7	8
Fraction name	A	B	C	D	E	F	E	-
Mass of catalyst [mg]	50	25	50	25	50	25	50	0
Reactor no.	9	10	11	12	13	14	15	16
Fraction name	A	B	C	D	E	F	B	-
Mass of catalyst [mg]	25	50	25	50	25	50	50	0

hours.

During the test the temperature and pressure of each reactor was measured. When no samples are collected, the mass of liquid product from each reactor is determined. In this way it is possible to determine the variation in flow between the reactors, and whether all of the liquid is recovered. At all conditions the total amount of liquid recovered was within ± 3 % of what was measured by the feed pump.

Table 5.3: List of test conditions

Condition	*P [barg]*	*Liquid flow [ml/hr]*	*H_2 flow [Nl/hr]*	*T_1 [°C]*	*T_2 [°C]*
1	30	3.75	0.94	340	340
2	30	1.88	0.47	340	340
3	30	3.75	0.94	300	320
4	30	3.75	0.94	320	360

The liquid samples were analyzed using a gas chromatograph. It seemed that due to the low boiling point of n-nonane, a significant part of it stayed in the vapor phase in the gas-liquid separators, and it was not possible to use it as standard for the GC analysis. Since the boiling points of naphthalene and tetralin are higher than for n-nonane it was assumed that the reactant and product stayed in the liquid phase, and the naphthalene conversions were calculated from the area percentages from the chromatogram as:

$$X = 1 - \frac{\frac{A_{naphthalene}}{M_{naphthalene}}}{\frac{A_{naphthalene}}{M_{naphthalene}} + \frac{A_{tetralin}}{M_{tetralin}} + \frac{A_{cis-decalin}}{M_{cis-decalin}} + \frac{A_{trans-decalin}}{M_{trans-decalin}}} \tag{5.1}$$

Here X is the conversion of naphthalene, A_i are the peak areas, and M_i are the molecular weights. Only very small amounts of the secondary products, cis- and trans-decalin, were seen in the product.

Table 5.4 shows the conversion in one of the reactors at three different run hours. The conversion is decreasing slightly with time, but the variation is so small, that it is assumed that a steady state has been reached.

Since a very small amount of catalyst was used in the experiments, it was tested whether any reaction took place in the absence of any catalytic material. With no catalyst in the reactor,

Table 5.4: Naphthalene conversion at different run hours, for size fraction F ($\sim 1450\ \mu m$). ($WHSV = 56\ hr^{-1}$, $T = 340\ ^{\circ}C$, $P = 30\ bar$ and $H_2/oil = 250\ Nl/l$)

Run Hour	Conversion
20	0.711
21	0.709
22	0.706

the naphthalene conversion was less than 2 %, which is so low, that it can be neglected.

5.4 Results

The conversion of naphthalene has been determined from the GC analysis. Since the effective diffusion coefficient for hydrogen is more than 3 times higher than for naphthalene, and since hydrogen is present in surplus, it is most likely, that naphthalene is the limiting reactant. A useful way of interpreting the results is by calculating pseudo first order rate constants using the naphthalene conversion, and thereby neglecting the hydrogen dependency, and any reactant / product inhibition of the reaction rate.

5.4.1 Kinetic analysis

Using the inverse of the Weight Hourly Space Velocity (WHSV) as a reaction time, the following differential equation can be used to describe the naphthalene concentration

$$\frac{dC_{nap}}{d\tau} = r_{nap} = -k_1 \cdot C_{nap} \tag{5.2}$$

Here τ is equal to $WHSV^{-1}$. Introducing the conversion of naphthalene, $X = 1 - \frac{C_{nap}}{C_{nap0}}$, the equation can be written as:

$$C_{nap0}\frac{dX}{d\tau} = k_1 \cdot C_{nap0} \cdot (1 - X) \tag{5.3}$$

C_{nap0} is the feed concentration of naphthalene. A first order rate constant can be calculated by solving the differential equation:

$$k_1 = -\ln(1 - X) \cdot WHSV \tag{5.4}$$

$X = 1 - \frac{C_{nap}}{C_{nap0}}$ is the naphthalene conversion. It is well-known, that hydrogenation reactions are limited by thermodynamic equilibrium at typical hydrotreating conditions. Since the reaction is exothermic the equilibrium is shifted towards the di-aromatic as the temperature increases. When the reaction approaches equilibrium, the rate will decrease and eventually

become zero. The irreversible first order rate expression, will not be suitable to describe the kinetics when the equilibrium becomes important. A simple way of accounting for the equilibrium is to assume that the forward reaction rate is first order in the naphthalene concentration while the backwards rate is first order in the tetralin concentration:

$$-r_{nap} = k_{1f} \cdot C_{nap} - k_{1b} \cdot C_{tet} \tag{5.5}$$

In terms of the conversion, X, the rate expression becomes:

$$-r_{nap} = k_{1f} \cdot C_{nap0} \cdot (1 - X) - k_{1b} \cdot C_{nap0} \cdot X \tag{5.6}$$

At equilibrium, the reaction rate is equal to 0, and the equilibrium ratio between tetralin and naphthalene is given by:

$$K_{ratio} = \frac{C_{tet,eq}}{C_{nap,eq}} = \frac{k_{1f}}{k_{1b}} \tag{5.7}$$

Introducing the equilibrium conversion, $X_{eq} = \frac{K_{ratio}}{1+K_{ratio}}$, the rate can be expressed as:

$$-r_{NAP} = k_{1f} C_{NAP0} \cdot \left(1 - \frac{X}{X_{eq}}\right) \tag{5.8}$$

From this equation, the rate constant for the forward reaction can be calculated as:

$$k_{1f} = -\ln\left(1 - \frac{X}{X_{eq}}\right) \cdot X_{eq} \cdot WHSV \tag{5.9}$$

For an irreversible first order reaction the equilibrium conversion becomes equal to 1, and k_{1f} reduces to k_1.

5.4.2 Calculation of equilibrium conversion

In order to be able to calculate the forward rate constant, it is necessary to know the equilibrium conversion, and thereby the equilibrium ratio between tetralin and naphthalene. The equilibrium constant for the hydrogenation of naphthalene to tetralin in the gas phase is given by [28]:

$$K_p = \frac{moles\ tetralin}{moles\ naphthalene \cdot f_{H_2}^2} \tag{5.10}$$

At the experimental conditions used in this work, 2 fluid phases can exist, and it is most

likely that the reaction is taking place in the liquid filled pores of the catalyst. Assuming that the equilibrium ratio between tetralin and naphthalene will be the same in the liquid phase as in the gas phase, and that the fugacity of hydrogen is equal to the partial pressure, K_{ratio} can be calculated as:

$$K_{ratio} = K_p \cdot f_{H_2}^2 = K_p \cdot p_{H_2}^2 \tag{5.11}$$

The partial pressure of H_2 is obtained from phase equilibrium calculations based on the total composition in the inlet using an equation of state (SRK), and is assumed to be constant. The equilibrium constant K_p in atm^{-2} is a function of temperature, and can be calculated as follows using equation (3.1) and parameters from table 3.2:

$$\log(K_p) = \frac{6460}{T} - 12.28 \tag{5.12}$$

Since tetralin does not react to form decalin under the investigated conditions, the ratio between tetralin and naphthalene is related to the conversion as follows:

$$\frac{moles\ tetralin}{moles\ naphthalene} = \frac{X}{1-X} \tag{5.13}$$

At equilibrium $K_{ratio} = \frac{moles\ tetralin}{moles\ naphthalene}$ and the equilibrium conversion is then given by:

$$K_{ratio} = \frac{X_{eq}}{1-X_{eq}} \Leftrightarrow \tag{5.14}$$

$$X_{eq} = \frac{K_{ratio}}{1+K_{ratio}} \tag{5.15}$$

Table 5.5 shows values of the equilibrium constant, and the equilibrium conversion at different temperatures. The equilibrium conversion is decreasing with increasing temperature. It can be seen in the table, that the partial pressure of hydrogen is decreasing with increasing temperature. This is because a larger part of the liquid is vaporized at high temperatures as can be seen from the value of the vapor fraction. At the highest temperature, 360 °C, only one phase is present at equilibrium, although due to capillary pressure the pores of the catalyst are most likely filled with liquid.

5.4.3 Apparent rate constants

Figure 5.2 show the calculated rate constant for one catalyst size fraction in one reactor. The rate constant increases with temperature from 300 to 340 °C, but decreases again when increasing the temperature to 360 °C. This is because the reaction is limited by thermodynamic equilibrium, and since the reaction is exothermic the equilibrium conversion decreases with

Table 5.5: Equilibrium properties for the reaction mixture at different temperatures

T [°C]	K_p $[atm^{-2}]$	Vapor fraction	P_{H_2} [atm]	K_{ratio}	X_{eq}
300	0.098	0.82	26.3	67.9	0.985
320	0.041	0.87	24.8	25.1	0.962
340	0.018	0.96	22.7	9.3	0.903
360	0.008	1.00	21.9	4.0	0.801

increasing temperature, leading to a lower reaction rate.

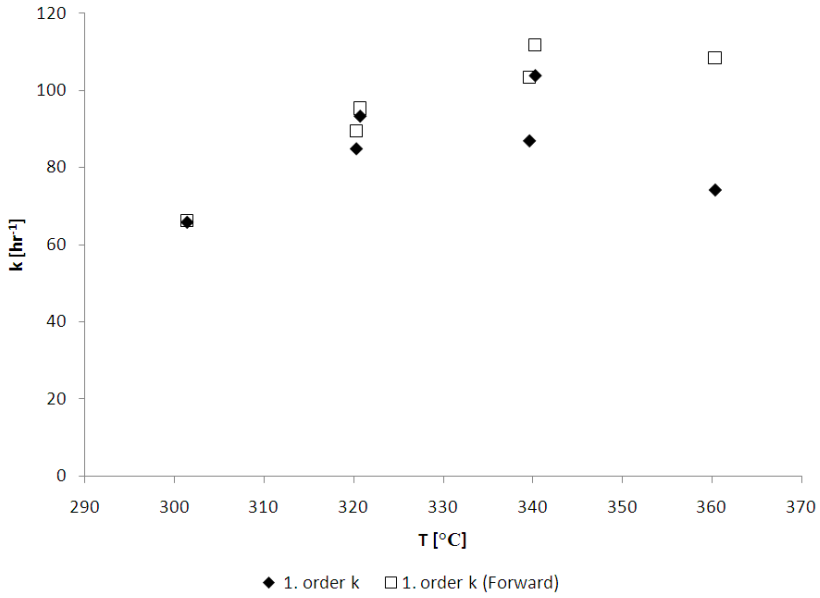

Figure 5.2: Effect of temperature on the pseudo first order rate constants for the 600-850 μm fraction

Figure 5.2 also shows, pseudo first order rate constants that have been corrected to take the equilibrium into account. In this case, it is the first order rate constant, for the forward reaction only that is plotted. At the lowest temperatures, the difference is not significant, but as the temperature increases the difference becomes more and more pronounced. There is still a decrease in the rate constant between 340 and 360 °C, which suggests that close to equilibrium, the reversible first order rate expression is not able to describe the effect of the equilibrium completely.

5.4.4 Evaluation of the experimental uncertainty

Two reactor tubes in each oven were loaded with the same amount of the same catalyst size fraction, to provide an estimate of the experimental uncertainty. Table 5.6 shows the comparison of the repeated experiments at one experimental condition (1), with respect to the conversion, pseudo first order rate constant and the first order rate constant corrected for thermodynamic equilibrium. At all the conditions (1-4), the difference is largest for the 850-1000 μm fraction, which has deviations between 22 and 29 % for the corrected rate constant. It appears to be

a systematic error, as the difference in conversion is practically the same at all conditions. It should be noted, that the differences in the rate constants are quite high, and if this is the typical magnitude of the error it is difficult to make any conclusions based on this experiment.

The differences between the repetitions of the 150-212 μm fraction are significantly smaller, giving an estimated error of less than 10 % in the rate constant corrected for equilibrium. The deviation between the two measurement for this fraction is in the range of what is typically observed using the experimental set-up.

Table 5.6: Estimation of experimental errors in the experiment at condition (1). ($T = 340\ ^\circ C$, $P = 30\ bar$ and $H_2/oil = 250\ Nl/l$)

Size fraction	$WHSV$	X	k_1	k_{1f} *(eq.)*
150-212 μm (1)	61.3	0.854	117.7	160.8
150-212 μm (2)	56.0	0.875	116.3	175.0
Average	58.6	0.864	117.0	167.9
Relative difference (%)	9.0	2.427	1.2	8.5
850-1000 μm (1)	55.9	0.731	73.5	83.8
850-1000 μm (2)	56.1	0.805	91.5	112.2
Average	56.0	0.768	82.5	98.0
Relative difference (%)	0.2	9.558	21.8	29.0

The cause of the systematic errors leading to similar differences at all conditions might be related to the catalyst: As the amount of catalyst in all cases is quite small, the conversion can be quite sensitive to errors in the determined mass. The crushed catalyst pellets were quite static, which might have led to the loss of some of the catalyst. This was especially a problem for the smallest fractions. Also if part of the catalyst is bypassed it can have a large influence on the conversion. The packing of the catalyst, and mixing with the dilution material may also have had an influence on the conversion.

Also, systematic differences in the gas and liquid flows in the different reactor tubes might lead to the differences in the conversion.

5.4.5 Effect of flow rate

If external mass transfer has an influence on the rate, the observed rate should change with the liquid velocity, even if the ratio between the feed flow rate and the catalyst mass is kept constant. Two different flow rates have been tested, and the comparison between the two is shown in figure 5.3. If external mass transfer were governing the rate, the rate would increase with increasing flow rate. According to the correlation for the gas-liquid mass transfer coefficient suggested by Goto and Smith [29], the mass transfer constant is proportional to the liquid flow rate to the power of 0.4. Similar the liquid-solid mass transfer coefficient depends on the liquid flow rate to the power of 0.5 according to the van Krevelen-Krekels equation [30]. If external mass transfer were rate controlling this would mean that doubling the flow rate should increase the rate by approximately 30-40 %. From figure 5.3 there is no obvious trend when changing the flow rate. For the two largest particle sizes, there is close to 30 % increase in the observed

rate constant, in going from the low to the high flow, but for the smaller particles there is no clear trend, and the difference is more likely to be due to experimental uncertainties.

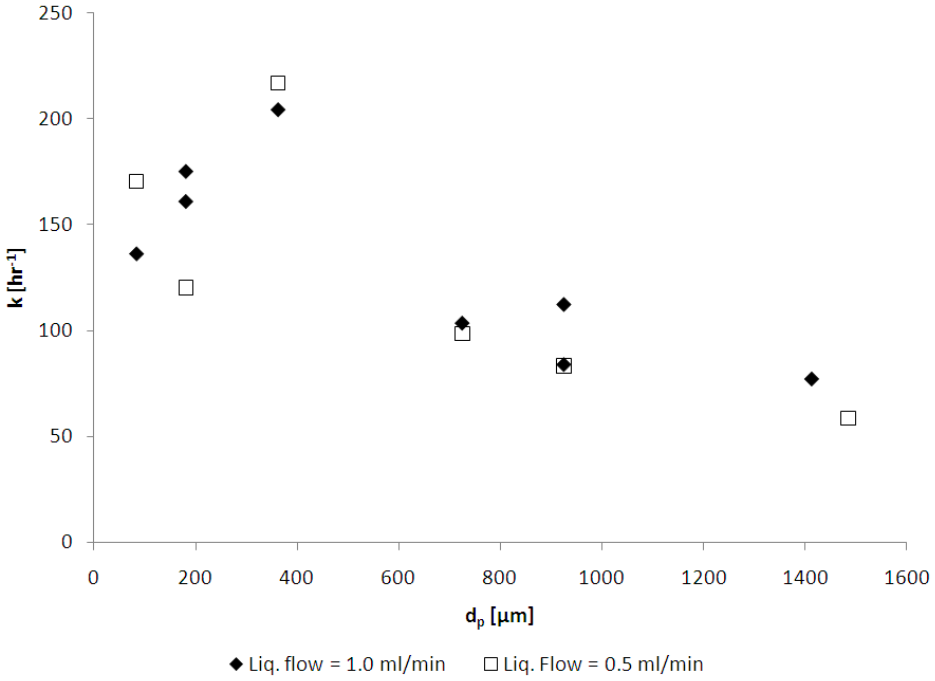

Figure 5.3: Effect of flow rate on the rate constant at constant $WHSV \sim 56hr^{-1}$. ($T = 340\ ^{\circ}C$, $P = 30\ bar$ and $H_2/oil = 250\ Nl/l$)

5.4.6 Effect of particle size

Figure 5.4 shows the average estimated rate constants for the different size fractions at all the investigated temperatures. In spite of the large uncertainties there appear to be some general trends. The largest particles yield the smallest rate constant at all conditions, and the rate appears to increase with decreasing particle size for the largest size fractions. This is a strong indication that the rate is limited by either internal or external mass transfer. At all conditions the largest rate constant is obtained for the 300-425 μm fraction. There is no obvious explanation for the decrease in rate when going below the 300-425 μm fraction. Decreasing the particle size will increase the external mass transfer rate, and limit the internal diffusion resistance. Therefore one would expect that the rate constant approached an asymptotic value, corresponding to an intrinsic rate constant, at these small particle sizes. Also a slightly higher rate is observed for the 63-105 μm fraction than the 150-212 μm fraction.

At 300 and 320 °C, the effect of correcting for the equilibrium is relatively small, whereas at 340 and 360 °C, it becomes significant. The difference between the irreversible / reversible rate constants is largest for the smallest particle fractions. This is because, the conversions are higher and therefore closer to equilibrium for the smallest particle sizes.

One way of determining whether external or internal diffusion resistance is rate limiting is investigating how much the rate constant changes with the particle size. Assuming that the

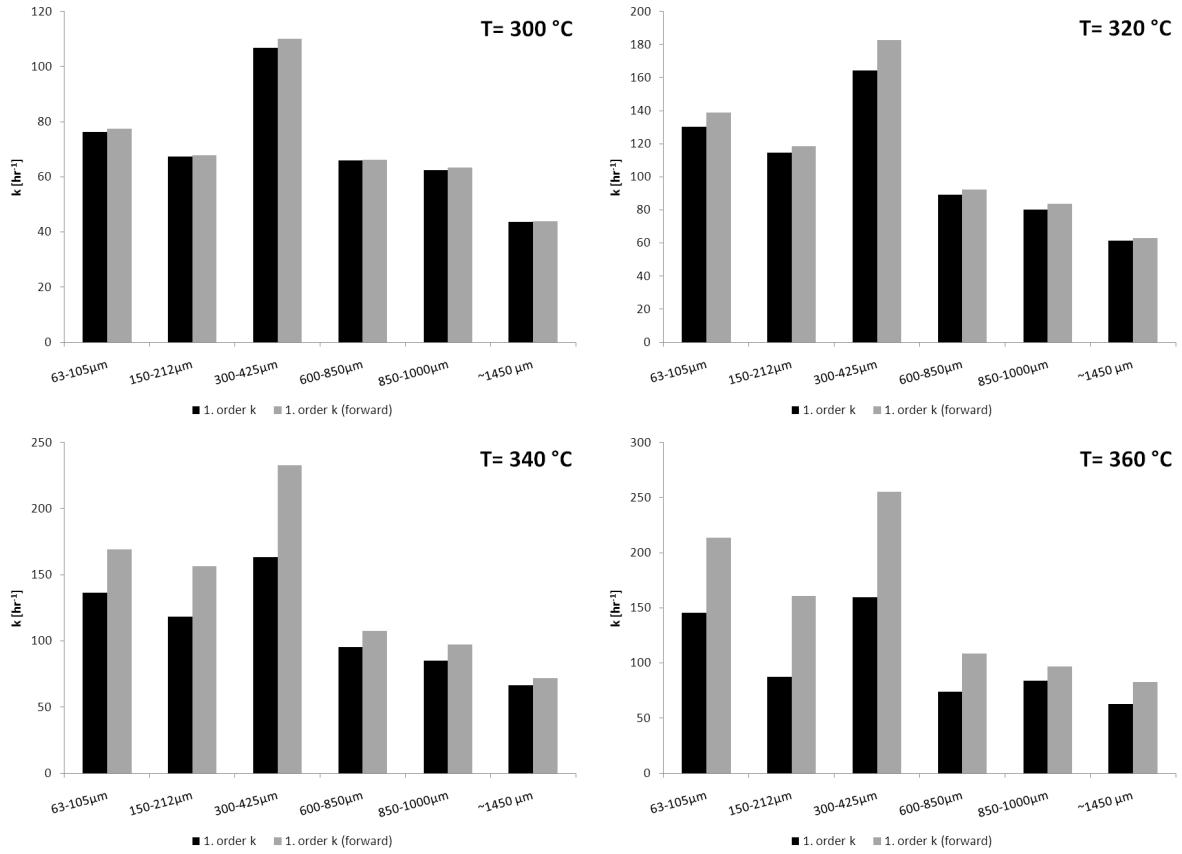

Figure 5.4: Effect of particle size, on the average apparent first order rate constants . ($P = 30barg$, $H_2/oil = 250Nl/l$ and $WHSV = 50 - 100\ hr^{-1}$)

liquid-solid mass transfer coefficient can be calculated from the van Krevelen-Krekels equation [30], it is proportional to the square root of the particle diameter. If external mass transfer is determining the rate, this means, a log-log plot of the rate constant as function of the particle diameter would yield a straight line with a slope equal to -1.5. If the rate is strongly limited by internal diffusion, the observed rate constant will be proportional to the inverse of the particle size, and a log-log plot of the rate constant as function of the particle diameter would yield a straight line with a slope equal to -1 [31].

Figure 5.5 shows the logarithm of the rate constant as function of the logarithm of the particle diameter at 340 °C. The slopes are in the range between -0.85 and -0.60. This suggests that external mass transfer does not play a major role, since the slopes are far from -1.5. It is more likely that the internal diffusion has an influence on the observed rate, although the slope shows deviations from -1. This might indicate, that the diffusion resistance is not strong enough, for the rate to follow the asymptotic behavior. It might also be due to experimental uncertainties.

5.4.6.1 Estimation of effectiveness factors

The effectiveness factor, η, for a catalytic reaction is defined as follows:

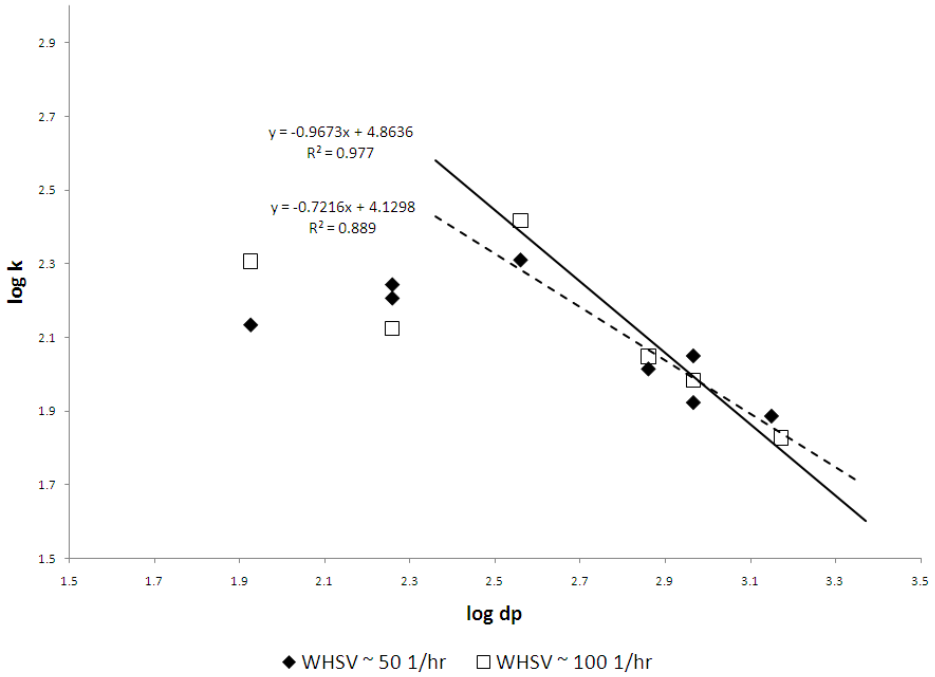

Figure 5.5: Log-log plot of the first order rate constant as function of the particles size. ($T = 340\ °C$, $P = 30\ bar$ and $H_2/oil = 250\ Nl/l$)

$$\eta = \frac{actual\ reaction\ rate}{reaction\ rate\ at\ surface\ conditions} \tag{5.16}$$

The experiments have shown, that the actual, or observed, reaction rate is a function of the size of the particles. In order to estimate the effectiveness factors, it will be assumed that the reaction rate is described by a first order rate expression. For a first order reaction, there is the following relation between the observed rate constant, and the rate constant in absence of any diffusion limitations, the intrinsic rate constant:

$$k_{obs} = \eta \cdot k_{int} \tag{5.17}$$

Here k_{obs} is the observed rate and k_{int} is the intrinsic rate constant for calculating the rate per volume of catalyst. The effectiveness factor is a function of the Thiele Modulus, which is defined as follows for a first order reaction in a spherical catalyst particle:

$$\phi = R_p \cdot \sqrt{\frac{k_{int}}{D_e}} \tag{5.18}$$

R_p is the radius of the catalyst particle and D_e is the effective diffusion coefficient for the reactant. For a reversible first order reaction the Thiele modulus can be calculated as follows,

assuming that reactant and product have the same diffusion coefficient:

$$\phi = R_p \cdot \sqrt{\frac{k_{int}}{D_e}\frac{1+K_{ratio}}{K_{ratio}}} = R_p \cdot \sqrt{\frac{k_{int}}{D_e \cdot X_{eq}}} \tag{5.19}$$

From the Thiele modulus, the effectiveness factor can be calculated as follows:

$$\eta = \frac{3}{\phi}\left[\frac{1}{\tanh\phi} - \frac{1}{\phi}\right] \tag{5.20}$$

For very small particles, the Thiele modulus approaches 0, and the effectiveness factor asymptotically approaches 1. Figure 5.4, shows, that the experimental rate constants, does not seem to approach a constant value for the smallest particle size fractions, and therefore the value of the intrinsic rate constant is not obvious. Instead it is possible to calculate an effectiveness factor, for each experimental point, iteratively from equation 5.20 and 5.18 by setting $k_{int} = k_{obs}/\eta$.

The rate constants in figure 5.4 are calculated based on the weight hourly space velocity, and not an actual residence time. Therefore the rate constants cannot be used directly in the calculation of the Thiele modulus. k_{int} should be based on the volume of the catalyst, and the volumetric flow rate of the liquid, and can be calculated as follows:

$$k_{int} = \frac{k_{1f}}{\eta} \cdot \frac{\rho_p}{\rho_L} \tag{5.21}$$

Here ρ_p is the density of the catalyst particle and ρ_L is the density of the liquid, at the reactor temperature. In this calculation, any vaporization of the liquid feed, is neglected. Phase equilibrium calculations based on the composition of the feed mixture, show that a significant part of the solvent and reactant, will be present in the gas phase at equilibrium, especially at the highest temperatures. The liquid densities are calculated using the equation suggested by Rackett [32], assuming it is pure n-tetradecane:

$$v_L = v_c \cdot Z_c^{[1-T_r]^{2/7}} = \left(\frac{RT_c}{P_c}\right) Z_c^{[1+(1-T_r)^{2/7}]} \tag{5.22}$$

Here v_L is the liquid molar volume and T_r is the reduced temperature. Table 5.7 lists estimated effective diffusion coefficients and liquid densities, $\rho_L = M_{n-tetradecane}/v_L$, at the different temperatures used in the experiments.

Using the estimated parameters, the effectiveness factors have been calculated. Figure 5.6 shows η as function of the particle size and it can be seen that, the effectiveness factors lies in a range between 0.5 and 1. The plot shows, that for the 2 smallest fractions, the internal diffusion resistance is absent with effectiveness factors above 0.99, but for particles above 300-425 μm the diffusion resistance is not negligible. On average, the effectiveness factors are decreasing slightly

Table 5.7: Effective diffusion coefficients and liquid densities of n-C14, at different temperatures

Temperature [°C]	D_e $[10^9 m^2/s]$	ρ_L $[kg/m^3]$
300	3.05	516
320	3.36	494
340	3.67	470
360	4.00	443

with increasing temperature from 300 °C to 340 °C, which is due to the higher rate constant. There is no significant difference between the effectiveness factor at 340 °C and 360 °C, which is probably because the effect of the thermodynamic equilibrium is not fully captured.

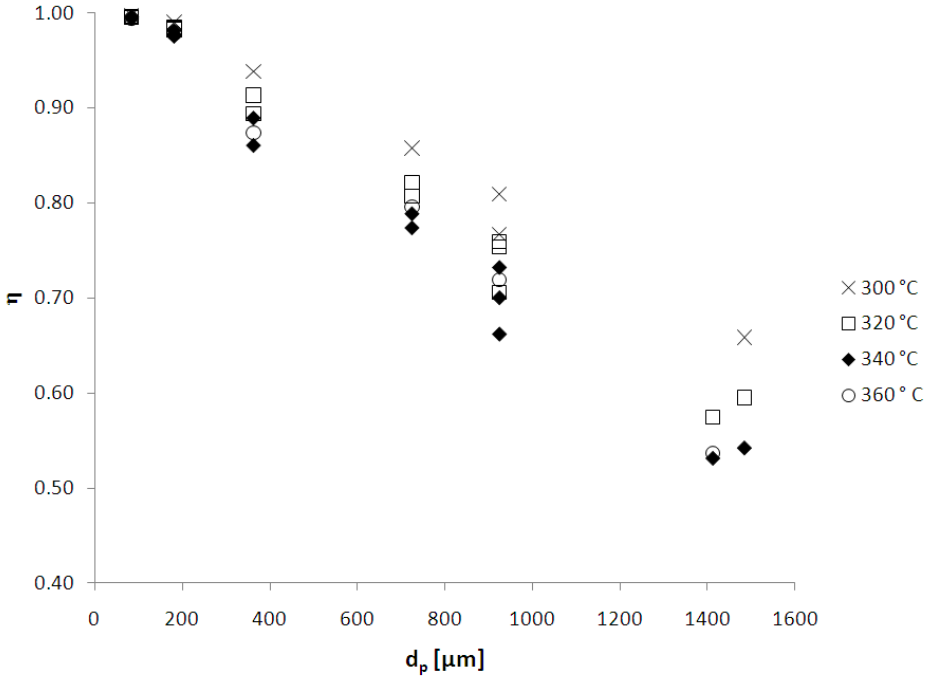

Figure 5.6: Estimated effectiveness factors as function of the average particle diameter. The effectiveness factor is calculated for each experimental point, assuming it follows 1. order kinetics

Knowing the effectiveness factors it is possible to calculate intrinsic rate constants, or rate constants in the absence of diffusion limitations, at all the investigated particle sizes, and comparing them. Figure 5.7 shows a plot of $k_{1,eq}/\eta$ as function of the particle size at 340 °C. There is some scattering in the values, but what should be noted, is that for the 300-425 μm fraction (average diameter of 362.5 μm) the rate constants lies above all the other rate constants. If this size is not considered, all other rate constants have values between 114 and 203 hr^{-1}. The rate constants for the particles with the average diameter of 362.5 μm has the values 223 and 301 μm. Since the rate constants, for all other sizes are relatively similar, this could indicate, that the maximum observed in the apparent rate constants for this size in figure 5.4, is due to an experimental error rather than a true maximum in the observed reaction rate for this size.

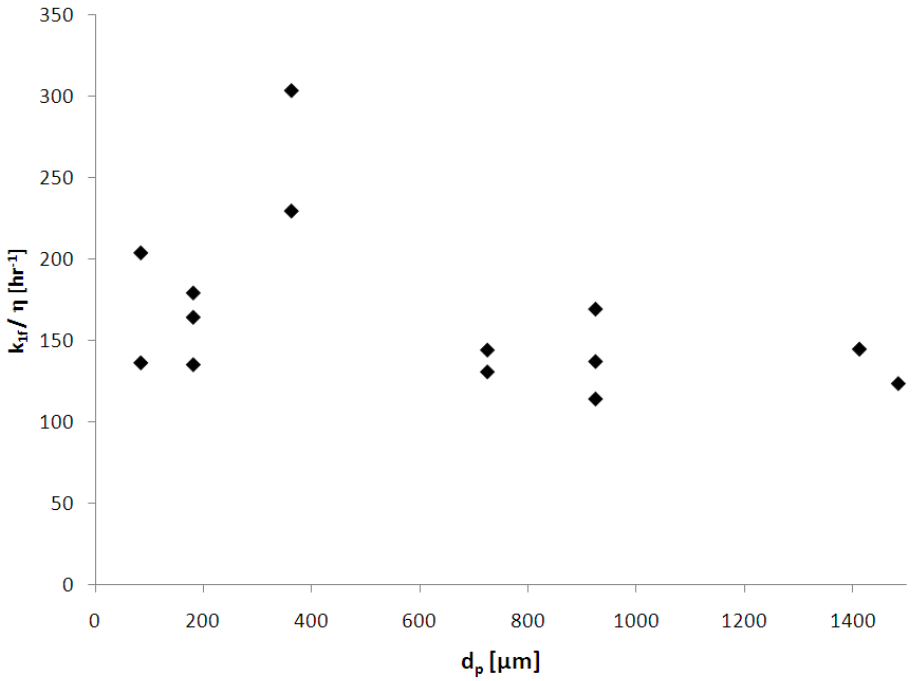

Figure 5.7: Estimated values for an intrinsic first order rate constant as function of the average particle diameter at 340 °C

5.4.7 Effect of temperature

5.4.7.1 Internal temperature gradient

The experiments show a maximum in the rate as function of the particle size. Since the reaction is exothermic with a reaction enthalpy equal to 124.68 kJ/mol [28], it is theoretically possible that the maximum is due to an internal temperature gradient, that results in effectiveness factors larger than 1 as illustrated by Weisz and Hicks [33]. According to Weisz and Hicks [33] this is unlikely to be significant for a liquid phase reaction, but as a test, the maximum temperature rise within the catalyst pellet can be estimated as follows:

$$\beta = \frac{T_{max} - T_s}{T_s} = \frac{C_s \cdot (-\Delta H_r) \cdot D_e}{\lambda \cdot T_s} \tag{5.23}$$

Table 5.8: Parameters used to estimate effect of internal temperature gradients at 340 °C.

C_s [mol/m^3]	38.2
ΔH_r [kJ/mol] from [28]	124.68
λ [J/s/m] from [34]	$1.39 \cdot 10^{-2}$
D_e [m^2/s]	$3.67 \cdot 10^{-9}$

As illustrated in figure 5.4 there is a maximum in the rate constants for the 300-425 μm particle size fraction at all temperatures. 340 °C is used as an example, and using the parameters

given in table 5.8, β becomes:

$$\beta = \frac{38.2\frac{mol}{m^3} \cdot 124.68 \cdot 10^3 \frac{J}{mol} \cdot 3.67 \cdot 10^{-9} \frac{m^2}{s}}{1.39 \cdot 10^{-2} \frac{J}{s \cdot m} \cdot 613.15K} = 2.1 \cdot 10^{-3} \tag{5.24}$$

This value of β correspond to a maximum temperature rise of 1.26 °C. This value indicates, that internal heat transfer effects does not play a major role, and it is highly unlikely, that this is the reason for the observed maximum in the reaction rate. Furthermore as pointed out by Carberry, the effect of an increase in temperature on the rate constant in the pellet, will to some degree be counter-balanced by a decrease in the equilibrium constant [35].

5.4.7.2 Effect of particle size on activation energy

The catalyst pellets have been tested at four different temperatures, 300, 320, 340 and 360 °C. As illustrated in figure 5.4, the limitations due to the reaction equilibrium are not significant at 300 and 320 °C. Therefore the results from these two temperatures have been used to estimate activation energies.

For a reaction that is strongly diffusion limited, the activation energy will be approximately equal to half of the true activation energy [34]. In the transition range when going from an effectiveness factor close to 1 and to a strongly limited reaction, the activation energy will change as a function of the particle size. Figure 5.8 shows the activation energy as a function of the particle size. The figure shows a clear trend in that the activation is decreasing from above 60 kJ/mol to just below 40 kJ/mol. This shows, that the reaction is limited by internal diffusion, but not to such a degree, that the activation energy has become equal to half of the true value.

According to Froment and Bischoff an activation energy on the order of 21-42 kJ/mol is an indication of strong diffusion resistance [30]. This is similar to the values obtained for the largest particles.

According to Cooper and Donnis, a typical observed activation energy for hydrogenation of the first ring in diaromatics lies between 105 and 115 kJ/mol [15]. Chu and Wang [36] defined a rate constant as, $k_1 = -\ln\left(1 - \frac{X}{X_{eq}}\right) \cdot WHSV$, and found an activation energy of 109 kJ/mol for naphthalene hydrogenation on a CoMo catalyst at 35 atm and a H_2 feed ratio of 6 mol/mol and temperatures between 270 °C and 320 °C. The activation energy found in this work, is considerably lower than these reported values even for the smallest of the catalyst size fractions.

5.5 Conclusion

This experimental investigation of the effect of catalyst particle size on the hydrogenation of naphthalene at industrial hydrotreating conditions, has shown that internal diffusion is limiting the overall reaction rate. The conversion of naphthalene, and therefore the reaction rate, clearly depends on the size of the catalysts particles, but there is no indication that external (gas-liquid

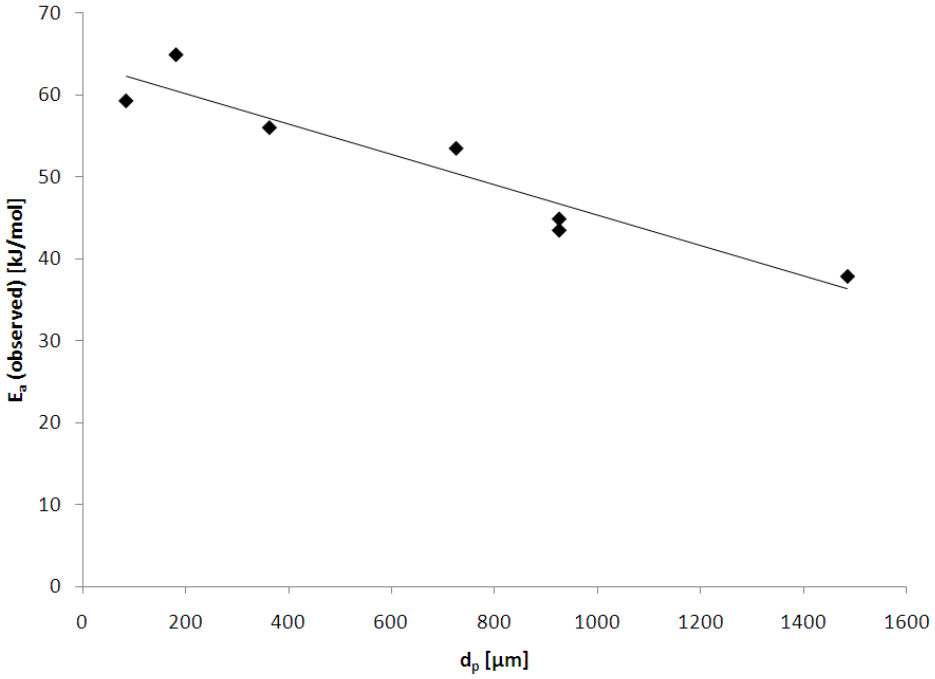

Figure 5.8: Activation energies calculated based on observed rate constants, at 300 and 320 °C. as function of the average particle diameter. ($P = 30\ barg$, $H_2/oil = 250 Nl/l$ and $WHSV = 50-100\ hr^{-1}$)

or liquid-solid) mass transfer is rate limiting. This shows, that the difference must be due to internal diffusion resistance.

The fact that two fluid phases possibly exists at equilibrium, and that the reaction is limited by thermodynamic equilibrium makes estimation of the effectiveness factors difficult. It appears to be a reasonable assumption, that the rate can be described by a reversible first order rate expression. Using this expression effectiveness factors have been calculated, and the values vary between approximately 0.5 for the largest particles and 1 for the smallest particles, at the investigated conditions. These values show, that internal diffusion has an effect on the rate, but the reaction is not strongly limited by diffusion.

As the conditions used in this work are close to those of industrial hydrotreaters, the calculated effectiveness factors should correspond to typical values in industrial units. One important factor that has not been accounted for is the hydrogen concentration. Since naphthalene was the limiting reactant, and also has a lower diffusivity, it is reasonable to neglect the hydrogen concentration as a factor. But in industrial ULSD units, the concentration of di- and polyaromatics will typically be higher than in this work, and hydrogen could then become the limiting reactant in the top of the reactor.

Chapter 6

Experimental Investigation of the Effect of Nitrogen Compounds on Hydrodesulfurization Reactions

In this chapter results are presented from an experimental investigation of the effect of different nitrogen compounds (acridine, 1,4-dimethylcarbazole and 3-methylindole), on the hydrodesulfurization of a real feed and of 4,6-dimethyldibenzothiophene.

6.1 Introduction

In deep desulfurization the sulfur content of diesel oil is reduced to 10-15 ppm [37], and it is well-known that certain nitrogen compounds act as inhibitors for the hydrodesulfurization (HDS) reaction [38, 39]. Understanding the inhibition mechanism and the effect of different types of nitrogen compounds is important in predicting feedstock reactivity, optimizing the hydrotreating process and in the development of higher activity catalysts. The average crude oil is getting heavier, which means that the sulfur and nitrogen content increases [40], with a greater need for optimizing the hydrotreating process and developing more active catalysts.

Among the most refractive sulfur compounds are dibenzothiophenes with side groups in the 4 and 6 position. 4,6-dimethyldibenzothiophene is thus a suitable model compound to get a better understanding of the kinetics of sulfur removal at high sulfur conversions of gas oils. The reason for the lower reactivity is believed to be sterical hindrance, which limits the direct sulfur removal [8, 9]. The sulfur compounds present in diesel feeds are mainly thiophenic compounds. The reactivity of the compounds depends on the size of the molecule, and the position of side groups.

Typical catalysts used for hydrotreating are sulfided CoMo or NiMo, and dibenzothiophenes are known to react through two parallel reaction routes as illustrated in figure 6.1. Dibenzothiophene without substituents adjacent to the sulfur atom (in the 4 and / or 6 position) prefers the direct desulfurization (DDS) route, while both the DDS and the pre-hydrogenation (HYD) route are important for the sterically hindered dibenzothiophenes [41]. In general a CoMo cat-

alyst has a higher activity for the DDS route, while a NiMo catalyst has a higher activity for the HYD route due to its higher hydrogenation activity [9, 41].

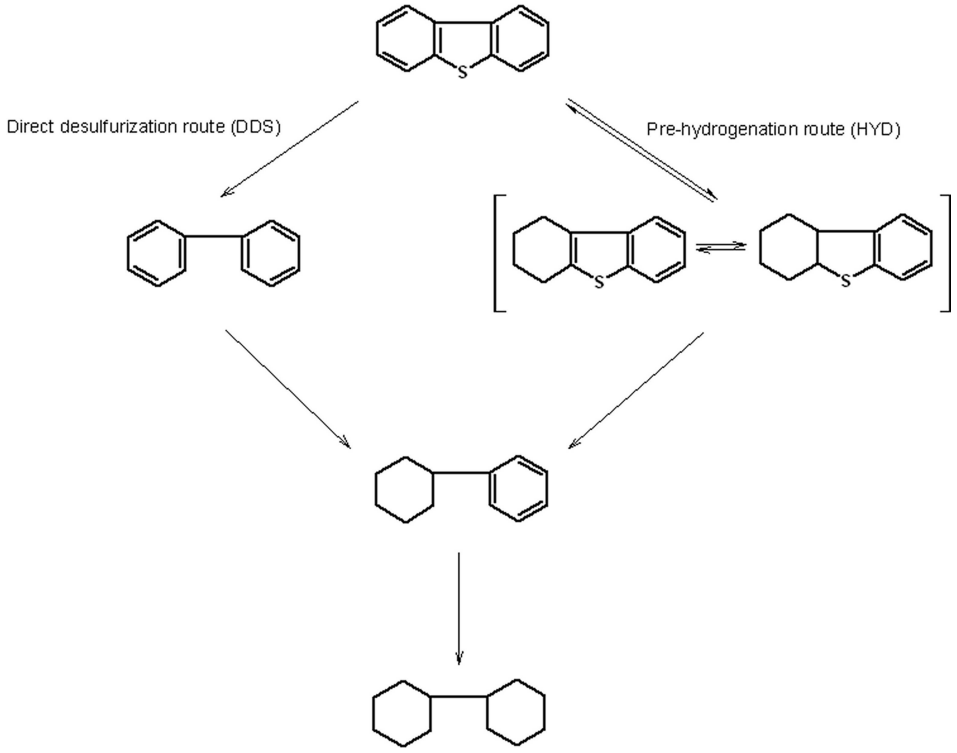

Figure 6.1: Parallel reaction pathways for hydrodesulfurization of dibenzothiophenes

Diesel oil consists of mixtures of hydrotreated straight run distillates and various hydrocracked products of heavier fractions. The nitrogen compounds present in the diesel feeds can be divided into different chemical classes: aliphatic amines, anilines and 2 types of heterocyclic aromatic compounds: five-membered pyrrolic and six-membered pyridinic ring systems. The pyrrolic heterocycles are components such as indoles and carbazoles, while quinolines and acridines are typical pyridinic species [16]. The nitrogen compounds are categorized as either basic or non-basic. In the non-basic heterocyclic nitrogen compounds, the lone-pair on the nitrogen atom is delocalized in the aromatic ring, and is not available for donation, while the opposite is the case for the basic heterocycles [17]. Aliphatic amines, anilines and pyridinic compounds belong to the family of basic nitrogen compounds while the pyrrolic compounds are non-basic [16].

Most of the nitrogen compounds in diesel feedstocks are non-basic. The typical nitrogen content of a straight run gas oil (SRGO) is approximately 30-1000 ppm, and the non-basic compounds such as indoles and carbazoles normally account for two thirds of the nitrogen compounds, while the basic compounds account for the remaining one third. The nitrogen content of light cycle oil (LCO) is higher than in SRGO, typically 500-2500 ppm, and consists mainly of indoles and carbazoles with only a small amount ($\sim$ 10 %) of basic compounds.

Specific basic N-containing compounds are considered to be among the strongest inhibitors for HDS reactions. It has been suggested that Brønsted acid sites (-SH or -OH groups) play a

role in the hydrogenation reaction mechanism on sulfided CoMo and NiMo catalysts, which can explain why especially basic nitrogen compounds are found to be strong inhibitors. Nagai et al. [42] and La Vopa and Satterfield [43] have correlated the adsorption constants of different nitrogen compounds with their gas phase basicities / proton affinities. A good correlation is found, which suggests that the nitrogen compounds adsorb on Brønsted acid sites. However nitrogen compounds with substituents close to the nitrogen atom shows large deviations from the correlation, since the observed adsorption constant is lower than the correlation suggests [42, 43]. Similarly Beltramone et al. find a good correlation between the adsorption constant of a series of nitrogen species originating from quinoline and indole, and calculated Mulliken charges on the nitrogen atom [44].

Sun et al. [45] have performed DFT calculations and estimated the adsorption energies of quinoline, acridine, indole and carbazole on the surface of a NiMoS catalyst. They find that it is energetically more favorable for the basic nitrogen compounds to interact with the surface through the lone pair on the nitrogen atom, while the non-basic compounds interact through the π electrons on the carbon atoms. They find that the adsorption energy of the basic compounds are higher, which can explain the stronger inhibition.

A combination of DFT calculations and STM studies has led to the discovery of the so-called brim sites which are located next to the edge of the catalyst crystals [22]. These sites have been shown to play an important role in hydrogenation reactions. Logadottir et al. [46] have investigated the inhibition effect of benzene, pyridine and H_2S on the HYD pathway on an unpromoted MoS_2 catalyst by estimating adsorption energies through DFT calculations. The brim sites are located next to the Mo-edge of the MoS_2 crystal, and it was found that H_2S adsorption on this edge was weak, which explains the weak effect of H_2S on the HYD pathway. The adsorption of pyridine was found to be much stronger than for benzene due to protonation to form a pyridinium ion. This explains the strong inhibition effect of basic nitrogen compounds, and why the inhibition effect can be correlated to the gas phase basicities / proton affinities. The inhibition of the nitrogen compound is not only due to blocking of the brim sites, but also due to the reaction with a Brøndsted acid site thereby reducing the number of -SH groups available for hydrogenation [46].

Several authors have investigated the effect of different nitrogen compounds on the HDS of 4,6-dimethyldibenzothiophene [18, 44, 47–51]. When investigating the effect of inhibitors, it is preferable to use continuous reactors for the experiments as opposed to batch reactors. In continuous reactors, and therefore also industrial reactors, it is expected that the catalyst surface coverage of strong inhibitors is high at steady state (or equilibrium). This high coverage can only by achieved when the catalyst has been exposed to a large amount of nitrogen compounds. Because of the nature of the batch reactor, the concentrations are changing in time, and the amount of the inhibitors that the catalyst is exposed to is less than in a continuous reactor, so the use of such a reactor might lead to erroneous conclusions.

Rabarihoela-Rakotovao et al. [18, 47] investigated the effect of acridine and its main hydrogenation product, 1,2,3,4,5,6,7,8-octahydroacridine, and 1,4-dimethylcarbazole on the HDS of 4,6-dimethyldibenzothiophene on a sulfided $NiMoP/Al_2O_3$ catalyst in a fixed bed microflowreac-

tor. It was found that acridine strongly inhibited the sulfur removal through both the DDS and the HYD pathway, even at low concentrations. The effect of acridine and its hydrogenation product on the HYD route was more pronounced than on the DDS route. For 1,4-dimethylcarbazole they found that it had a similar effect on both of the two reaction routes. In a competitive experiment, they found that acridine was a strong inhibitor for the HDN of 1,4-dimethylcarbazole. At typical hydrotreating conditions acridine is easily hydrogenated, and the main hydrogenation product is 1,2,3,4,5,6,7,8-octahydroacridine. It was found that this compound had a very similar inhibition effect on the HDS of 4,6-dimethyldibenzothiophene as acridine. This suggests that the parent compound is not necessarily the main contributor to the inhibition.

Kwak et al. [48] have investigated the effect of carbazole and quinoline on the HDS of dibenzothiophene, 4-methyldibenzothiophene and 4,6-dimethyldibenzothiophene on sulfided $CoMo/Al_2O_3$ in a slurry tank batch reactor. They found that the basic quinoline is a stronger inhibitor than the non-basic carbazole. The HDS of 4-methyldibenzothiophene and 4,6-dimethyldibenzothiophene is significantly inhibited at small nitrogen concentrations, where the effect on the HDS of dibenzothiophene is negligible. The HDS of dibenzothiophene is also inhibited when the nitrogen compounds are present in much larger quantities. It is found that for 4-methyldibenzothiophene and 4,6-dimethyldibenzothiophene the DDS route is suppressed more by the nitrogen compounds than the HYD route, whereas for dibenzothiophene the opposite trend is observed. The stronger inhibition of the DDS route for sterically hindered dibenzothiophenes is not in agreement with other studies [18, 49].

Egorova and Prins [49] have investigated the effect of 2-methylpyridine and 2-methylpiperidine on the HDS of 4,6-dimethyldibenzothiophene on a $NiMo/\gamma\text{-}Al_2O_3$ in a fixed bed reactor. They found that 2-methylpiperidine, a 2-methylpyridine hydrogenation product, was a slightly stronger inhibitor of both the DDS and the HYD pathway than 2-methylpyridine. Especially the desulfurization of 4,6-dimethyltetrahydrodibenzothiophene was difficult in the presence of the nitrogen compounds. They found that both 4,6-dimethyldibenzothiophene and dibenzothiophene inhibited the hydrogenation of 2-methylpyridine, while they had no effect on the cleavage of the C-N bond in 2-methylpiperidine. They conclude that the adsorption of 2-methylpiperidine is stronger than that of 4,6-dimethyldibenzothiophene on both DDS and HYD sites.

Koltai et al. [50] have investigated the effect of acridine, carbazole and polyaromatics such as anthracene, phenanthrene and fluorene on the HDS of 4,6-dimethyldibenzothiophene on a commercial $NiMo/Al_2O_3$ catalyst in a slurry tank reactor operated in the batch mode. They find that acridine is a stronger inhibitor than carbazole. They also recognize that the hydrogenation of acridine is very fast which suggests that the effect of the partially hydrogenated nitrogen compound is more important than the parent molecule.

Beltramone et al. have [44] investigated the effect of quinoline, tetrahydroquinoline, indole, indoline and ammonia on the hydrogenation of phenanthrene and tetralin and the HDS of dibenzothiophene and 4,6-dimethyldibenzothiophene on a commercial NiMo/alumina catalyst in a continuous flow reactor. They find that the inhibiting effect increases in the order quinoline $<$ tetrahydroquinoline $<$ indole $<$ indoline $<$ ammonia for all the reactions.

Turaga et al. [51] have investigated the effect of quinoline and carbazole on HDS of 4,6-dime-

thyldibenzothiophene on MCM-41- and γ-Al_2O_3-supported CoMo catalysts in a fixed bed flow reactor. They find that carbazole has practically no effect on the HDS reaction over the γ-Al_2O_3-supported catalyst, while quinoline severely inhibits the reaction. On the MCM-41-supported catalyst both quinoline and carbazole have a large negative effect on the HDS reaction. They find that the basic quinoline inhibits hydrogenation sites on the γ-Al_2O_3-supported catalyst, which is reflected in a change in the selectivity towards hydrogenolysis products.

There is general agreement that basic nitrogen compounds are the strongest inhibitors for the HDS reaction. Also, several authors find that hydrogenation products may be responsible for the inhibition rather than the parent molecule itself [18, 49, 50]. This is either because the hydrogenated species adsorbs more strongly on the catalyst, or simply because the parent molecule is so reactive that it is immediately hydrogenated at typical hydrotreating conditions. For the HDS of 4,6-dimethyldibenzothiophene it is generally found, that the HYD route is more affected by the presence of the nitrogen compound than the DDS route.

In this work the effect of three nitrogen compounds (acridine, 1,4-dimethylcarabazole and 3-methylindole) on the hydrodesulfurization of a real feed and of 4,6-dimethyldibenzothiophene on NiMoP catalysts have been investigated at conditions similar to those used in industrial hydrotreating units.

6.2 Experimental

Three different types of experiments have been performed to investigate the effect of nitrogen compounds on hydrodesulfurization reactions over sulfided NiMoP catalysts: (1) Test of the effect of well-defined nitrogen compounds on the HDS of a real feed (mixture of SRGO and LCO). (2) Competitive HDN of model nitrogen compounds in the absence of thiophenic sulfur. (3) HDS of 4,6-dimethyldibenzothiophene in the presence of nitrogen compounds.

6.2.1 HDS of real feed

In order to be able to study the effect of individual nitrogen compounds on the HDS of a real feed, a practically nitrogen free (5 ppm N) oil was prepared using a chromatographic method as described in Knudsen et al. [39]. The original feed was a blend of 75 % (w/w) of a Kuwait Gasoil and 25 % (w/w) of a LCO from a Kuwait crude. The properties of the oil blend are given in table 6.1. The separation method involved running the oil through a column containing silica-gel. The column was saturated with sulfur compounds and polyaromatics much faster than it was saturated with nitrogen compounds, which allowed separation of the nitrogen compounds from the oil. Figure 6.2 shows the N and S concentration in the effluent of the column as function of the treated volume. As shown in the figure, the column is saturated with sulfur compounds after approximately 4 l of oil were treated. Since the column was saturated with sulfur compounds and polyaromatics much faster than it was saturated with nitrogen compounds, it was possible to separate almost all of the nitrogen compounds from the oil.

Different feeds were prepared by doping the N-free oil with known nitrogen compounds. The

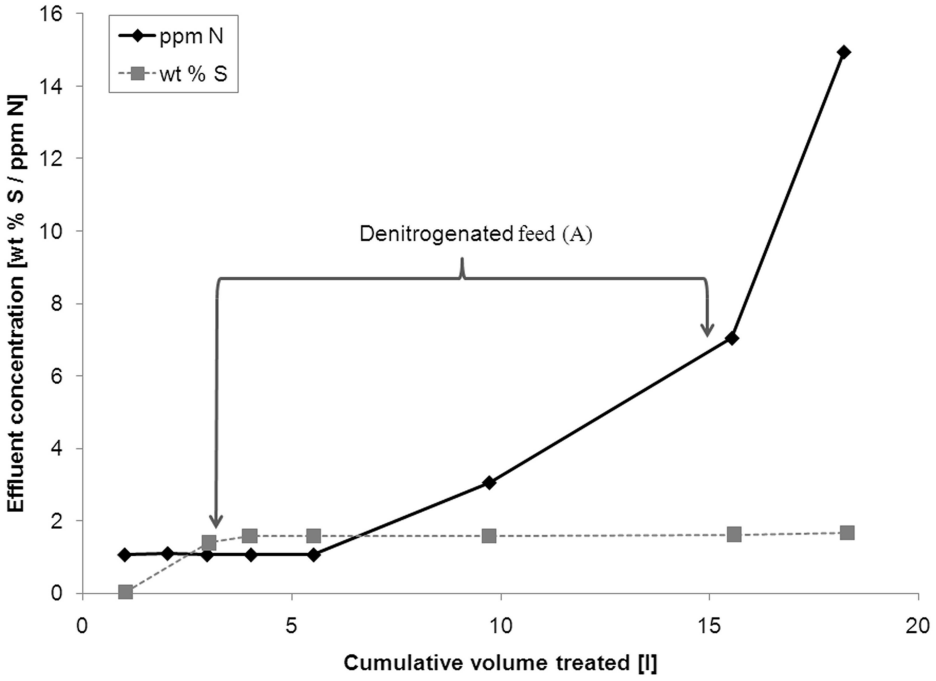

Figure 6.2: Effluent concentration of N and S in the oil after passing through a column with silica-gel. (N-content shown as 1 ppm N indicates that the concentration is < 1 ppm N)

amount of nitrogen added was in all cases 300 wt ppm, which matched the nitrogen content of the original oil. The model compounds used were acridine, 1,4-dimethylcarbazole and 3-methylindole, which are shown in table 6.2. A feed was also prepared in which 100 ppm N of all three nitrogen compounds were added. The S and N content of the different feeds are summarized in table 6.3. The removal of the nitrogen was done essentially without changing the sulfur compounds present in the oil. As shown in table 6.3, the amount of sulfur was reduced from 1.61 % w/w to 1.46 % w/w, but an analysis using gas chromatography followed by Sulfur Chemiluminescence Detector (SCD-GC) showed, that the amount of the sterically hindered S-compound, 4,6-dimethyldibenzothiophene, was the same in the the denitrogenated feed as in the original feed.

Table 6.1: Properties of the 75 % (w/w) SRGO and 25 % (w/w) LCO blend

SG	0.8733
Hydrogen	12.3 %
Sulfur	1.5 %
Nitrogen	300 ppm
Aromatics (Total)	33 %
Mono-aromatics	13.0 %
Di-aromatics	14.8 %
Tri-aromatics	5.2 %

The oils were all hydrotreated at 330 °C, 30 bar and with a hydrogen to oil ratio of 500 Nl/l

Table 6.2: Model nitrogen compounds used for experiments

Acridine	1,4-dimethylcarbazole	3-methylindole
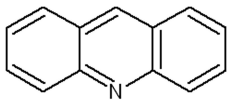	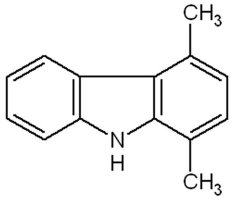	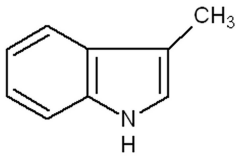

Table 6.3: S and N content of the SRGO-LCO feed mixtures

Feed	S (wt %)	N (wt ppm)
Original feed	1.61	300
SiO_2 treated feed (A)	1.46	5
A + 300 wt ppm N as 3-methylindole	1.45	300
A + 300 wt ppm N as 1,4-dimethylcarbazole	1.45	300
A + 300 wt ppm N as acridine	1.45	300
A + 100 wt ppm N of each of the above	1.45	300

in a fixed bed reactor with co-current down-flow at two different space velocities (1.5 hr^{-1} and 2.4 hr^{-1}). The reactor was loaded, with 15 ml of a NiMo catalyst.

All experiments were started by presulfiding the catalyst, and using a standard feed until a stable performance was obtained. Liquid product samples were collected and analyzed for sulfur and nitrogen.

6.2.1.1 HDS and HDN of Model Compounds

The experiments using only model compounds were carried out using a smaller laboratory scale fixed bed reactor with co-current down-flow, with an internal diameter of 7.5 mm, and a thermo couple is placed in the middle of the catalyst bed to measure the temperature.

The catalyst was a NiMo catalystavailable in the form of trilobes which was crushed to smaller particles of a size between 600 and 850 μm. In all of the experiments the volume of the reactor bed was between 1 and 2 ml. The position of the bed was adjusted such that the temperature was measured in the middle of the bed. Ballotini, with a diameter of 150 and 250 μm, was used to dilute the bed, such that the minimum volume was 1 ml. The catalyst was sulfided by first heating the reactor from room temperature to 150 °C with approximately 5 °C/min. When 150 °C was reached the sulfiding feed, a solution of 2.5 % (w/w) of dimethyldisulfide (DMDS) in *n*-heptane was fed to the reactor. The reactor was heated by 2 °C/min to 350 °C. During the sulfiding, the hydrogen flow was set to 250 Nml/min. After 4 hours at 350 °C, the catalyst was considered completely sulfided, and the temperature was changed to the desired reaction temperature, and the liquid feed was changed to a solution

containing the model sulfur and/or nitrogen compounds. The experiments were carried out at a temperature of 350 °C and a pressure of 50 barg, which was chosen to match typical hydrotreating conditions. The H_2 / oil ratio was 125 Nl/l. The amount of catalyst was varied between 0.35 and 2 g during the series of experiments.

The hydrodenitrogenation of acridine and 1,4-dimethylcarbazole, individually and in a mixture, was investigated in the absence of sulfur compounds. The composition of the feeds used for these experiments is shown in table 6.4. The effect of nitrogen compounds on the hydrodesulfurization of 4,6-dimethyldibenzothiophene was tested, and the composition of the different feeds is summarized in table 6.5. *n*-dodecane was used as solvent for the HDS experiments, to ensure that the reaction took place in a liquid phase rather than in a gas phase, as is the case in industrial units.

100 ppm S as DMDS was added to all solutions in table 6.4 and 6.5. At reactor conditions DMDS reacted instantly to yield methane and hydrogen sulfide. This was done to ensure that the catalyst was kept in the sulfided state, even when no other sulfur compounds were present.

The liquid product was analyzed online on a gas chromatograph.

Table 6.4: N concentrations of model feed mixtures. (100 ppm S as DMDS was added to all solutions)

Feed	Solvent	Acridine (ppm N)	1,4-dmcbz (ppm N)
1	*n*-C7	300	0
2	*n*-C7	0	300
3	*n*-C7	150	150

Table 6.5: S and N concentrations of model feed mixtures. (100 ppm S as DMDS was added to all solutions)

Feed	Solvent	4,6-dmdbt (ppm S)	Acridine (ppm N)	1,4-dmcbz (ppm N)	3me-in (ppm N)
I	*n*-C12	1000	0	0	0
II	*n*-C12	1000	300	0	0
III	*n*-C12	1000	0	300	0
IV	*n*-C12	1000	0	0	300
V	*n*-C12	1000	150	150	0

6.3 Results and Discussion

6.3.1 HDS of real feed

Results from the hydrotreating of the feeds listed in table 6.3 have previously been given by Cooper and Knudsen [52] and Zeuthen et al. [53], and are shown in figure 6.3. The figure shows how much sulfur was left in the product after hydrotreating. The figure clearly shows that the non-basic nitrogen compounds 1,4-dimethylcarbazole and 3-methylindole are not major

inhibitors, while the basic compound, acridine, severely inhibits the HDS reaction. The oil containing equal amounts of the 3 nitrogen inhibitors seems to behave as a linear combination of the three compounds.

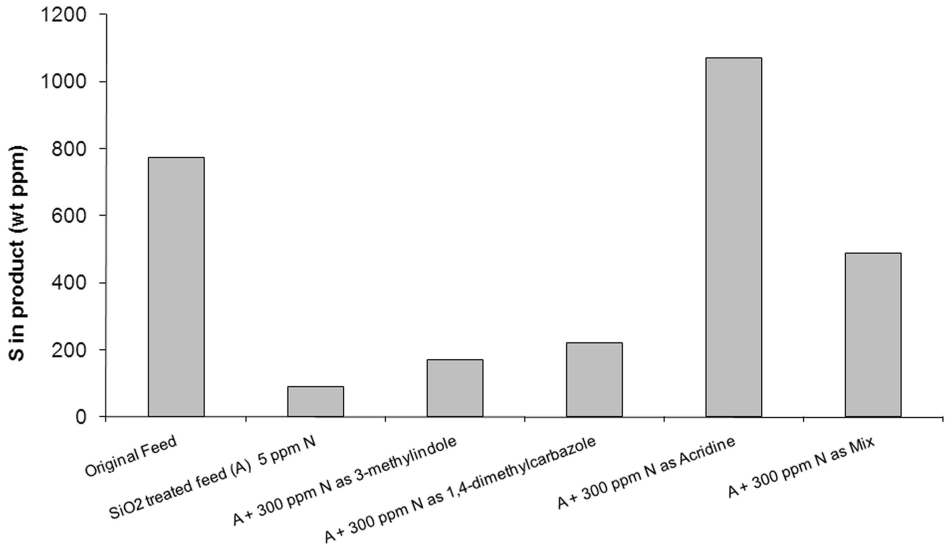

Figure 6.3: Sulfur in the product after hydrotreating of the feeds in table 6.3 ($T = 330\ ^{\circ}C$, $P = 30\ bar$, $H_2/oil = 500\ Nl/l$ and $LHSV = 1.5\ hr^{-1}$)

The products were analyzed in detail to see how much of the nitrogen was still left in the oil after the hydrotreating. These, previously unpublished results, are shown in figure 6.4 and 6.5.

The nitrogen content in the product is shown as function of the space velocity in figure 6.4. It shows that the highest amount of nitrogen in the product is found in the untreated fuel. The oil containing acridine and the oil with the mixture of the three nitrogen compounds show very similar behavior, and some nitrogen is still left in the product. 3-methylindole is very reactive and is almost completely removed, while 1,4-dimethylcarbazole is a little less reactive, but still fairly easy to remove. Based on the results the following order of HDN reactivity is found: 3-methylindole > 1,4-dimethylcarbazole > acridine.

The order of reactivity is found to be the opposite of the inhibition strength, in that the strongest inhibitor acridine also has the lowest reactivity for hydrodenitrogenation (HDN).

The oil containing all three inhibitors was investigated in more detail to see how much nitrogen was left from the individual compounds. This is illustrated in figure 6.5, which shows that in the mixture 3-methylindole is still easily removed. But the figure also shows that a significant amount of nitrogen originating from 1,4-dimethylcarbazole is left in the oil, while almost all acridine has been removed. This is a very strong indication of competitive adsorption, as the basic nitrogen compound inhibits the HDN reaction of 1,4-dimethylcarbazole due to a stronger adsorption on the active sites of the catalyst. This suggests that although substituted carbazoles are the most abundant class of nitrogen compounds found in hydrotreated diesel oil fractions as shown by Wiwel et al. [16], they are probably not the major inhibitors.

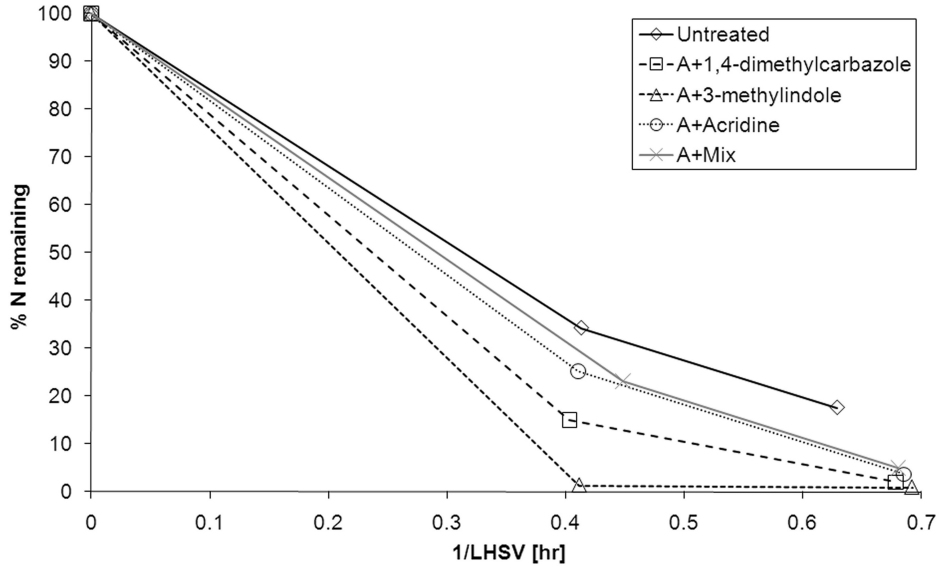

Figure 6.4: Nitrogen in product after hydrotreating of the feeds in table 6.3 ($T = 330\ °C$, $P = 30\ bar$ and $H_2/oil = 500\ Nl/l$)

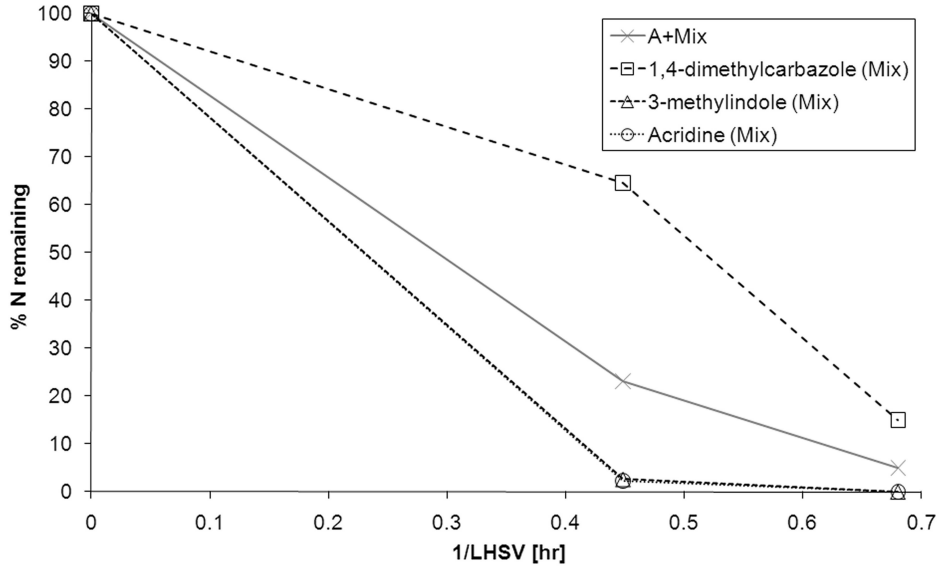

Figure 6.5: Total N and individual nitrogen compounds remaining after hydrotreating of SRGO-LCO feed added a mixture of nitrogen compounds ($T = 330\ °C$, $P = 30\ bar$ and $H_2/oil = 500\ Nl/l$)

6.3.2 HDN of acridine and 1,4-dimethylcarbazole

The hydrodenitrogenation (HDN) of acridine and 1,4-dimethylcarbazole was investigated in the absence of sulfur compounds using the feeds shown in table 6.4. The results are summarized in table 6.6, which lists the HDN conversions. From the experiments with only one nitrogen compound it can be seen that 1,4-dimethylcarbazole is more reactive than acridine at the investigated conditions, although the difference is more pronounced at the high space velocity than at the low space velocity. In the HDN of acridine, 5 main products was observed, which accounted for more than 85 % of the mass balance. These were 1,2,3,4,-tetrahydroacridine; 1,2,3,4,5,6,7,8-octahydroacridine, 1,2,3,4,4a,9,9a,10-octahydroacridine; benzylcyclohexane and 1,1'-methylenebis(cyclohexane) (dicyclohexylmethane). The hydrogenation of the first ring is very fast, and at the investigated space velocities practically no (< 3 %) acridine is left in the product. Due to the assymetric nature of 1,4-dimethylcarbazole, several possible reaction products exist, which could not easily be distinguished. The main ones were found to be dimethylcyclohexylbenzenes.

The mixture in table 6.6 contained 150 ppm N as acridine and 150 ppm N as 1,4-dimethylcarbazole. It should be noted that in the mixture, the conversion of acridine is significantly higher than the 1,4-dimethylcarbazole, even though that 1,4-dimethylcarbazole has a higher reactivity when the N compounds are studied individually at similar conditions. This shows that acridine is a very strong inhibitor of the HDN of the substituted carbazole, which indicates that acridine adsorbs more strongly on the catalyst. These observations are in agreement with what was observed previously in the real feed experiments, as illustrated in figure 6.5, and a similar observation was made by Rabarihoela-Rakotovao et al. [47]. Similarly Ferdous et al. have observed that acridine inhibits the hydrodenitrogenation of carbazole [54].

Table 6.6: HDN conversions in solutions containing 300 ppm N. ($T = 350\ ^{\circ}C$, $P = 50\ barg$ and $H_2/oil = 125\ Nl/l$)

	WHSV = 8 hr^{-1}			**WHSV = 12 hr^{-1}**		
Feed	**Acridine**	**1,4-dmcbz**	**Total**	**Acridine**	**1,4-dmcbz**	**Total**
1 (Acridine)	0.66	-	0.66	0.35	-	0.35
2 (1,4-dmcbz)	-	0.75	0.75	-	0.59	0.59
3 (Mixture)	0.50	0.05	0.28	0.46	0.02	0.25

6.3.3 HDS of 4,6-dimethyldibenzothiophene in the presence of N-compounds

Experiments were done using the feed solutions shown in table 6.5. Figure 6.6 shows the total conversion of 4,6-dimethyldibenzothiophene as a function of the inverse space velocity for the 5 different solutions. The main reaction products were 3,3'-dimethylbiphenyl and 3-(3'-methylcyclohexyl)toluene. As the total conversion of 4,6-dimethyldibenzothiophene increased the amount of other products, probably products from hydrogenation of 3-(3'-methylcyclohexyl)-toluene, became higher. Especially in the absence of nitrogen, these compounds account for up

to 40 % of the the 4,6-dimethyldibenzothiophene mass balance.

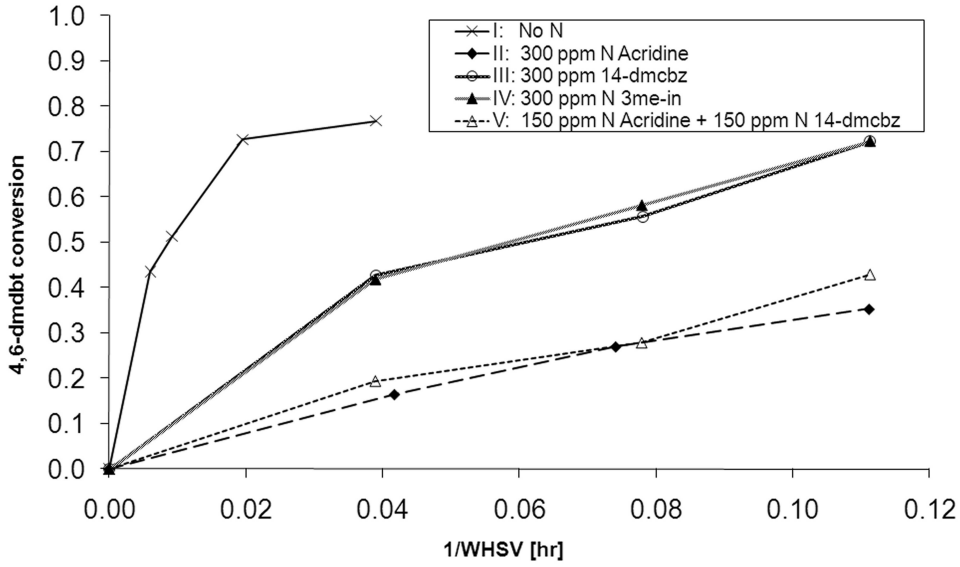

Figure 6.6: HDS conversion of 4,6-dimethyldobenzothiophene in the feeds listed in table 6.5 ($T = 350\ ^{\circ}C$, $P = 50\ barg$ and $H_2/oil = 125\ Nl/l$)

The rate of sulfur removal from 4,6-dimethyldibenzothiophene was the highest when no nitrogen is present, so evidently all of the nitrogen compounds have a significant inhibition effect. For solutions III and IV the conversion of 4,6-dimethyldibenzothiophene is very similar and suggests that the two non-basic nitrogen compounds have very similar inhibition strength, which was also observed in the real feed experiments. The order of the inhibiting strength is the same as was observed in the real feed experiments.

Interestingly, the conversion in solutions II and V are also very similar, which might be because the catalytic sites are mainly covered by adsorbed acridine species even in the mixture where the acridine concentration is lower (150 ppm N). A similar cooperative effect has been observed by Laredo et al. [40], who investigated the effect of quinoline, indole and carbazole on the initial rate of the HDS of dibenzothiophene. They found that a mixture of the three compounds had a larger inhibition strength than the individual compounds, when they were present in the same amount. As the concentration increased, the effect of the mixture approached that of the strongest inhibitor, indole [40].

As shown in figure 6.1, dibenzothiophenes react via two reaction routes. As a measure of the relative rate between the two reaction routes a selectivity can be defined as:

$$S = \frac{amount\ of\ mcht\ in\ product}{amount\ of\ dm-bp\ in\ product} \tag{6.1}$$

3-(3'-methylcyclohexyl)toluene (mcht) is the primary product of the HYD route, while 3,3'-dimethylbiphenyl (dm-bp) is the primary product of the DDS reaction route. Thus the selectivity is a measure of the relative reaction rates between the two parallel routes. This is strictly only

valid if the further hydrogenation of 3,3'-dimethylbiphenyl to 3-(3'-methylcyclohexyl)toluene does not take place.

So, in order to test whether 3,3'-dimethylbiphenyl is hydrogenated to 3-(3'-methylcyclohexyl)toluene at these experimental conditions, a solution similar to feed IV in table 6.5, with 0.5 % of 3,3'-dimethylbiphenyl added, was made. This feed was hydrotreated at a temperature of 350 °C, a pressure of 50 barg, hydrogen to oil ratio of 125 Nl/l and at WHSV equal to 8 hr^{-1}. The results using the feeds with and without 3,3'-dimethylbiphenyl, are shown in table 6.7. Adding 3,3'-dimethylbiphenyl has no effect on the overall conversion of 4,6-dimethyldibenzothiophene, so it does not act as an inhibitor for either the HYD route or the DDS route. With the feed containing 4,6-dimethyldibenzothiophene and 3,3'dimethylbiphenyl, the product concentration of 3,3'dimethylbiphenyl is 0.34 %, which is less than the feed concentration. If the 3,3'dimethylbiphenyl that is formed through direct sulfur removal from 4,6-dimethyldibenzothiophene is subtracted, this shows, that approximately 50 % of the 3,3'-dimethylbiphenyl in the feed has been converted. The hydrogenation of 3,3'-dimethylbiphenyl is therefore not necessarily negleglible at these conditions.

Even though the hydrogenation of 3,3'-dimethylbiphenyl cannot be ignored, the selectivity, as given in equation 6.1, can still be used as a measure of the ratio between the hydrogenation activity and the desulfurization activity.

Table 6.7: Effect of adding 3,3'-dimethylbiphenyl (dm-bp) on the HDS of solution IV in table 6.5 ($T = 350\ °C$, $P = 50\ barg$, $H_2/oil = 125\ Nl/l$ and $WHSV = 8\ hr^{-1}$)

Feed	**4,6-dmbt conversion**	**dm-bp in product [%]**	**mcht/dm-bp**
IV (table 6.5)	0.86	0.09	2.78
IV (table 6.5) + 0.5 % dmbp	0.87	0.34	1.32

Figure 6.7 shows the selectivities as a function of the reaction time. In all cases the selectivity is higher than 1, which is in agreement with the fact, that due to sterical hindrance dibenzothiophenes with substituents in the 4 and 6 positions react mainly through the HYD route.

From figure 6.7 it seems clear that the inhibitors have a higher effect on the hydrogenation activity than on the direct desulfurization. The weakest inhibitors 1,4-dimethylcarbazole and 3-methylindole, yield similar selectivities as they also gave similar conversions. The strongest of the inhibitors (acridine) gives the lowest selectivity, while solution V, containing a mixture of acridine and 1,4-dimethylcarbazole has a selectivity between the pure solutions. All the nitrogen compounds appears to lower the selectivity. At $WHSV^{-1} = 0.04\ hr^{-1}$ one can see, that the selectivity towards the hydrogenation product is decreasing, with the increasing strength of the inhibitor. 1,4-dimethylcarbazole and 3-methylindole which showed a similar inhibition strength have the same selectivity. The solutions with the strongest inhibition taking place, II and V, yields the smallest values of the selectivity. These results show that the HYD pathway is more affected than the DDS pathway by all of the nitrogen compounds. This is different than what is observed by Rabarihoela-Rakotovao et al. [47] who find that that 1,4-dimethylcarbazole inhibits both reaction pathways to the same degree. Similar to this work, they find that acridine is a

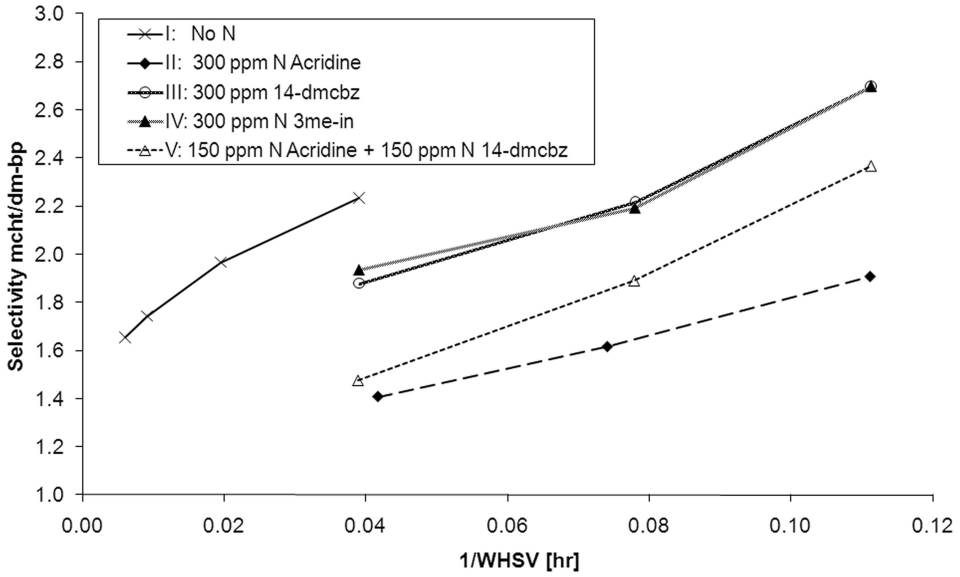

Figure 6.7: Ratio bewteen 3-(3'-methylcyclohexyl)toluene (mcht) and 3,3'-dimethylbiphenyl (dm-bp) in the product after hydrotreating of the feeds in table 6.5 ($T = 350\ ^{\circ}C$, $P = 50\ barg$ and $H_2/oil = 125\ Nl/l$)

much stronger inhibitor of the HYD route than of the DDS route.

A common feature for solution I-V is that the observed selectivity is not constant, but increases with the reaction time (and HDS conversion). As has been discussed previously, the most plausible explanation, is that this is because some of the 3,3'-dimethylbiphenyl formed is hydrogenated further to yield 3-(3'-methylcyclohexyl)toluene, thereby increasing the value of the selectivity. Ho and Sobel [55] observed a similar behavior as the selectivity increased as a function of conversion in the hydrodesulfurization of dibenzothiophene.

It should be noted that while the HDS conversion for solution II and V are very similar, the selectivity towards 3-(3'-methylcyclohexyl)toluene is higher for solution V, and the difference increases with the space time.

To take a closer look at the HDN reaction in the presence of a sulfur compound, the HDN conversion is plotted in figure 6.8 for the solutions containing acridine or 1,4-dimethylcarbazole, and the mixture of the two. Again it is seen that 1,4-dimethylcarbazole has a higher HDN reactivity than acridine, and that the total HDN conversion of the mixture is lower than for the two pure solutions. This is equivalent to what was observed in the HDN experiments, in the absence of sulfur, for which the results are given in 6.6. Similar to the real feed experiment 3-methylindole was the most reactive nitrogen compound, and the HDN conversion was above 90 % at the investigated conditions.

Figure 6.9 shows the HDN conversions of the individual compounds in the mixture. Again it can be observed, that acridine reacts faster than 1,4-dimethylcarbazole, because the conversion of 1,4-dimethylcarbazole is inhibited by the presence of acridine. Since ring hydrogenation has to happen prior to the nitrogen removal it appears that acridine adsorbs more strongly on the active sites used for hydrogenation and thereby inhibits the hydrogenation of 1,4-dimethylcarbazole.

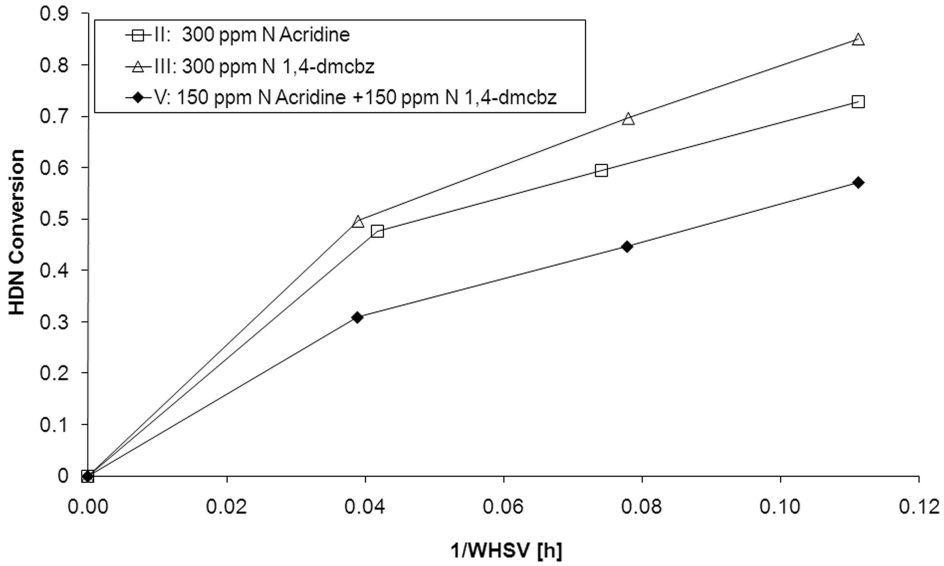

Figure 6.8: HDN conversion of acridine and 1,4-dimethylcarbazole ($T = 350\ °C$, $P = 50\ barg$ and $H_2/oil = 125\ Nl/l$)

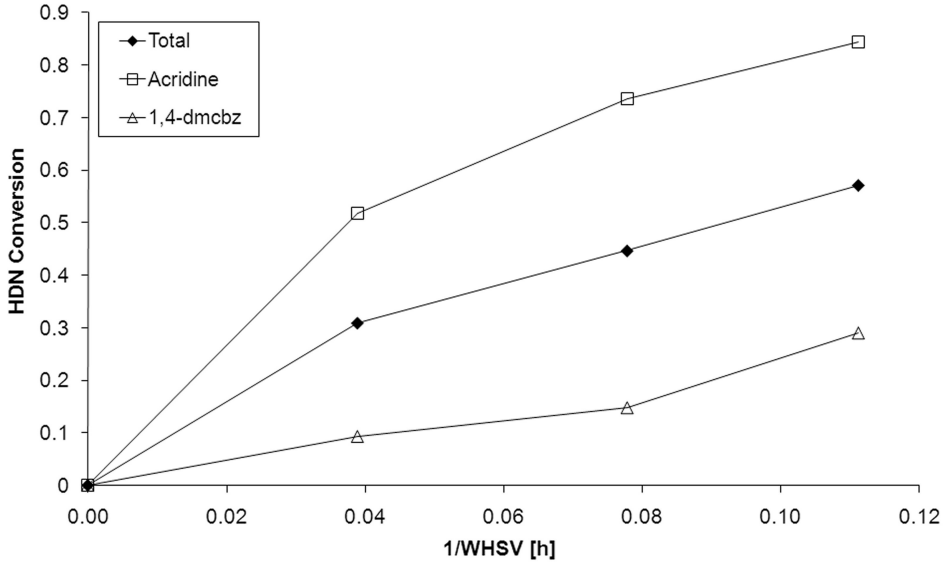

Figure 6.9: HDN conversion in feed containing both acridine and 1,4-dimethylcarbazole ($T = 350\ °C$, $P = 50\ barg$ and $H_2/oil = 125\ Nl/l$)

This can also explain the difference in selectivity between solution II and V shown in figure 6.7. As acridine, the strongest inhibitor for the HYD pathway, is removed, the selectivity towards 3-(3'-methylcyclohexyl)toluene increases.

There is found to be a very good agreement between the real feed experiments and the model compound experiments. One small exception is, that the effect of a mixture of nitrogen compounds on the HDS reaction is different in the model compound experiments than in the real feed experiments. As can be seen in figure 6.3, mixing the strongest inhibitor, acridine, with the less inhibiting non-basic compounds results in a significant increase in the HDS activity, whereas the conversion of 4,6-dimethyldibenzothiophene is similar in the presence of 300 ppm N as acridine and 300 ppm N as acridine and 1,4-dimethylcarbazole as can be seen in figure 6.6. The reason might be that the overall nitrogen conversion is very high (> 95 %) in the real feed experiments, while it is somewhat lower (< 60 %) in the model experiments.

It is difficult to directly compare the strength of the inhibitors on the HDS reactions of the SRGO/LCO feed and on 4,6-dimethyldibenzothiophene, as temperature, pressure, hydrogen to oil ratios and space times are different. To get an idea, it is possible to compare the relative sizes of the observed rate constants. Since the sulfur compounds in the SRGO/LCO mixture cover a large range of reactivities, a first order rate expression is not suitable to describe the sulfur conversion. Instead it will be assumed that the HDS rate of the real feed is 1.7th order in the total sulfur concentration, which is a good approximation if the conversion is not too high [56]. Table 6.8 show the rate constants in presence of 1,4-dimethylcarbazole and 3-methylindole, relative to the rate constant when acridine is present. There is good agreement between the model feed and the real feed in terms of the relative effect of the individual inhibitors.

Table 6.8: Relative HDS rate constants in the HDS of a SRGO/LCO mixture and of 4,6-dimethyldibenzothiophene

Inhibitor	**Reaction order**	**Acridine**	**1,4-dmcbz**	**3-mein**
k_{HDS} Real feed (LHSV ≈ 2.5 hr^{-1})	1.7	100	234	267
k_{HDS} Model feed (WHSV ≈ 8 hr^{-1})	1	100	294	413

6.4 Conclusion

The effect of three different nitrogen compounds (acridine, 1,4-dimethylcarbazole and 3-methylindole) on the HDS of a SRGO/LCO blend and on 4,6-dimethyldibenzothiophene has been investigated. There was found to be very good agreement between the effect of the nitrogen compounds on the real feed and on the model compound. The order of inhibiting strength was the same for both HDS of the real feed and of 4,6-dimethyldibenzothiophene. The most basic compound acridine, was also the strongest inhibitor, while 1,4-dimethylcarbazole and 3-methylindole showed similar inhibition strengths to each other, but lower than acridine.

A study of the HDN of the individual compounds showed a good agreement between the HDN reactivity and the inhibition strength. The strongest inhibitor acridine, showed the lowest HDN reactivity.

Dibenzothiophenes reacts through two parallel reaction pathways. It has been shown that the nitrogen compounds have a stronger inhibiting effect on the hydrogenation pathway than on the direct desulfurization pathway. This is important, as the refractive sulfur compounds, such as 4,6-dimethyldibenzothiophene, that has to be removed in order to meet ULSD demands reacts mainly through the HYD route.

It has been shown that acridine is not only a strong inhibitor of HDS reactions, but can also inhibit the HDN of 1,4-dimethylcarbazole. This can explain why carbazoles are the main nitrogen compounds found in hydrotreated oils. Also it is a very strong indication that the inhibition is due to competitive adsorption, as the basic nitrogen compound acridine blocks the active sites used for hydrogenation reactions.

Chapter 7

Hydrotreating of a Model Diesel Mixture

One of the challenges when modelling and measuring kinetics of hydrotreating reactions, is the vast number of components present in real diesel feeds. This makes detailed analysis of real feedstocks quite difficult. A useful way to obtain fundamental understanding of the types of reactions taking place during hydrotreating of diesel is using model compounds. In this chapter, experimental results from the hydrotreating of a 13 component model diesel mixture are presented. The experiments were carried out using the experimental set-up described in chapter 2. The purpose of these experiments was to study individual reactions in a mixture that is similar in composition to a real diesel feed, but with fewer components.

7.1 Feed composition

A feed mixture with compounds from the following different classes were used for these experiments: Aromatics, naphthenes, paraffins, sulfur compounds and nitrogen compounds. The composition of the feeds, and the structures of the model compounds are presented in the following sections.

Table 7.1: Aromatic compounds in the model diesel mixture

Pentylbenzene	**Tetralin**	**Naphthalene**
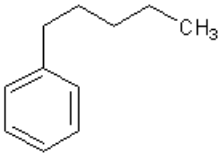	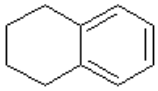	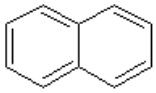
Phenanthrene		
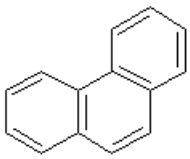		

Aromatics

The total aromatics concentration of the model mixture is approximately 20 % (w/w). Pentylbenzene and tetralin represent the relatively slow reacting mono-aromatics. Naphthalene represents the diaromatics with a concentration approximately equal to 4.5 % (w/w). Phenanthrene was used as a tri-aromatic with a concentration equal to 1.5 % (w/w). The compounds are shown in table 7.1.

Naphthenes

2 different naphthenes were used for the feed, butylcyclohexane and decalin, which are shown in table 7.2. The total concentration of naphthenes was approximately 30 % (w/w).

Table 7.2: Naphthenic compounds in the model diesel mixture

Butylcyclohexane	**decalin**
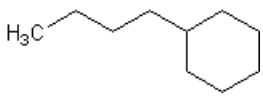	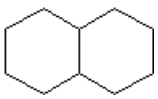

Paraffins

The total concentration of paraffins in the feed was close to 44 % (w/w). n-Hexadecane was used as the only component to represent this compound class, although the solution also contained 0.5 % (w/w) n-nonane to be used as internal standard for the GC analysis.

Sulfur compounds

The total sulfur concentration in the feed was approximately 1.1 % S. 3 different sulfur compounds, which are shown in table 7.3, were used to cover different levels of reactivity. Benzothiophene represents the most reactive sulfur species, while dibenzothiophene is a less reactive sulfur compound. Two similar feeds were prepared, one of them also containing the particularly refractive sulfur compound 4,6-dimethyldibenzothiophene.

Table 7.3: Sulfur compounds in the model diesel mixture

Benzothiophene	Dibenzothiophene	4,6-dimethyl-dibenzothiophene
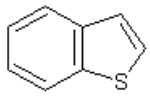	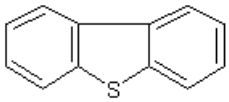	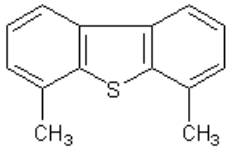

Nitrogen compounds

3 different nitrogen compounds were used, representing both basic and non-basic compounds. The structures of the nitrogen compounds are shown in table 7.4. Two non-basic nitrogen compounds were used: 3-methylindole, the most reactive of the N compounds, and 1,4-dimethylcarbazole. Acridine was used as a basic compound. The total nitrogen concentration was around 230 ppm N.

Table 7.4: Nitrogen compounds in the model diesel mixture

Acridine	1,4-dimethylcarbazole	3-methylindole
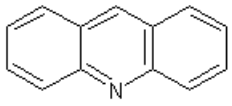	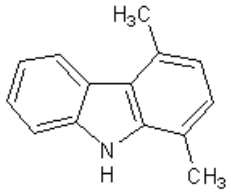	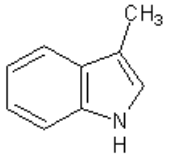

The composition of the two feeds are given in table 7.5. The specific gravity of both were 0.84.

Properties of the feed components are given in table 7.6. The boiling points of the compounds range 181 to 345 °C.

Table 7.5: Composition of model diesel feeds. Concentrations are in weight percent

	Feed A	**Feed B**
Aromatics (total)	**20.0**	**20.3**
pentylbenzene	8.0	7.9
tetralin	6.0	6.4
naphthalene	4.5	4.5
phenanthrene	1.5	1.5
Naphthenes (total)	**30.0**	**29.7**
butylcyclohexane	18.0	17.8
decalin	12.0	11.9
Paraffins (total)	**44.2**	**43.8**
n-nonane	0.5	0.5
n-hexadecane	43.7	43.3
Sulfur Compounds (total)	**5.4**	**5.9**
benzothiophene	2.0	2.0
dibenzothiophene	3.4	3.4
4,6-dimethyldibenzothiophene	0.0	0.59
Nitrogen Compounds (total)	**0.3**	**0.3**
acridine (basic)	0.06	0.06
3-methylindole (non-basic)	0.06	0.06
1,4-dimethylcarbazole (non-basic)	0.18	0.18

Table 7.6: Molecular weight and boiling points of the model compounds [57–59].(*) indicates the boiling point is estimated using a group contribution method [60]

	Mw [g/mol]	**T_B [°C]**
Aromatics		
pentylbenzene	148.25	205.5
tetralin	132.21	207.6
naphthalene	128.17	218.0
phenanthrene	178.23	339.9
Naphthenes		
butyl-cyclohexane	140.26	181.0
decalin	138.25	195.8
Paraffins		
hexadecane	226.45	286.9
Sulfur Compounds		
benzothiophene	134.20	219.9
dibenzothiophene	184.26	332.6
4,6-dimethyldibenzothiophene (*)	212.31	327.9
Nitrogen Compounds		
acridine (basic)	179.22	344.9
3-methylindole (non-basic) (*)	131.17	257.3
1,4-dimethylcarbazole (non-basic) (*)	195.26	326.4

An analysis of the aromatics content of feed A using ASTM D6591, yields a total aromatics content of 27.2 % (w/w). This is significantly larger than the 20 % (w/w), which is added in the feed. The reason for the difference is that the sulfur and nitrogen compounds, also contain aromatic rings. Furthermore it is possible that the presence of a heteroatom in a compound will make it interfere with the analyis [61]. Table 7.7 shows the concentration of the aromatics obtained from the analysis, and based on the amount of chemicals added to the feed. It shows, that the concentrations of mono- and tri-aromatics are relatively similar, while there is a large difference in the di-aromatics concentration. This shows, that the sulfur compounds (benzothiophene and dibenzothiophene) and possibly also the nitrogen compounds (acridine, 3-methylindole and 1,4-dimethylcarbazole), will mainly contribute with an error in the di-aromatics concentration.

Table 7.7: Aromatics concentrations (% (w/w)) of feed A in table 7.5, by experimental analysis (ASTM D6591)

Method	Mono-	Di-	Tri-	Total
Added amount	14.0	4.5	1.5	20.0
ASTM D6591	15.0	10.5	1.7	27.2

7.2 Phase equilibria calculations

Typically hydrotreating is done at conditions where both a liquid phase and a gas phase is present in the reactor. Changing conditions such as temperature and pressure and composition at the reactor inlet, will have an influence on the reactor performance. In this section results from equilibrium calculations are presented. It is assumed that the behavior in the reactor can be described by considering the feed mixture at the reactor inlet. No considerations about any reactions or the effect of gas / liquid hold-up in the reactor is done in this section. The calculations are done using the Soave-Redlich-Kwong equation of state as described in section 8.4. The influence of temperature, pressure and gas-to-oil ratio is investigated, and it is assumed that the liquid feed has a composition equal to that of feed B in table 7.5 and that the gas feed is pure hydrogen.

7.2.1 Effect of temperature

Increasing the temperature results in increased vaporization which is illustrated as an increase in the vapor fraction in table 7.8. At 340 °C , the vapor fraction is 1, and at higher temperatures all of the liquid evoporates and only one gas phase is present at equilibrium. Still it is likely that liquid will be present in a hydrotreating reactor due to the capillary pressure in the pores of the catalyst pellets.

Table 7.8: Effect of temperature on gas- and liquid-phase mole fractions (y and x) of selected compounds at equilibrium. The liquid feed has a composition as feed B in table 7.5. (H_2/oil = 500 Nl/l and $P = 50\ barg$)

T [°C]	Vapor fraction	x_{H_2}	y_{H_2}	x_{NAP}	x_{PHE}	x_{BT}	x_{DBT}	$x_{4,6-DMDBT}$
300	0.935	0.056	0.871	0.039	0.027	0.017	0.054	0.010
310	0.954	0.058	0.855	0.037	0.031	0.016	0.059	0.011
320	0.975	0.060	0.837	0.034	0.035	0.015	0.064	0.013
330	0.9996	0.062	0.818	0.032	0.042	0.014	0.071	0.017
340	1	-	0.818079	-	-	-	-	-

7.2.2 Effect of pressure

Table 7.9 shows results of phase equilibrium calculations at different pressures. It should be noted, that increasing the pressure has a large effect on the liquid phase hydrogen concentration, that almost triples when going from 30 to 80 barg. The effect on the oil components is much smaller, although the liquid phase concentrations decrease slightly with increasing pressure.

Table 7.9: Effect of pressure on gas- and liquid-phase mole fractions (y and x) of selected compounds at equilibrium. The liquid feed has a composition as feed B in table 7.5. (H_2/oil = 125 Nl/l and $T = 350\ °C$)

P [barg]	Vapor fraction	x_{H_2}	y_{H_2}	x_{NAP}	x_{PHE}	x_{BT}	x_{DBT}	$x_{4,6-DMDBT}$
30	0.763	0.063	0.674	0.047	0.021	0.020	0.043	0.0072
40	0.686	0.087	0.732	0.049	0.018	0.021	0.037	0.0061
50	0.633	0.109	0.772	0.049	0.016	0.021	0.034	0.0055
60	0.593	0.131	0.802	0.048	0.015	0.021	0.032	0.0051
70	0.561	0.152	0.824	0.048	0.014	0.020	0.030	0.0048
80	0.533	0.172	0.842	0.047	0.013	0.020	0.029	0.0045

7.2.3 Effect of gas-to-oil ratio

Table 7.10 shows results of phase equilibrium calculations at different gas-to-oil ratios. Increasing the gas-to-oil ratio has very little effect on the liquid phase hydrogen concentration, but the vapor fraction increases when more hydrogen is fed to the reactor. When more of the gaseous hydrogen is present in the feed, more of the light oil compounds will evaporate to the gas phase. Therefore the liquid phase mole fraction of light compounds such as benzothiophene and naphthalene will decrease, while the mole fraction of heavy compounds such as dibenzothiophene and 4,6-dimethyldibenzothiophene in the liquid will increase with increasing hydrogen to oil ratio.

7.3 Reactions

In this section the most important of the investigated reactions are discussed.

Table 7.10: Effect of gas-to-oil ratio on gas- and liquid-phase mole fractions (y and x) of selected compounds at equilibrium. The liquid feed has a composition as feed B in table 7.5. ($P = 50\ barg/l$ and $T = 350\ ^{\circ}C$)

H_2/oil [Nl/l]	Vapor fraction	x_{H_2}	y_{H_2}	x_{NAP}	x_{PHE}	x_{BT}	x_{DBT}	$x_{4,6-DMDBT}$
125	0.633	0.109	0.772	0.049	0.016	0.021	0.034	0.005
200	0.788	0.111	0.786	0.046	0.019	0.020	0.039	0.006
300	0.895	0.112	0.802	0.042	0.023	0.018	0.045	0.008
400	0.953	0.113	0.816	0.038	0.027	0.016	0.051	0.010
500	0.987	0.113	0.827	0.035	0.032	0.015	0.058	0.012

Although not a very reactive compound, the monoaromatic pentylbenzene can be hydrogenated and form the main product pentylcyclohexane. The other monoaromatic in the feed, tetralin, is part of the reaction network for naphthalene as shown in figure 1.7. Naphthalene can react to form tetralin, which can be further hydrogenated to yield decalin. Since the hydrogenation reactions are reversible, the backward reactions are also possible.

The 5 main products, not counting isomers, from phenanthrene hydrogenation can be seen in the reaction network of given in figure 1.8. They are dihydrophananthrene, tetrahydrophenanthrene, symmetric and assymmetric octahydrophenanthrene and perhydrophenanthrene.

One possible reaction network for benzothiophene is shown in figure 1.5. Since it is a relatively reactive compound, it has been completely converted at the investigated conditions. The main product, that is observed is ethylbenzene, but some of the ethylbenzene has been further hydrogenated to ethylcyclohexane.

Dibenzothiophenes follow the reaction scheme given in figure 1.6. The main products from the reaction of dibenzothiophene are biphenyl, from the DDS route, and cyclohexylbenzene from the HYD route. The further hydrogenation of the monoaromatic ring in cyclohexylbenzene to form 1,1'-bicylcohexyl is also possible. Similar, but methylsubstituted, products are expected from the reaction of 4,6-dimethyldibenzothiophene.

The reaction network, including possible intermediate products, for acridine hydrodenitrogenation is shown in figure 1.9. 3-methylindole is expected to follow a reaction network similar to indole. The main product is isopropylcyclohexane rather than ethylcylcohexane. In hydrodenitrogenation of 1,4-dimethylcarbazole a lot of products are observed, which are not easily identified, but the main ones are likely to be dimethylcyclohexylbenzenes and dimethyldicyclohexanes.

Although at certain conditions cracking of the paraffins are a possibility, no significant changes in the concentrations have been observed, so it is assumed that it is not taking place.

7.4 Experimental conditions

The NiMo catalyst with properties given in table 2.1 has been used, and the reactor has been loaded with either 1 or 2 g of catalyst. The liquid feed flow were 0.2 ml/min in all the experiments. The temperature was varied between set points of 300 and 360 °C. Due to the exothermic

nature of the reactions, the measured temperature was at some conditions 2-10 °C higher than the set point. The total pressure was varied between 30 and 80 barg, and the hydrogen to oil ratio between 125 and 500 Nm^3/m^3.

When the feed without 4,6-dimethyldibenzothiophene (A) was used, the weight hourly space velocity was kept constant at 10 hr^{-1}, and when the feed with 4,6-dimethyldibenzothiophene (B) was used WHSV was 5 hr^{-1}.

7.5 Hydrodesulfurization

In this section the effect of different parameters on the hydrodesulfurization reactions are presented. The most reactive sulfur compound in the feeds listed in table 7.5 is benzothiophene. At all the conditions that have been applied in these experiments, benzothiophene was completely converted, i.e. all the sulfur was removed from this compound. The main desulfurization product was ethylbenzene, but small amounts of ethylcyclohexane were also produced.

7.5.1 Effect of temperature

Figure 7.1 shows the sulfur concentration in the product as a function of the temperature, using a feed without 4,6-dimethyldibenzothiophene. Since benzothiophene is very reactive, all sulfur that is left in the product originates from dibenzothiophene. As the temperature increases, more and more of the sulfur is removed. The sulfur product concentration is shown at two different pressures. At the highest pressure, 50 barg, the sulfur conversion decreases faster than at the low pressure, 30 barg. Increasing the pressure increases the liquid phase concentration of hydrogen, and has a positive effect on the removal of sulfur. The reason for this is that the rate of the hydrodesulfurization reaction increases with increasing hydrogen concentration, but also because the removal of inhibiting compounds is faster.

7.5.2 Effect of pressure

Figure 7.2 shows the effect of the pressure on the product sulfur concentration at three different conditions. Increasing the pressure has a positive effect on the rate of sulfur removal, at all the conditions. Again this is probably related to an increase in the equilibrium concentration of hydrogen in the liquid phase. Increasing the temperature and the hydrogen to oil ratio results in a decrease in the product concentration of sulfur. The slope in the logarithmic plot when increasing the pressure is steeper, when the product concentration is low. The reason for this could be that limitations of the reaction rate due to adsorption of dibenzothiophene, or other species, becomes less important when a large part of the components has already been converted. Also, at these conditions the conversion of the inhibitors has increased, and the importance of the hydrogenation route, which probably has a stronger dependence on the hydrogen concentration, becomes more significant.

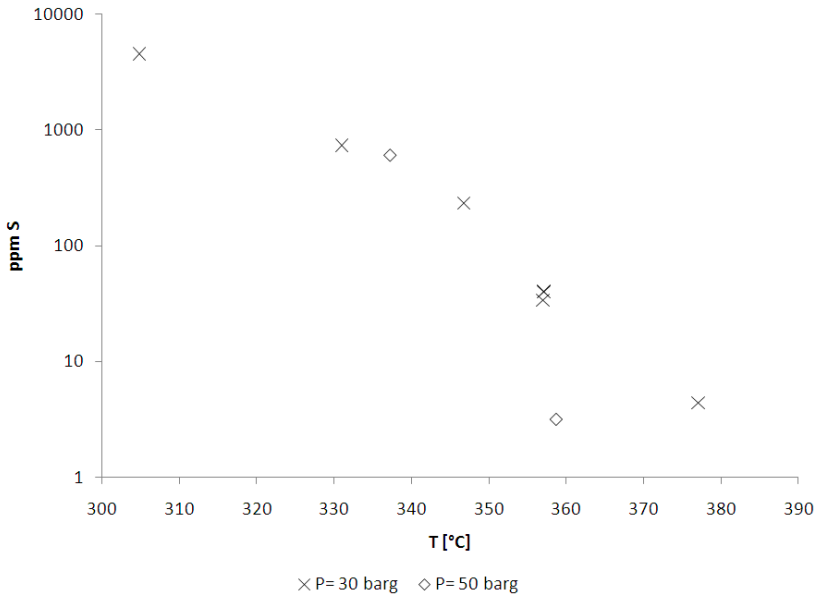

Figure 7.1: Sulfur concentration in the product after hydrotreating of Feed A in table 7.5. ($H_2/oil = 500\ Nl/l$ and $WHSV = 10\ hr^{-1}$)

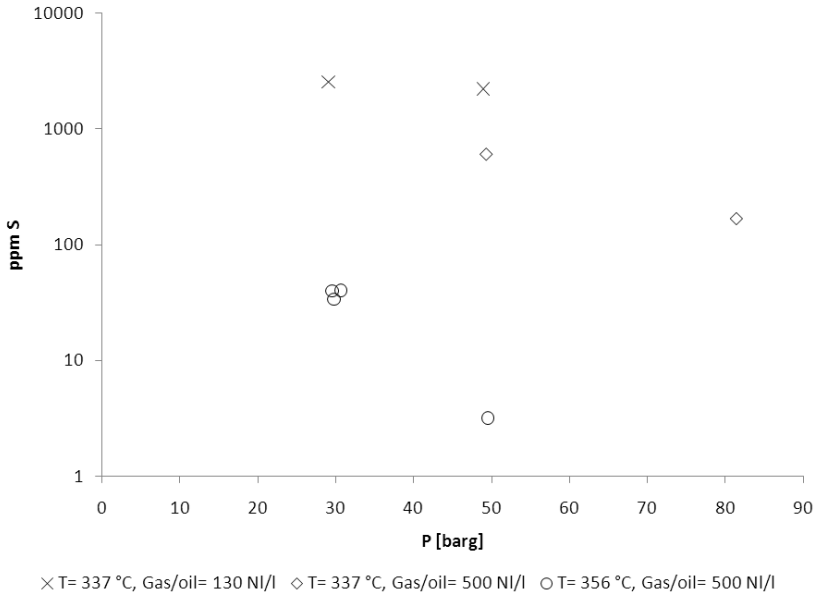

Figure 7.2: Sulfur concentration in the product after hydrotreating of Feed A in table 7.5. ($WHSV = 10\ hr^{-1}$)

7.5.3 Effect of gas-to-oil ratio

Figure 7.3 shows the effect of changing the gas-to-oil ratio on the conversion of 4,6-dimethyldibenzothiophene. At these conditions, the conversion of dibenzothiophene is close to 1 and is not affected by the hydrogen-to-oil ratio. Increasing the hydrogen-to-oil ratio from 120 to 480 Nl/l has a strong effect on the conversion of 4,6-dimethyldibenzothiophene, as it increases from 0.37 to 0.92. Increasing the hydrogen to oil ratio does not have a very large effect on the liquid phase mole fraction of hydrogen, which is practically constant. When increasing the hydrogen to oil ratio the vapor fraction increases, and the amount of oil compounds in the gas phase at equilibrium increases. Hoekstra [7] has observed an increase in the sulfur conversion with increasing gas-to-oil ratio at ULSD conditions. A possible reason for the increase in reaction rate, is that the liquid phase concentration of a heavy compound such as 4,6 dimethyldibenzothiophene increases because lighter hydrocarbons are stripped from the liquid. At the conditions applied here, the other sulfur compounds have already been completely converted, so a light compound such as benzothiophene is not affected in a negative way due to the high vaporization. Also the increase in the amount of hydrogen will lead to smaller concentrations of ammonia and hydrogen sulfide, thereby reducing the inhibiting effect.

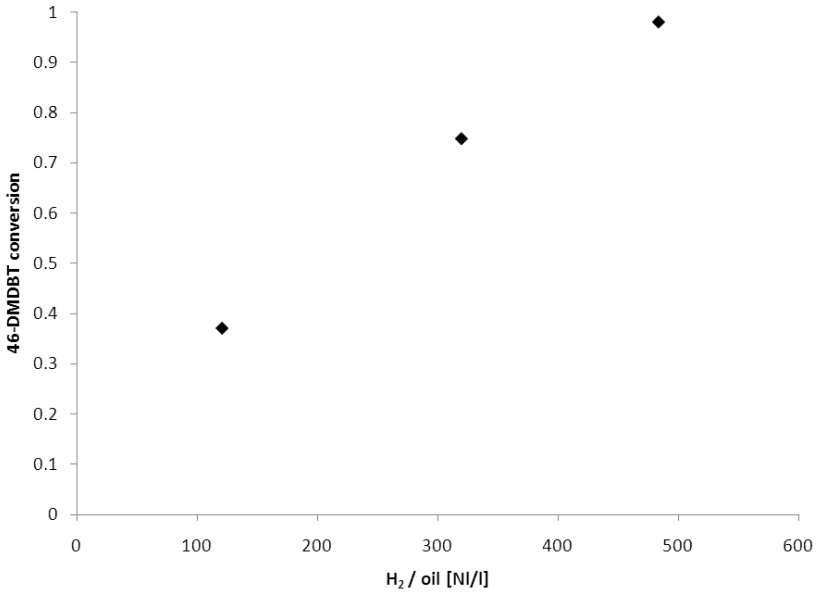

Figure 7.3: Conversion of 4,6-dimethyldibenzothiophene after hydrotreating of Feed B in table 7.5. Benzothiophene and dibenzothiophene have practically been completely desulfurized. ($P = 50\ barg$, 350 $°C$ and $WHSV = 5\ hr^{-1}$)

7.5.4 Reaction pathways

As has been illustrated previously, dibenzothiophenes react through either the DDS or the HYD route. The main product from the DDS route is biphenyl, while the main product from the HYD route is cyclohexylbenzene. Figure 7.4 shows how the product concentration of biphenyl and cyclohexylbenzene changes with the conversion of dibenzothiophenes. It is obvious that

the main product is biphenyl illustrating that the DDS pathways is the main reaction route. At very high conversions the biphenyl concentration decreases, while the cyclohexylbenzene concentration increases sharply. This is most likely because this happens at conditions, where the saturation of the mono-aromatic ring in biphenyl after sulfur removal from dibenzothiophene becomes significant.

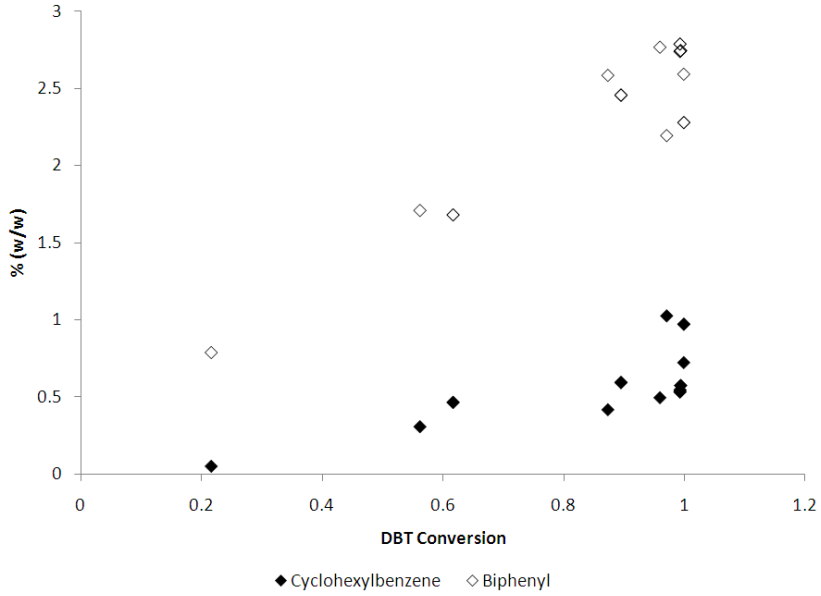

Figure 7.4: Product concentration of biphenyl and cyclohexylbenzene after hydrotreating of Feed A and B in table 7.5, as function of the conversion of dibenzothiophene (DBT). ($H_2/oil = 125 - 500\ Nl/l$, $T = 305 - 377\ °C$, $P = 30 - 80\ barg$, and $WHSV = 5 - 10\ hr^{-1}$)

7.5.5 Difference in reactivity between DBT and 4,6-DMDBT

One of the reasons that it is difficult to reach ULSD levels through hydrotreating are the difference in reactivity between the sulfur compounds present in the feed, since some of them are very refractive. Figure 7.5 shows a comparison between the conversion of a sterically hindered sulfur compound, 4,6-dimethyldibenzothiophene, and a non-sterically hindered compound, dibenzothiophene. As tetrahydrophenanthrene, a product from the hydrogenation of phenanthrene, has interfered with the determination of the dibenzothiophene concentrations, the calculated conversions for this compound are conservative, and probably lower than the actual conversion at some of the conditions. Nevertheless, the figure illustrates that the conversion of 4,6-dimethyldibenzothiophene is lower than that of dibenzothiophene. Except for one point where the dibenzothiophene conversion is approximately 0.5 it is above 0.8 at all the investigated conditions, whereas the conversion of 4,6-dimethyldibenzothiophene lies in between 0.2 and 1. This shows, that a significant part (above 80 %) of the dibenzothiophene has reacted before the reaction of 4,6-dimethyldibenzothiophene becomes important. A few experimental points show an observed conversion for 4,6-dimethyldibenzothiophene that is larger than for dibenzothiophene, but this should be assigned to uncertainties in the dibenzothiophene con-

version. Since the conversions have been measured at different temperatures, pressures and gas-to-oil ratios, it is difficult to see any direct correlation between the two conversions. Both compounds react through two parallel pathways, DDS or HYD, and since the pathways are affected differently by changing the conditions, the relative reactivity is not constant, which is why, there is no direct correlation. However it is clear, that the 4,6-dimethyldibenzothiophene is less reactive than dibenzothiophene, and that at the investigated conditions, the rate of 4,6-dimethyldibenzthiophene removal changes more than the rate of dibenzothiophene removal.

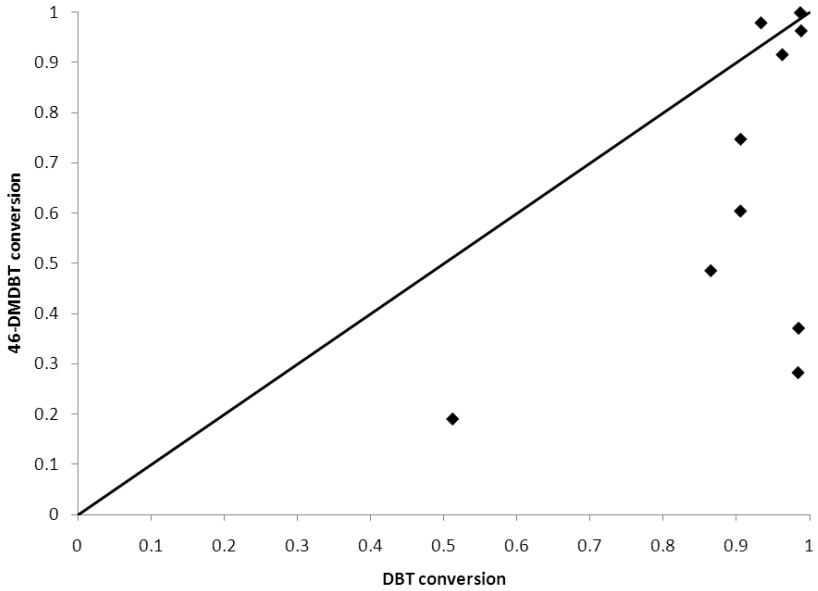

Figure 7.5: Conversion 4,6-dimethyldibenzothiophene (46-DMDBT) after hydrotreating of Feed B in table 7.5, as function of the conversion of dibenzothiophene (DBT). ($H_2/oil = 125 - 500\ Nl/l$, $T = 330 - 359\ °C$, $P = 30 - 80\ barg$, and $WHSV = 10\ hr^{-1}$)

7.6 Hydrodearomatization

7.6.1 Effect of temperature

The liquid products have been analyzed for the total amount of mono-, di- and tri-aromatics present. Figure 7.6 shows the effect of temperature on the product concentration of the different aromatic groups. The total aromatics content is decreasing slightly with increasing temperature from 26.7 % to 25.6 %. Inititally the monoaromatics concentration is increasing, but then it goes through a maximum and starts to decrease. The opposite is the case for both the di- and tri-aromatics, where a minimum is observed. The reason for the minimum in concentrations for the di-and tri-aromatics is a limitation due to the equilibrium being moved towards the aromatic compounds when the temperature is increased.

The maximum in the mono-aromatics concentration is observed because a significant amount of mono-aromatics is formed as a product from the reaction of the di- and tri-aromatics. Although the conversion is relatively low, some of the mono-aromatics are converted into naph-

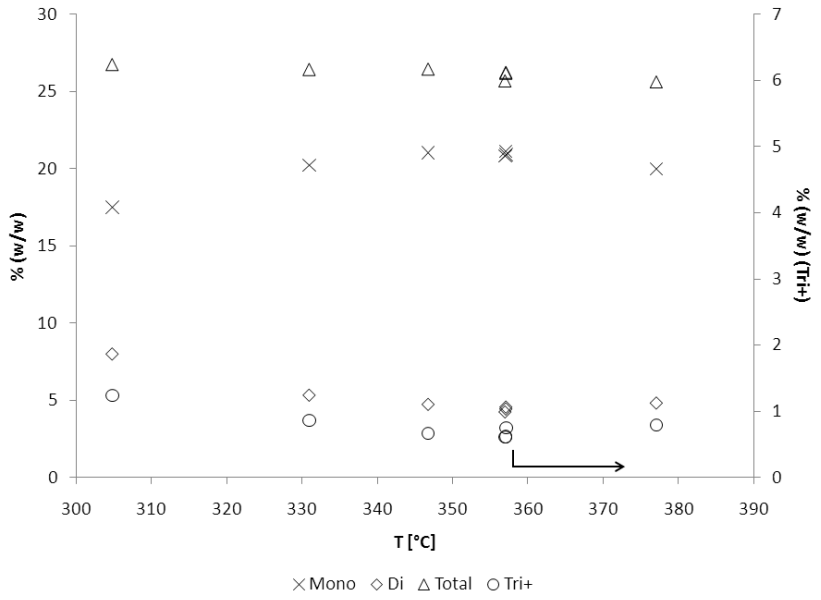

Figure 7.6: Concentration of aromatics in the product after hydrotreating of Feed A in table 7.5. There is a maximum in the mono-aromatics concentration, and minima in the concentration of di- and tri-aromatics. ($P = 30\ barg$, $H_2/oil = 500\ Nl/l$ and $WHSV = 10\ hr^{-1}$)

thenes. This is illustrated in figure 7.7 which shows the conversion of 3 individual compounds present in the feed. At the lowest temperatures, the calculated pentylbenzene conversion is negative, which is most likely due to the uncertainty in determining the concentration of pentylbenzene, but as the temperature increases, the conversion increases up to 3.7 % at 377 °C. Both napthalene and phenanthrene experience a maximum that is located at around 360 °C.

Since the hydrogenation reactions are reversible, it is possible for naphthenic compounds to dehydrogenate to aromatic compounds, in the process releasing hydrogen. As illustrated in figure 7.8, the concentration of butylbenzene in the product increases with temperature, while the butylcyclohexane concentration decreases. But the conversion of butylcyclohexane is less than 1 % at all the investigated conditions, showing that the dehydrogenation of a naphthene is negligible at the investigated condition.

Figure 7.7 and 7.8 show that the hydrogenation of a mono-aromatic (pentylbenzene) to a mono-naphthene (pentylcyclohexane) and the similar but reverse reaction of butylcyclohexane to butyl benzene are quite slow.

Table 7.6.1 shows a comparison of the conversion of pentylbenzene and butylcyclohexane, which are compounds present in the feed, that are not formed by other reactions. Although the product concentrations are determined from several GC chromatograms, there are some uncertainties and scattering in the values. At temperatures below 340 °C small (< 0.01) negative conversions were seen for both pentylbenzene and butylcyclohexane, which suggest that the measured product concentrations are a little too high. One reason could be the loss of a small fraction of the liquid phase leaving with the gas phase at the reactor outlet, but this would be such a small amount, that it is negligible. The difference in product and feed concentrations is still less than 1 % and it shows, that no reaction is taking place at low temperatures. But at

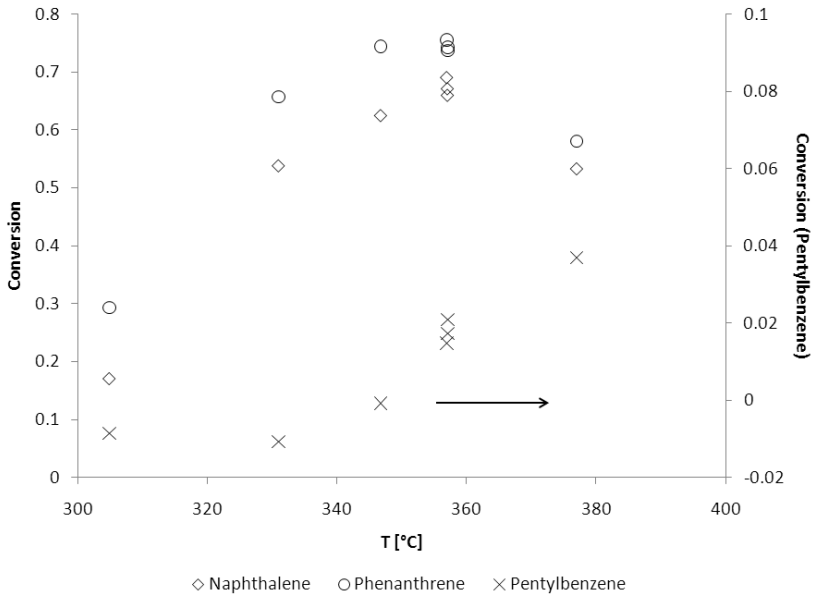

Figure 7.7: Conversion of pentylbenzene, naphthalene and phenanthrene after hydrotreating of Feed A in table 7.5. ($P = 30\ barg$, $H_2/oil = 500\ Nl/l$ and $WHSV = 10hr^{-1}$)

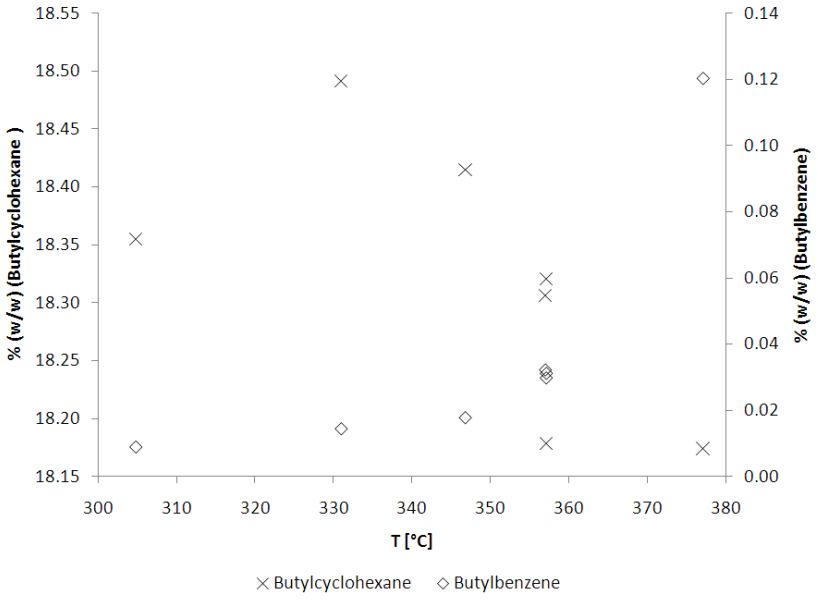

Figure 7.8: Product concentrations of butylcyclohexane and butylbenzene after hydrotreating of Feed A in table 7.5. ($P = 30\ barg$, $H_2/oil = 500\ Nl/l$ and $WHSV = 10hr^{-1}$)

higher temperatures it is clear from table 7.6.1 that hydrogenation of pentylbenzene is faster than the dehydrogenation of butylcyclohexane. At high temperatures the thermodynamic equilibrium will favor the aromatic compound, provided that the hydrogen concentration is low enough. That the hydrogenation of pentylbenzene is taking place at all, shows that the reaction has not reached equilibrium. The dehydrogenation of butylcyclohexane is also not limited by equilibrium, and the lower conversion is probably due to a lower adsorption constant and reactivity for naphthenes, than for mono-aromatics. A weak adsorption for butylcyclohexane means that other compounds are more likely to adsorp on the active sites of the catalyst, and thereby lead to a low apparent reaction rate.

Table 7.11: Conversion of pentylbenzene and butylcyclohexane after hydrotreating of Feed A in table 7.5. ($P = 30\ barg$, $H_2/oil = 500\ Nl/l$ and $WHSV = 10hr^{-1}$)

T [°C]	Pentylbenzene	Butylcyclohexane
347	≈0	≈0
357	0.0177	0.0023
377	0.0369	0.0075

7.6.2 Effect of pressure

Figure 7.9 shows the effect of changing the pressure on the conversion of the aromatics. The conversion of naphthalene and phenanthrene are very similar, and increasing the pressure results in an increase in the conversion. At the highest pressure, they are practically completely transformed, as the conversion is above 0.98. It appears that increasing the pressure from 29 to 48 barg results in a decrease in the conversion of pentylbenzene. The reason for this is likely to be because the measured temperature at the middle pressure (48 barg) was 5-7 °C lower than, at the two other pressures. At the highest pressure the pentylbenzene conversion is 0.25 which is high for this otherwise slow reacting compound. The main reason seems to be that other compounds, inhibiting the conversion, have been almost completely removed. These compounds could be the di- and triaromatics or the nitrogen compounds. At the highest pressure the total nitrogen conversion is above 0.99.

7.6.3 Effect of gas-to-oil ratio

The effect of the amount of hydrogen on the conversion of the three aromatic compounds, pentylbenzene, naphthalene and phenanthrene, is illustrated in figure 7.10. It can be seen that the conversion of pentylbenzene is practically constant as the hydrogen to oil ratio increases from 120 to 480 Nl/l. The effect is strongest on the triaromatic phenanthrene, as the conversion increases from 0.72 to 0.95. It also appears that the increased hydrogen flow results in an increased conversion, when increasing the gas-to-oil ratio from 120 to 320 Nl/l for both naphthalene and phenanthrene, but the conversion does not seem to be affected much when going from 300 to 480 Nl/l. For naphtalene, the reason might be an increased vaporization and

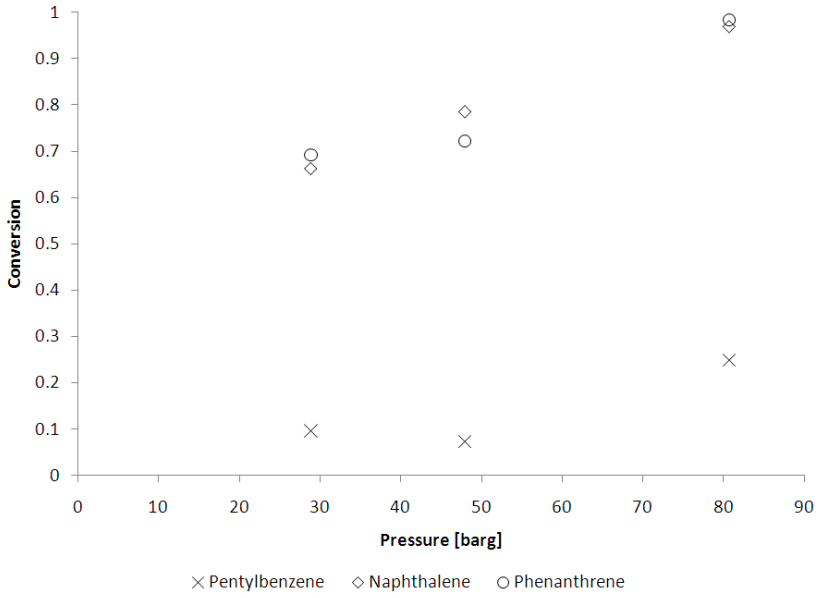

Figure 7.9: Conversion of pentylbenzene, naphthalene and phenanthrene after hydrotreating of Feed B in table 7.5. ($H_2/oil = 125\ Nl/l$, $T = 350\ °C$ and $WHSV = 5hr^{-1}$)

a decrease in the liquid phase concentration, as is seen in table 7.10, which is the opposite effect of what was observed for 4,6-dimethyldibenzothiophene. But this is not the case for the heavier compound phenanthrene, which experiences an increase in the liquid phase mole fraction.

7.7 Hydrodenitrogenation

7.7.1 Effect of temperature

Figure 7.11 shows the nitrogen content of the product as a function of the temperature at 2 different pressures. As the temperature increases, more and more nitrogen is removed. Similar to the hydrodesulfurization, it appears that the effect of increasing the temperature is stronger at the highest pressure. At a pressure of 30 barg the hydrodenitrogenation is not very sensitive towards a temperature change, increasing the temperature from 304 to 377 °C, results in a decrease in the concentration from 206 to 89 ppm N, but at a pressure of 50 barg the nitrogen content of the product is reduced from 70 to 1 ppm N by increasing the temperature from 337 to 359 °C. Comparing with figure 7.1, it can be seen, that the nitrogen compounds are much less reactive than the sulfur compounds in feed A (benzothiophene and dibenzothiophene).

7.7.2 Effect of pressure

Increasing the pressure results in an increase in the nitrogen conversion as is illustrated in figure 7.12. The main reason for the increase is a higher liquid phase concentration (and partial pressure) of hydrogen at higher pressures. The increase from 50 barg to 80 barg has a very strong effect on the nitrogen removal and the result is a complete removal of nitrogen, since the product concentration is less than 1 ppm. The reason that increasing the pressure from 30 to 50 barg

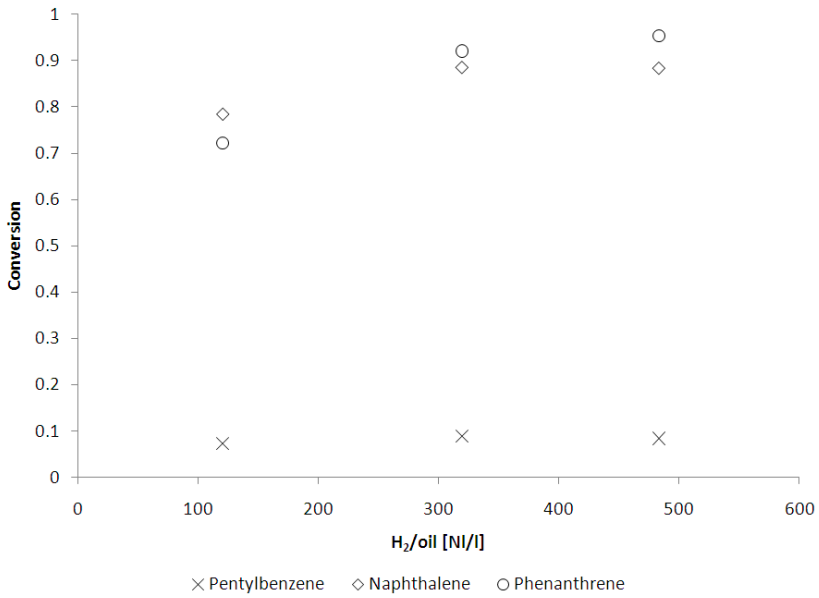

Figure 7.10: Conversion of pentylbenzene, naphthalene and phenanthrene after hydrotreating of Feed B in table 7.5. ($P = 50\ barg$, $T = 350\ ^{\circ}C$ and $WHSV = 5hr^{-1}$)

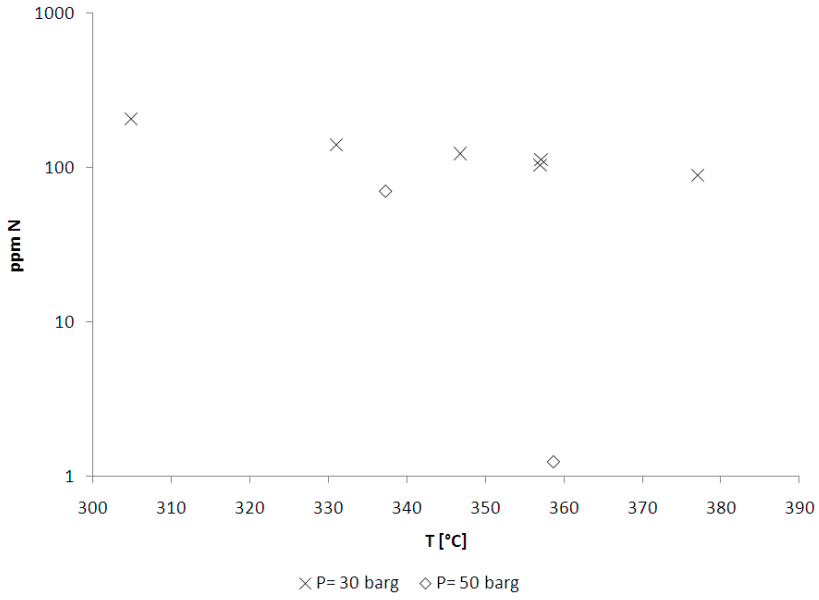

Figure 7.11: Nitrogen concentration in the product after hydrotreating of Feed A in table 7.5. ($H_2/oil = 500\ Nl/l$ and $WHSV = 10\ hr^{-1}$)

only decrease the product concentration from 92 to 74 ppm N is quite possibly because the less reactive acridine has to be removed before reaction of the faster reacting 1,4-dimethylcarbazole can take place.

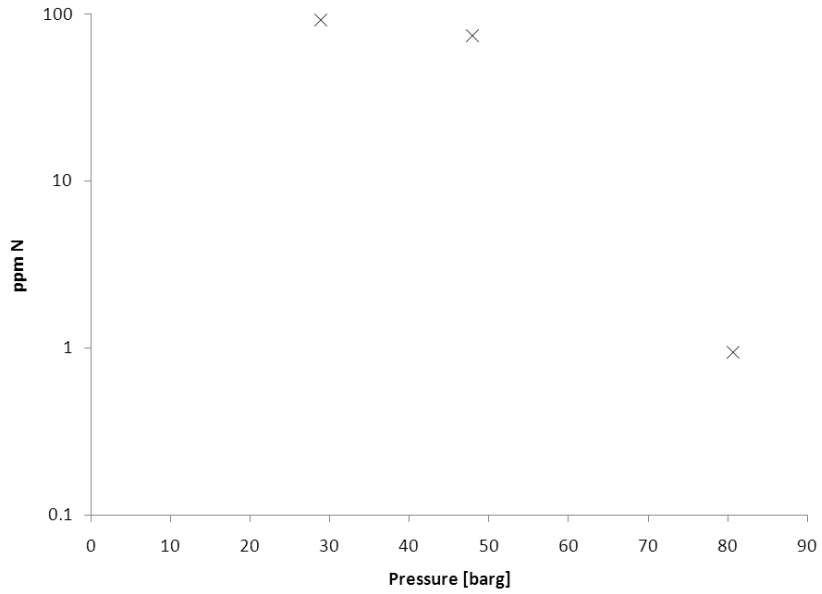

Figure 7.12: Nitrogen concentration in the product after hydrotreating of Feed B in table 7.5. ($H_2/oil = 125\ Nl/l$, $T = 350\ ^{\circ}C$ and $WHSV = 5hr^{-1}$)

7.7.3 Effect of gas-to-oil ratio

Figure 7.13 shows the total nitrogen product concentration at 2 different temperatures. Increasing the hydrogen flow has a positive effect on the nitrogen conversion. At the lowest hydrogen to oil ratio, the product concentrations at the two temperatures are almost the same. This might be due to uncertainties in the analysis, but as figure 7.11 showed, at some conditions the hydrodenitrogenation rate does not change very much with temperature. If this is the case, figure 7.13 shows that the effect of the hydrogen to oil ratio on the hydrodenitrogenation is larger at the highest temperature.

7.7.4 Comparison of reactivities

3-methylindole is the most reactive of the nitrogen compounds, and practically all nitrogen is removed from this compound at all the investigated conditions. It has previously been shown, in chapter 6, how acridine is an inhibitor for the hydrodenitrogenation of 1,4-dimethylcarbazole. This has been illustrated in figure 7.14, that shows the amount of nitrogen present as 1,4-dimethyldibenzothiophene as function of the total amount of nitrogen. It shows, that as the total amount of nitrogen is reduced from around 230 to around 150 ppm N, corresponding to a 35 % of the in the total nitrogen, only 20 % of the 1,4-dimethylcarbazole has reacted. As the total nitrogen concentration decreases and becomes lower than 150 ppm N, the 1,4-dimethylcarbazole nitrogen concentration is approaching the total nitrogen concentration. The figure shows, that

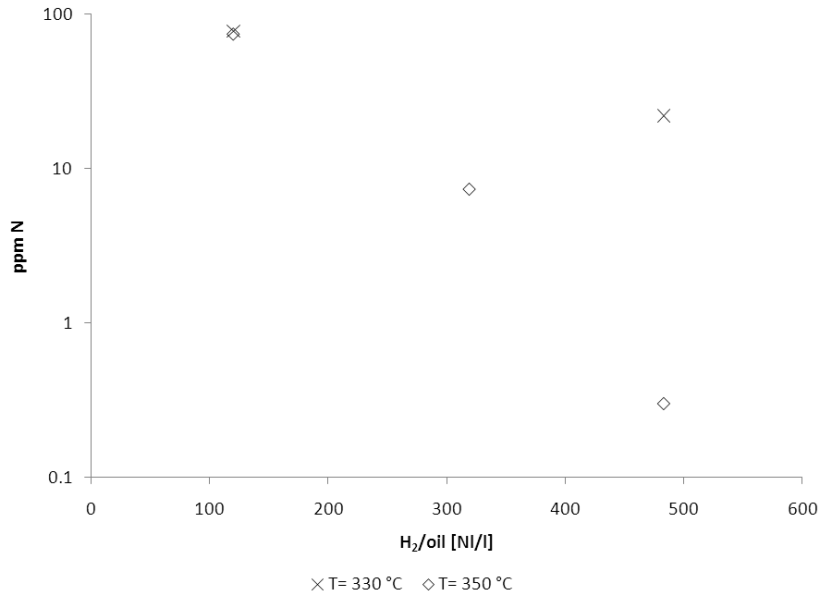

Figure 7.13: Nitrogen concentration in the product after hydrotreating of Feed B in table 7.5. ($P = 50\ barg$ and $WHSV = 5\ hr^{-1}$)

the carbazole is the main remaining nitrogen compound, because the presence of the basic compound acridine limits the conversion. When most of the acridine has been removed the 1,4-dimethylcarbazole will react more rapidly.

7.8 Conclusion

The effect of temperature, pressure and hydrogen to oil ratio on the hydrotreating of a model diesel mixture has been investigated.

Benzothiophene was the most reactive of the sulfur compounds, and was completely desulfurized at all the investigated conditions. The conversion of the sulfur compounds, dibenzothiophene and 4,6-dimethyldibenzothiophene increased with increasing temperature, pressure and hydrogen to oil ratio. When increasing the pressure the liquid feed hydrogen concentration increases, which is responsible for the higher conversion. A higher conversion of nitrogen compounds, that act as inhibitors for hydrogenation reactions, will have increase the reaction rate. When the gas-to-oil ratio is increased, the liquid phase mole fraction of hydrogen is almost constant, but due to evaporation of the lighter liquid phase components, the liquid phase concentration of the heavy sulfur compounds increases. Furthermore it is likely, that the inhibiting effect of gaseous compounds such as hydrogen sulfide and ammonia is reduced. As expected, the reactivity of 4,6-dimethyldibenzothiophene was lower than for dibenzothiophene due to the sterical hindrance. At the investigated conditions there is no obvious correlation between the conversion of dibenzothiophene and of 4,6-dimethyldibenzothiophene.

When increasing the temperature, a maximum is observed in the concentration of a diaromatic, naphthalene, and a triaromatic, phenanthrene. The reason for this is that, the exothermic

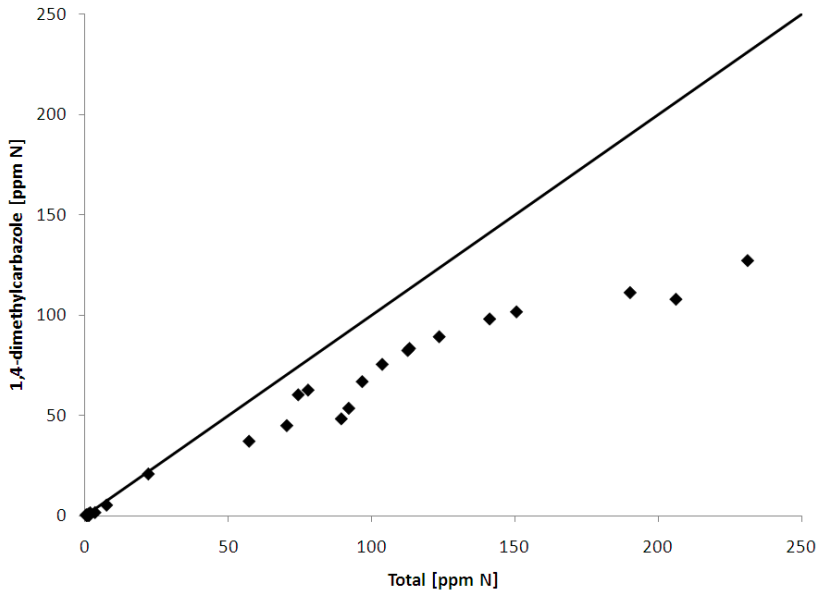

Figure 7.14: 1,4-dimethylcarbazole concentration after hydrotreating of Feed A and B in table 7.5, as function of the total nitrogen concentration. ($H_2/oil = 125 - 500\ Nl/l$, $T = 305 - 377\ °C$, $P = 30 - 80\ barg$, and $WHSV = 5 - 10\ hr^{-1}$)

hydrogenation reactions becomes limited by thermodynamic equilibrium at high temperatures. It has been shown, that the reactivity of a monoaromatic compound, pentylbenzene, is significantly smaller than of di- and tri-aromatics. Because of the low reactivity, no maximum is observed in the conversion of pentylbenzene as the reaction is far from equilibirium. A maximum is observed in the total concentration of monoaromatics, since the primary products from the hydrogen of diaromatics are monoaromatics. The aromatics hydrogenation reactions are known to be reversible, but the reaction of a butylcyclohexane, a mononaphthene, to butylbenzene have been shown to be negligible.

Three different nitrogen compounds were present in the mixture, and practically all nitrogen was removed from the most reactive of the three, 3-methylindole. The last of the nitrogen compounds to be removed was 1,4-dimethylcarbazole. The total nitrogen concentration decreased with increasing temperature, pressure and hydrogen to oil ratio.

Chapter 8

Mathematical Model of a Trickle-bed Hydrotreater

In this chapter the mathematical model of an isothermal trickle-bed reactor is described in detail. First of all the equations describing the concentration profiles inside the catalyst pellets is given. By solving these equations, the apparent reaction can be calculated. The model for the individual catalyst pellets is coupled to a model for the entire fix-bed reactor. The fix-bed reactor model contains mass balance equations for both the liquid phase and the gas phase.

Methods for estimating physical properties that are needed in the model, such as density, viscosity, diffusion and mass transfer coefficients, is presented.

8.1 Model of a catalyst pellet

For a number of hydrotreating reactions, the rate can be so fast, that diffusion inside the catalyst pellets can become rate limiting. Therefore it is necessary to have a model for a single pellet, that can be used to calculate the apparent rate of reaction. For simplicity it is assumed that the pellet is spherical, with a radius R_p. The concentration of a component k is a function of the distance from the center of the pellet, r. In general the steady state concentration can be described by the following differential equation:

$$D_{e,k}\frac{d}{dr}\left(r^2\frac{dc_k}{dr}\right) - r^2 R_k(\underline{c}) = 0 \tag{8.1}$$

c_k is the concentration, $D_{e,k}$ is the effective diffusion coefficient and $R_k(\underline{c})$ the rate of consumption of component k in moles / second per m^3 of the catalyst pellet. The reaction rate is given by the following expression:

$$R_k(\underline{c}) = -\rho_p \cdot \sum_{m=1}^{NR} \nu_{km} \cdot r'_m(\underline{c}) \tag{8.2}$$

Here NR is the number of reactions, ν_{km} is the stoichiometric coefficient of component k in reaction m (negative for reactants, positive for products and zero if component k is not part of the reaction), and r'_m is the rate of reaction m in $\frac{mol}{s \cdot kg\ cat.}$. ρ_p is the density of the catalyst pellet, so the unit of $R_k(\underline{c})$ becomes $\frac{mol}{m^3 \cdot s}$. The differential equation (8.1) can be rewritten as:

$$D_{e,k} \cdot \left[r^2 \frac{d^2 c_k}{dr^2} + 2r \frac{dc_k}{dr} \right] - r^2 \cdot R_k(\underline{c}) = 0 \tag{8.3}$$

Since the concentration profile has to be symmetrical around the center of the pellet the first derivative of the concentration must be 0 at $r = 0$. Furthermore it is assumed that the surface concentration, $c_{k,0}$, of the component is known. Thus the two necessary boundary conditions becomes:

$$B.C.\ \ 1 : r = 0 \qquad \frac{dc_k}{dr} = 0 \tag{8.4}$$

$$B.C.\ \ 2 : r = R_p \qquad c_k = c_{k,0} \tag{8.5}$$

The variables $x = \frac{r}{R_p}$ and $y_k = \frac{c_k}{c_0}$ can be introduced in equation (8.3) to make it dimensionless. c_0 is a reference concentration for example one of the surface concentrations:

$$x^2 \frac{d^2 y_k}{dx^2} + 2x \frac{dy_k}{dx} - \phi_k^2 x^2 \cdot \rho_k(\underline{y}) = 0 \tag{8.6}$$

Here $\phi_k = \sqrt{\frac{R_p^2 R_k(\underline{c}_0)}{D_{e,k} c_0}}$ is the Thiele modulus for the component and $R_k(\underline{c}_0)$ is the reaction rate at a set of reference conditions, in this case the surface conditions. The Thiele modulus is a measure of how fast the reaction rate of a component is compared to the diffusion rate. $\rho_k(\underline{y})$ is a dimensionless reaction rate defined as $\rho_k(\underline{y}) = \frac{R_k}{R_k(\underline{c}_0)}$. The corresponding boundary conditions for the dimensionless model are:

$$B.C.\ \ 1 : x = 0 \qquad \frac{dy_k}{dx} = 0 \tag{8.7}$$

$$B.C.\ \ 2 : x = 1 \qquad y_k = y_{k,0} \tag{8.8}$$

where $y_{k,0} = \frac{c_{k,0}}{c_0}$. When more than one component / reactant is present a set of coupled second order differential equations has to be solved. This is done numerically by using an optimal collocation method given by Villadsen and Michelsen [62]. Further details of the solution are given in appendix C.

8.1.1 Calculation of apparent rate

The reactions inside the catalyst pellet may be limited by diffusion, and thus the apparent reaction rate observed in the reactor will often be different from what it would be if it occurred at bulk conditions. The purpose of setting up a model for the concentration inside a catalyst pellet is to be able to calculate the apparent reaction rate at a given surface concentration. For a given surface concentration the concentration profile inside the catalyst pellet can be

determined by solving equation (8.6). From the solution the apparent reaction rate can be determined by evaluating the following integral:

$$R_{k,app} = \frac{\int_0^{R_p} R_k(r) \cdot 4\pi r^2 dr}{\frac{4}{3}\pi R_p^3} \tag{8.9}$$

$$= \frac{\int_0^1 R_k(x) \cdot 4\pi x^2 R_p^3 dx}{\frac{4}{3}\pi R_p^3} \tag{8.10}$$

$$\tag{8.11}$$

The integral is evaluated numerically using a quadrature method [62], and the apparent rate is used in the model for the entire reactor.

8.2 Fixed bed reactor model

In this section a steady state model for the entire reactor is presented. An illustration of the reactor is shown in figure 8.1. Two streams are entering at the top of the reactor, one liquid oil stream and one gas stream consisting mainly of hydrogen. It is assumed that there is plug flow in the reactor, which means that both the gas and liquid velocity (in m/s) does not change across the reactor. Furthermore the linear gas and liquid velocity is assumed to be constant down through the reactor. Reaction only occurs in the catalyst pellets and not in the gas or liquid phase.

Mass transfer from the gas to the liquid phase, and from the liquid phase to the surface of the catalyst particles is described by using a mass transfer coefficient for transport through the film layers. Transport through the gas film layer is considered to be very fast compared to the transport through the liquid film layer, and thus it is assumed that there is equilibrium between the gas and the liquid at the gas-liquid interface. The molar flux, N_k $[\frac{mol}{m^2 \cdot s}]$ from gas to liquid is then given by:

$$N_{k,LG} = k_{k,LG} \cdot (c_k^{eq} - c_k^L) \tag{8.12}$$

and from the liquid to the surface of the catalyst particles

$$N_{k,LS} = k_{k,LS} \cdot (c_k^L - c_k^S) \tag{8.13}$$

The unit of the mass transfer coefficients $k_{k,LG}$ and $k_{k,LS}$ are $\frac{m}{s}$. A stationary mass balance for component k in the liquid phase gives:

$$u_L \frac{dc_k^L}{dl} = k_{k,LG} \cdot a_{LG} \cdot (c_k^{eq} - c_k^L) - k_{k,LS} \cdot a_{LS} \cdot (c_k^L - c_k^S) \tag{8.14}$$

l is the position in the reactor, u_L is the superficial liquid velocity, a_{LG} and a_{LS} are the contact area per unit volume between gas and liquid and liquid and solid respectively. c_k^{eq} is the

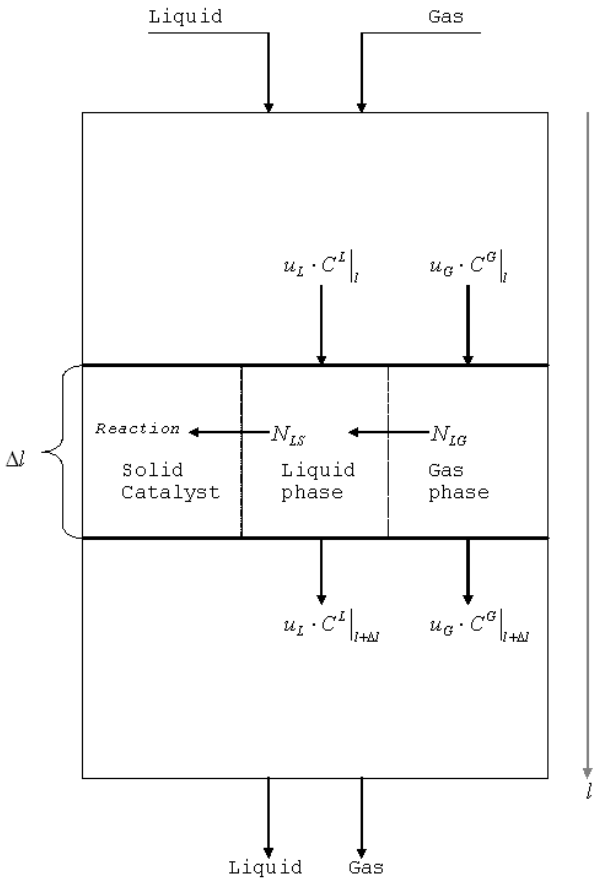

Figure 8.1: Illustration of the reactor and the inlet and outlet streams

concentration at the gas-liquid interface. A stationary mass balance for component k in the gas phase yields:

$$u_G \frac{dc_k^G}{dl} = -k_{k,LG} \cdot a_{LG} \cdot (c_k^{eq} - c_k^L) \tag{8.15}$$

u_G is the superficial gas velocity. Figure 8.2 illustrates how the concentration of a reactant (for instance H_2) is changing in the different phases at a certain point in the reactor. The relevant concentrations c_k^{eq}, c^S, c^L, c_k^{eq} and c^G is also shown.

Introducing the dimensionless reactor length $z = \frac{l}{L}$ and rearranging yields the following two first order differential equations:

$$\frac{dc_k^L}{dz} = \frac{L}{u_L} \left[k_{k,LG} \cdot a_{LG} \cdot (c_k^{eq} - c_k^L) - k_{k,LS} \cdot a_{LS} \cdot (c_k^L - c_k^S) \right] \tag{8.16}$$

$$\frac{dc_k^G}{dz} = -\frac{L}{u_G} \cdot k_{k,LG} \cdot a_{LG} \cdot (c_k^{eq} - c_k^L) \tag{8.17}$$

The flux of component k from the liquid phase to the surface of the catalyst has to be equal

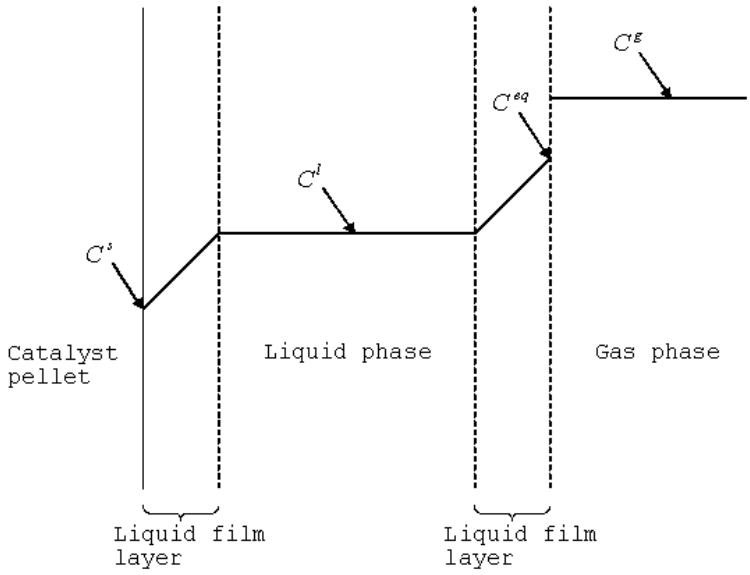

Figure 8.2: Illustration of the concentration of a reactant in the different phases

to the rate at which the component is consumed in the pellet. Thus the following algebraic equation has to hold.

$$0 = k_{k,LS} \cdot a_{LS} \cdot (c_k^L - c_k^S) - R_{k,app}(c_k^S) \cdot (1 - \epsilon_{bed}) \tag{8.18}$$

ϵ_{bed} is the porosity of the catalyst bed, and the expression $(1 - \epsilon_{bed})$ is the volume of catalyst per volume of reactor.

This addition of this equation means that the model for the reactor is a system of differential and algebraic equations (DAE). If C components are considered there will be $2C$ differential equations and C algebraic equations.

8.2.1 Initial conditions

In order to solve the system of equations a set of initial conditions has to be specified. It will be assumed that there is physical equilibrium between the gas and the liquid at the inlet of the reactor. These are determined by doing a flash calculation of the entering feed mixture.

The concentrations at the surface of the catalyst are still unknown, but these can be calculated from the liquid phase concentrations by solving the algebraic equations (equation (8.18)).

When dealing with trickle-bed reactors the reaction times is often expressed in terms of WHSV^{-1} or LHSV^{-1}. The relation between z and WHSV^{-1} and LHSV^{-1} is:

$$WHSV^{-1} = \frac{zL \cdot A_{reactor} \cdot \rho_{bed}}{L_0} \tag{8.19}$$

$$LHSV^{-1} = \frac{zL \cdot A_{reactor}}{L_0 \cdot \rho_L} \tag{8.20}$$

Here $A_{reactor}$ is the cross section area of the reactor, ρ_{bed} is the density of the catalyst bed (kg

cat./ m^3 reactor), ρ_L is the density of the liquid feed and L_0 is the liquid feed flow rate in kg/h.

8.3 Estimation of physical parameters for the model

The models for the pellet and for the reactor contain some physical parameters that need to be estimated. This can be done by using correlations, or by fitting to experimental data. In this section some correlations are presented, and methods for calculating some parameters are shown.

8.3.1 Estimation of diffusion coefficients

It is necessary to estimate values for liquid phase diffusion coefficients since these are used to calculate effective diffusion coefficients in the catalyst pellets. Furhtermore they are needed when estimating mass transfer coefficients. A reasonable assumption is to use infinite dilution diffusion coefficients, which can be estimated using the following correlation suggested by Wilke and Chang [57]:

$$D_k = 7.4 \cdot 10^{-8} \frac{(\phi M_L)^{1/2} T}{\mu_L v_k^{0.6}} \tag{8.21}$$

ϕ is a dimensionless association factor, that is set to 1.0 for a non-associating solvent. The unit of D_k is cm^2/s. T is the temperature in K, μ_L is the viscosity of the solvent in mPa·s, M_L is the molar weight of the solvent in g/mol and v_k are the molar volume of the solute at the normal boiling point. This can be estimated from the critical volumes using the following correlation:

$$v = 0.285 \cdot v_c^{1.048} \tag{8.22}$$

v and v_c are in cm^3/mol. The viscosity (in $mPa \cdot s$) of a liquid hydrocarbon mixture can be calculated from this correlation:

$$\mu_L = 3.141 \cdot 10^{10} \cdot (1.8 \cdot T - 460)^{-3.444} \cdot [\log(API)]^a \tag{8.23}$$

where a is given by

$$a = 10.313 \cdot [\log(1.8 \cdot T - 460)] - 36.447 \tag{8.24}$$

T is the temperature in K. The API gravity can be calculated as [63]:

$$API = \frac{141.5}{\gamma_0} - 131.5 \tag{8.25}$$

where the specific gravity, γ_0, can be calculated from the mixture density , ρ_0, and the density of water, ρ_{H_2O}, at 60 ° F (15.56 °C) as

$$\gamma_0 = \frac{\rho_0}{\rho_{H_2O}} \tag{8.26}$$

Any pressure dependency of the viscosity will be neglected.

If the size of the diffusing molecules is considerably smaller than the pores in the catalyst pellets, then the effective diffusion coefficient can be calculated using the infinite dilution coefficient, the porosity, ϵ_p, and the tortuosity, τ_p [64]:

$$D_{k,e} = D_k \frac{\epsilon_p}{\tau_p} \tag{8.27}$$

A value of $\epsilon_p = 0.60$ and of the tortuosity $\tau_p = 3$ are assumed in this project. If the size of the diffusing molecules is comparable to the size of the pores, then the effective diffusion coefficient is a function of the Stokes radius of the molecule and the pore radius. An empirical expression is given by Tsai et al. [65]. If λ_k is equal to the ratio of the molecule and the pore diameter ($d_{molecule}/d_{pore}$), then the effective diffusion coefficient can be estimated from the following expression if $\lambda_i \leq 2$:

$$D_{k,e} = D_k(1 - \lambda_k)^4 \cdot \frac{\epsilon_p}{\tau_p} \tag{8.28}$$

If the size of the pores is considerably larger than the molecules then λ approaches 0, and equation (8.28) reduces to equation (8.27).

8.3.2 Mass transfer coefficients

For the reactor model estimates of the mass transfer coefficients for all the compounds are needed. This includes both the gas-liquid mass transfer coefficient and the liquid-solid mass transfer coefficient. Correlations for these are suggested by Korsten and Hoffmann [66] and these will be used here.

8.3.2.1 Gas-liquid mass transfer coefficient

The gas-liquid mass transfer coefficient can be calculated from a correlation given by Goto and Smith [29]. They carried out experiments with three different particle sizes. They found that the product $k_{k,LG}a_{LG}$ was independent of the gas flow rate, and used a correlation of the following form:

$$\frac{k_{k,LG}a_{LG}}{D_k} = \alpha_L \left(\frac{G_L}{\mu_L}\right)^{n_L} \left(\frac{\mu_L}{\rho_L D_k}\right)^{0.5} \tag{8.29}$$

G_L is the superficial mass velocity of the liquid in $\frac{kg}{cm^2 \cdot s}$. The viscosity and the diffusion coefficient can be estimated using correlations. The parameters α_L and n_L are dependent on

the diameter of the particles. The values at different particle sizes are listed in table 8.1. The values suggest that n_L is almost independent of the particle size and have a value around 0.40. This value will be used in this case. The value of α_L can be estimated roughly by interpolation. It should be noted that two of the particle types used by Goto and Smith [29] had diameters that are considerably larger than what is used in this project. From the values in table 8.1 one would assume that the value for particles with diameter 600-850μm probably lie in the region of 7 to 8, thus the value for the smallest particles, 7.8, will be used. The expression shows that increasing the superficial liquid velocity will increase the mass transfer rate, which means that if the liquid feed flow is increased then the mass transfer rate is also increased.

Particles	diameter [cm]	$\alpha_L[cm^{n_L-2}]$	n_L
Glass beads	0.413	2.8	0.40
CuO·ZnO	0.291	6.0	0.41
CuO·ZnO	0.0541	7.8	0.39

Table 8.1: Parameters determined by Goto and Smith for their correlation [29]

8.3.2.2 Liquid-solid mass transfer coefficient

The liquid-solid mass transfer coefficient in the low interaction regime can be calculated from a correlation given by van Krevelen and Krekels as given in [30]. This correlation also shows that the mass transfer coefficient is independent of the gas flow rate.

$$\frac{k_{LS}}{D_k \cdot a_S} = 1.8 \left(\frac{G_L}{a_S \cdot \mu_L} \right)^{1/2} \left(\frac{\mu_L}{\rho_L D_k} \right)^{1/3} \tag{8.30}$$

a_S is the specific surface area of the packing. This can be calculated from the equivalent particle diameter, d_p, and the void fraction of the bed, ϵ_{bed}:

$$a_S = \frac{6}{d_p}(1 - \epsilon_{bed}) \tag{8.31}$$

This correlation also shows that increasing the superficial liquid velocity will increase the mass transfer coefficient.

8.4 Phase equilibrium calculations

A typical industrial hydrotreater is operated at conditions where two fluid phases, a gas- and a liquid-phase, exists. In order to model, and to understand the behavior of a hydrotreater at different conditions, it is necessary to perform phase equilibrium calculations. In this work the Soave-Redlich-Kwong (SRK) equation of state is used to calculate equilibrium compositions of the gas and the liquid phase. SRK is a cubic equation of state, and the relation between pressure, P, temperature, T, and molar volume, V_m, is [67]:

$$P = \frac{RT}{V_m - b} - \frac{a}{V_m(V_m + b)} \tag{8.32}$$

The parameter a is related to interaction energy between different molecules, while b is related to the molecular volume. When applied to a single compound, the parameters a and b are given by:

$$a = 0.042747 \cdot \frac{R^2 T_c^2}{P_c} \left(1 + m(\omega)(1 - \sqrt{T_r})\right)^2 \tag{8.33}$$

$$b = 0.08664 \cdot \frac{RT_c}{P_c} \tag{8.34}$$

$m(\omega)$ is a function of the acentric factor ω and for SRK it is given by:

$$m(\omega) = 0.48 + 1.574\omega - 0.176\omega^2 \tag{8.35}$$

In systems with 2 or more components, the parameters a and b are calculated using a set of mixing rules. In this work the following mixing rules have been used:

$$a = \sum_i \sum_j x_i x_j a_{ij} \tag{8.36}$$

$$b = \sum_i b_i \tag{8.37}$$

The cross-interaction parameter a_{ij} is calculated using the following combining rules:

$$a_{ij} = \sqrt{a_i a_j}(1 - k_{ij}) \tag{8.38}$$

For interactions between hydrocarbons, it will be assumed that the binary interaction coefficient, k_{ij}, is equal to zero. Due to the low critical temperatures of gas components such as hydrogen, hydrogen sulfide and ammonia, use of binary interaction coefficients can provide more accurate description of the equilibrium. Gray et al. [68] have used binary VLE data for hydrogen-hydrocarbon systems and fitted the corresponding interaction parameters. The correlated the $k_{H_2,j}$ to the critical temperature of the hydrocarbon using the following expression, which is valid for a critical temperatures (T_{cj}) between 50 and 1000 K:

$$k_{ij} = A + \frac{BX^3}{1 + X^3} \tag{8.39}$$

$$X = \frac{T_{cj} - 50}{1000 - T_{cj}} \tag{8.40}$$

For SRK, the parameters A and B are equal to 0.0067 and 0.63375 respectively [68].

The interaction coefficients involving the hydrogen sulfide and ammonia will be assumed to be equal to zero.

In order to do the equilibrium calculations it is necessary to know values of the critical temperature and pressure and the acentric factor for all of the compounds. In cases where data was not available they were estimated using a program using group contribution methods for property prediction. The normal boiling point, critical temperature, critical pressure, critical volume and acentric factors has been estimated using the methods of Marrero and Gani [60], Constantinou et al. [69] and Joback and Reid [70]. Values for selected compounds, that have been used for equilibrium calculations are given in table B.1. The binary interaction coefficient between hydrogen and various compounds are given in table 8.2.

Table 8.2: Binary interaction calculated from equation (8.39)

Compound	T_c [K]	k_{i,H_2}
Pentyl-benzene	675	0.562
Tetralin	719	0.597
Naphthalene	748.4	0.612
Phenanthrene	873	0.638
Butyl-cyclohexane	667	0.554
Decalin (cis-)	702.3	0.585
n-Nonane	594.6	0.455
n-Hexadecane	722	0.599
Benzothiophene	754	0.615
Dibenzothiophene	897	0.639
4,6-dimethyldibenzothiophene	907.91	0.640
acridine (basic)	891.1	0.639
3-methylindole (non-basic)	769.64	0.620
1,4-dimethylcarbazole (non-basic)	838.21	0.635

8.5 Liquid molar volume

Since cubic equations of state can give large errors in the calculation of liquid volumes, the density of liquid mixtures have been calculated using the equation suggested by Rackett [32]. The following is a correlation for the saturated liquid volume of a pure compound, as a function of the reduced temperature and the critical properties:

$$v_L = v_c \cdot Z_c^{[1-T_r]^{2/7}} = \left(\frac{RT_c}{P_c}\right) Z_c^{[1+(1-T_r)^{2/7}]} \tag{8.41}$$

Here v_L is the liquid molar volume and T_r is the reduced temperature. For a mixture of compounds, the following equation can be used to estimate the molar volume of the liquid [57]:

$$v_L = R\left(\sum_i \frac{x_i T_{ci}}{P_{ci}}\right) Z_{RAm}^{[1+(1-T_r)^{2/7}]} \tag{8.42}$$

Z_{RAm} is equal to $Z_{RAm} = \sum_i x_i Z_{RAi}$, where Z_{RAi} can be found from:

$$Z_{RAi} = 0.29056 - 0.08775\omega_i \tag{8.43}$$

T_r in equation (8.42) is equal to $T_r = T/T_{cm}$, where T_{cm} can be calculated from the following expressions:

$$T_{cm} = \sum_i \sum_j \phi_i \phi_j T_{cij} \tag{8.44}$$

$$\phi_i = \frac{x_i v_{ci}}{\sum_j x_j v_{cj}} \tag{8.45}$$

$$1 - k_{ij} = \frac{8(v_{ci} v_{cj})^{1/2}}{(v_{ci}^{1/3} + v_{cj}^{1/3})^{1/3}} \tag{8.46}$$

$$T_{cij} = (1 - k_{ij})(T_{ci} T_{cj})^{1/2} \tag{8.47}$$

The effect of pressure on the liquid volume is assumed to be negligible.

8.5.1 Calculation of equilibrium concentrations

To know the gas to liquid mass transfer rate it is necessary to calculate the equilibrium liquid concentrations. It is assumed that at the gas-liquid interface the liquid is in equilibrium with the gas. The driving force for the mass transport is difference between this equilibrium concentration and the actual bulk liquid concentration. The equilibrium concentration is calculated from the gas phase concentrations at the given position in the reactor. From the gas phase concentrations the mole fractions, y_k, in the gas phase can be calculated:

$$y_k = \frac{c_k^G}{\sum_k c_k^G} \tag{8.48}$$

The equilibrium factors, K_k, are calculated from the SRK equation of state. Using these K-factors the liquid equilibrium composition that correspond to the gas phase composition can be calculated:

$$x_k^{eq} = \frac{y_k}{K_k} \tag{8.49}$$

Knowing the equilibrium mole fraction, the equilibrium concentration can be calculated using the molar volume of the solution:

$$c_k^{eq} = \frac{x_k^{eq}}{v_L} \tag{8.50}$$

8.6 Model assumptions

The basic assumptions in the models for the catalyst pellets and for the trickle-bed reactor is listed in this section. The basic equations to describe the reactor are equation (8.1) which gives the concentration profiles in the pellet at a certain position z in the reactor. Equation (8.11) which uses the solution to equation (8.1) to calculate the apparent reaction rate. The gas and liquid phase concentrations in the reactor are given by the equations (8.16), (8.17) and (8.18).

8.6.1 Assumptions in the pellet model

The most important assumptions regarding the model for the concentration profiles inside the catalyst pellet are listed here.

- The pellet is isothermal
- The surface concentrations are known, and they are the same all over the surface
- The pellet is spherical
- The system is in steady state, i. e. the concentrations don't change with time
- The pellet is treated as a continuum
- The flux in the pellet can be described by Fick's law using an effective diffusion coefficient

8.6.2 Assumptions in the reactor model

The important assumptions and simplifications in the reactor model are listed here:

- Three phases exist: A solid catalyst phase, a liquid phase and a gas phase
- Only liquid exists in the catalyst pores
- Reaction only takes place inside the catalyst pellets
- Mass transport from gas to liquid are described using the two-film theory
- Mass transport in the gas film are so fast that there is equilibrium at the gas-liquid interface
- The catalyst pellet surface is covered with liquid, so transport to the surface happens only from the liquid phase

- Mass transport from liquid to the catalyst surface are described with the film-theory
- The reactor operates at steady state
- The reactor is isothermal
- There is no pressure drop in the reactor
- The superficial gas and liquid velocities u_G and u_L are constant down through the reactor
- The mass transfer coefficients $k_{LG} \cdot a_{LG}$ and $k_{LS} \cdot a_{LS}$ are constant down through the reactor
- A gas-liquid equilibrium has been established in the feed, before entering the reaction zone

8.7 Conclusion

In this chapter a heterogeneous reactor model for a trickle-bed hydrotreater has been presented. It consists of a model describing the concentration profiles inside a catalyst pellet coupled with a fixed bed reactor model with two-phase flow operated in the trickle flow regime. Methods for estimating physical properties, such as diffusion coefficients, mass transfer coefficients, densities and equilibrium compositions have been presented. The model assumes constant linear velocities of the 2 fluid phases and that the reactor is isothermal. Industrial hydrotreaters are adiabatic, and due to the exothermic nature of the hydrotreating reactions, the temperature in the reactor will not be constant. Therefore the model described in this chapter will mainly be suited to simulate the behavior of laboratory reactors. Future work would include testing the validity of the model by simulating a single reaction, and subsequently add more reactions, and eventually try to simulate the experiments described in chapter 7. In order to be able to simulate industrial hydrotreating units, further work on the model would involve including energy balances such that the temperature changes in the reactor could be accounted for.

Chapter 9

Modelling of Naphthalene Hydrogenation in a Robinson-Mahoney Reactor

The work described in this chapter has been carried out during a 5 month external stay, at the Laboratory of Chemical Technology at Ghent University, under the supervision of professor Guy B. Marin and assistant professor Joris W. Thybaut.

9.1 Introduction

An important part of simulating industrial hydrotreaters is understanding the kinetics of different reactions. Laboratory experiments with model compounds can provide useful information about reaction pathways and reactivities of different compounds, and provide data that can be used to develop rate laws for the different reactions. Several types of laboratory reactors exist, which can be used to measure kinetics of gas-liquid-solid reactions: fixed-bed reactors, simple stirred tank reactors, spinning basket reactors and fixed basket reactors [71].

One type of reactor that can be applied to measuring reaction rates of gas-liquid-solid reactions is a Robinson-Mahoney reactor [72]. Figure 9.1 shows a sketch of the Robinson-Mahoney reactor used in this work. The reactor consists of a stainless steel vessel containing a cylindrical fixed basket. The catalyst is placed in the middle of the basket, with inert material above and below. A gas liquid mixture is fed from the bottom of the reactor and the product mixture leaves the reactor downward through a tube from the top of the reactor. In the center of the reactor is an impeller which forces the gas liquid mixture through the basket and establishes a good contact between the reactants and the catalyst. Figure 9.2 shows a suggested flow pattern inside the reactor, and it can be seen that part of the gas and liquid is recycled internally. Provided that the recycle ratio (the ratio of the recircling gas/liquid divided by the feed flow) is sufficiently high, the reactor will behave as a Continuous Stirred Tank Reactor (CSTR).

Robinson-Mahoney reactors are suitable for kinetic experiments at a wide range of condi-

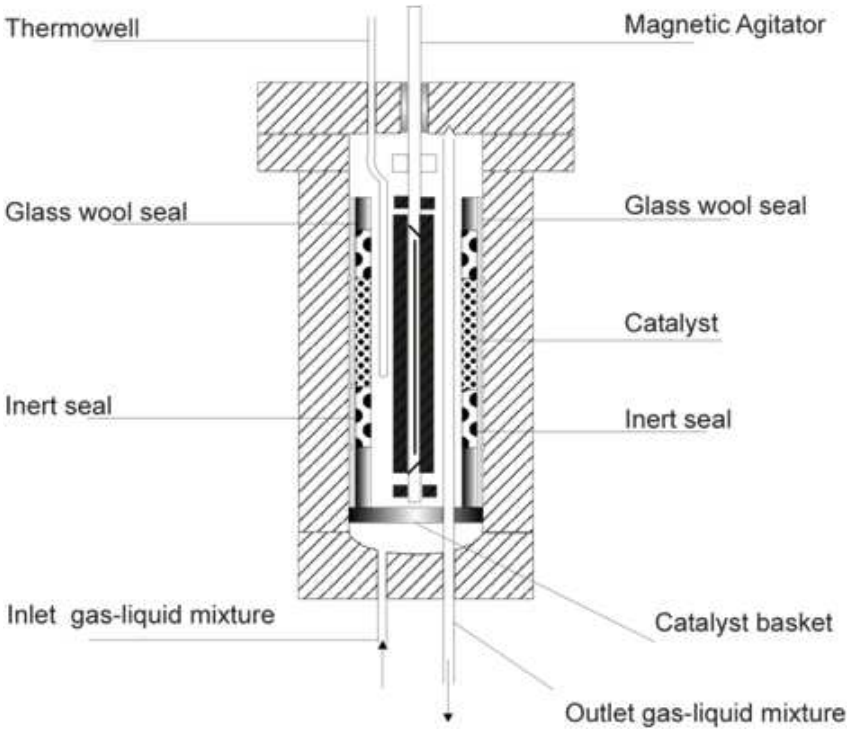

Figure 9.1: A schematic representation of a Robinson-Mahoney reactor

tions. One of the advantages of using a Robinson-Mahoney is that the reaction rate can be measured directly. If this is to be done in a fixed bed reactor, it is necessary to operate in a differential mode, meaning, that one is limited to low conversions. The Robinson-Mahoney reactor has been applied by several authors for the study of hydroprocessing reactions, such as hydrocracking [73], hydrodesulfurization [74, 75] and hydrogenation of aromatics [76, 77]. In most studies the conditions of the experiments are chosen such that mass transfer and diffusion resistance is negligible. For this reason kinetic studies are often carried out at temperatures and pressures lower than in industrial units. Thus when applying intrinsic rate expressions developed from laboratory experiments in simulation of hydrotreaters there is no guarantee for their validity, since they are used outside of the temperature and pressure range for which they have been developed.

Pitault et al. [71] have investigated the liquid-solid and the gas-liquid mass transfer in 2 different stationary basket reactors for an air-water system. One of the reactors designed and produced by Autoclave Engineers Company is similar to the one used in this work. They find that the liquid-solid mass transfer in both reactors is very similar to that in a stirred tank reactor, though a little slower. But the liquid-solid mass transfer is significantly larger, up to a factor of 10, than in a trickle-bed reactor.

The gas-liquid mass transfer in the 2 reactors showed different behavior. The authors found that the reactor from Autoclave Engineers Company basically behaved as a classical tank with a diameter equal to the inner diameter of the basket, and they concluded that correlations developed for classical stirred tanks can be used to estimate the transport coefficients.

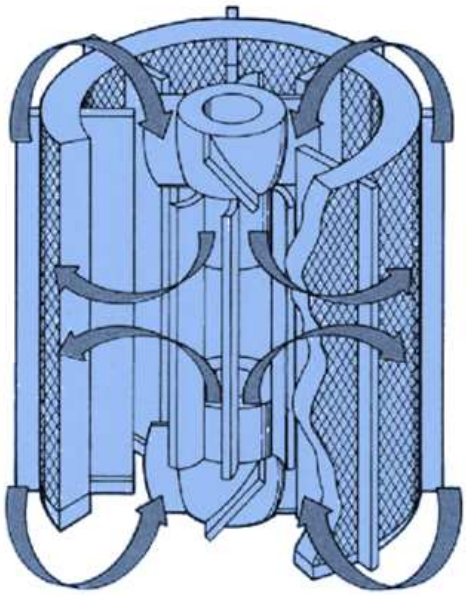

Figure 9.2: An illustration of the flow patterns internally in a Robinson-Mahoney reactor

Mitrovic et al. [78] determined liquid-solid mass transfer coefficients in a Robinson-Mahoney reactor. They measured global and local coefficients using naphtol particles in water and heptane, and developed a first correlation for the mass transfer coefficients as function of agitation speed. The mass transfer coefficients were compared with kinetic parameters for a hydrocracking reaction as presented by Schweitzer et al. [73]. They showed that the liquid-solid mass transfer coefficients are hundreds of times higher, and therefore the observed reaction rate is not influenced by liquid-solid mass transfer.

In this work a model was developed for a Robinson-Mahoney reactor which takes internal and external mass transfer into account. In this way kinetic models that have been developed at lower temperature and pressure can be tested at industrial conditions. If a model is able to describe the mass transfer phenomena, it can eventually be used to obtain intrinsic kinetic information in situations where transport limitations cannot be avoided.

9.1.1 Hydrogenation of naphthalene

In this work, the hydrogenation of naphthalene has been investigated in a Robinson-Mahoney reactor. In compounds containing fused rings, the rings are hydrogenated one at a time. The reaction pathway of naphthalene hydrogenation is shown in figure 9.3. First tetralin is formed which can then be further hydrogenated into cis- and trans-decalin. These reactions have been investigated in a Robinson-Mahoney reactor previously by Romero [77], who developed detailed kinetic models based on two different suggested reaction mechanisms by assuming different rate-determining steps. The reaction mechanism assumes 2 different types of sites, coordinatively unsaturated metal sites and sulfur anion sites. Based on an analysis of the statistical significance of the parameters and the quality of the fit the best kinetic models were found for hydrogenation of naphthalene to tetralin and for hydrogenation of tetralin to cis- and trans-decalin respectively.

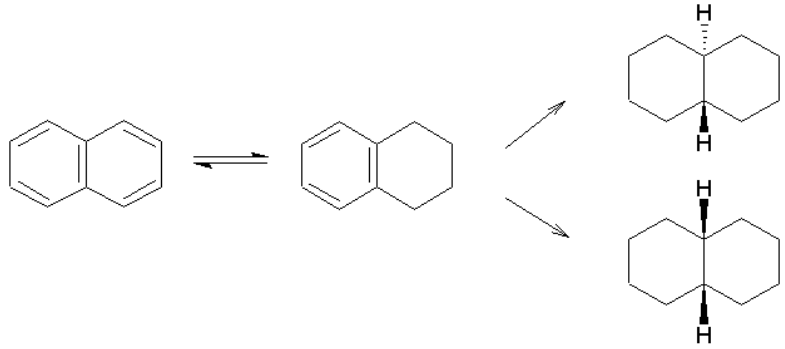

Figure 9.3: The reaction pathway for hydrogenation of naphthalene

The mechanisms that lead to the best kinetic models assumed a heterolytic adsorption of hydrogen and hydrogen sulfide. The rate expressions are expressed in terms of liquid fugacities, f_i, which are related to the liquid phase concentration of component i as follows:

$$f_i = \phi_i^L P V_m^L C_i^L \tag{9.1}$$

P is the total pressure, V_m^L the liquid molar volume and C_i^L the liquid phase concentration. The best rate expression for naphthalene hydrogenation has the following form:

$$-r_N = \frac{k_{comp,N} f_N f_{H_2}^2}{\sqrt{\mu\delta}(\sqrt{\mu}+\sqrt{\delta})^2} \cdot \left(1 - \frac{f_{TT}}{K_{eq,N} f_N f_{H_2}^2}\right) \tag{9.2}$$

The subscript *comp* denotes, that it is a composite rate constant, which is a product of the real rate constant, and various adsorption equilibrium constants. The following rate expression was found best to describe the hydrogenation of tetralin:

$$-r_T = \frac{k_{comp,T} f_T f_{H_2}}{\delta(\sqrt{\mu}+\sqrt{\delta})^2} \cdot \left(1 - \frac{f_D}{K_{eq,T} f_T f_{H_2}^3}\right) \tag{9.3}$$

The denominator terms are given by $\delta = 1 + K_N f_N + K_T f_T + K_{cD} f_{cD} + K_{tD} f_{tD}$ and $\mu = K_{H_2} f_{H_2} + K_{H_2S} f_{H_2S}$. Romero et al. [76] report that the surface concentrations of any hydrocarbon species are found to be negligible, and therefore the value of δ close to 1.

For practical purposes the distinction of cis- and trans-tetralin is not important, and therefore they are treated as one compound, decalin, in this work. The parameters used in the rate equations, 9.2 and 9.3 are given in table 9.1. The parameters for equation 9.2 were determined by fitting the model to experimental data obtained at different space times and at temperatures between 523 and 583 K and pressures between 20 and 40 bar. For determining the parameters for 9.3 experimental data at temperatures between 523 and 593 and pressures between 60 and 80 bar were used [77]. The equilibrium coefficients were calculated using thermodynamic

properties estimated using a group contribution as suggested by Benson et al. [79].

Table 9.1: Parameters used in equation 9.2 and 9.3

Parameter	Value
$A_{comp}[kmol/kg/s/bar^3]$ 9.2	$7.0 \cdot 10^{-6}$
$E_{A,comp})$ $[kJ/mol]$ 9.2	-37.9
$A_{comp}[kmol/kg/s/bar^2]$ 9.3 (cis-decalin)	$1.28 \cdot 10^{-5}$
$E_{A,comp})$ $[kJ/mol]$ 9.3 (cis-decalin)	-30.0
$A_{comp}[kmol/kg/s/bar^2]$ 9.2 (trans-decalin)	$13.1 \cdot 10^{-5}$
$E_{A,comp})$ $[kJ/mol]$ 9.2 (trans-decalin)	-25
$\Delta S^0_{H_2}$ $[J/mol/K]$	-161
$\Delta S^0_{H_2S}$ $[J/mol/K]$	-189
$\Delta H^0_{H_2}$ $[kJ/mol]$	-82.5
$\Delta H^0_{H_2S}$ $[kJ/mol]$	-109

9.2 Experimental Procedures

9.2.1 Catalyst and chemicals

The catalyst used for the series of naphthalene hydrogenation experiments was a commercial CoMo catalyst. The particles were in the form of trilobes with a diameter of 1/20". The catalyst was sulfided using a solution of 1 vol % dimethyldisulfide in parapur. For the naphthalene hydrogenation experiments, a solution of 5 wt % naphthalene, was prepared. The solvent, parapur, is a commercial mixture of n-alkanes, mainly n-decane (10 wt %),n-undecane (26 wt %), n-dodecane (44 wt %), n-tridecane (19 wt %) and smaller amounts of other hydrocarbons (1 wt %). 0.1 vol. % of dimethyldisulfide was added to the liquid feed, in order to keep the catalyst in its active sulfided state. At the applied reaction conditions, dimethyldisulfide reacts instantaneously with hydrogen to produce H_2S.

9.2.2 Experimental setup and procedures

The hydrogenation experiments were performed in a three-phase Robinson-Mahoney reactor. A detailed description of the set-up and operating procedures has been given in publications by Vanrysselberghe et al. [74] and Arroyo et al.[80]. 20 g of the catalyst was placed in the basket in the reactor, and to reduce local overheating the catalyst bed was diluted with 40 vol % of glass beads with a diameter of 1.5-2.5 mm. Experiments were done at two sets of temperatures, 553 and 593 K, and two sets of pressures, 50 and 100 bar. The range of investigated space velocities (LHSV's) was 2-4 hr^{-1}. The molar ratio of hydrogen to naphthalene was 5.

The liquid phase product was analyzed using a Chrompack CP-9001 gas chromatograph.The actual peak areas were determined by integration of the chromatogram using the X-Chrom software package. For all experimental points the naphthalene molar balance was in the range 89 to 103 %. The molar yields are calculated from the liquid outlet flows as follows:

$$Y_i = \frac{F_i}{F_N + F_T + F_{cD} + F_{tD}} \tag{9.4}$$

In order to make sure that the catalyst did not suffer a significant loss of activity during the experimental campaign one set of conditions was investigated twice: After 29 and 51 days on stream. Table 9.2 shows the product yields, at the two times, and the difference is so small, that any loss of activity is negligible.

Table 9.2: Yields at set of base conditions after 29 and 51 days on stream

	29 days on stream	*51 days on stream*
Yield Naphthalene	0.77	0.84
Yield Tetralin	10.94	9.77
Yield trans-Decalin	70.55	71.42
Yield cis-Decalin	17.74	17.97

9.2.2.1 Step-response experiment

A single step-response experiment was done to measure the liquid hold-up in the reactor. This was done at slightly different conditions than the hydrogenation experiments, and using feeds that did not contain any naphthalene. The composition of the 2 different feeds used in the experiment (I and II) is shown in table 9.3. Feed I was pure parapur, while feed II was 50 wt % parapur and 50 wt % n-dodecane. The temperature was 633 K and the pressure was 135 bar. The liquid hourly space velocity (LHSV) was 4 hr^{-1}, corresponding to a liquid feed flow of 1.32 ml/min, and the hydrogen to oil ratio was 1750 Nl/l.

Feed I was fed to the reactor for at least 2 hours, such that a steady state was reached. Then the feed was switched to feed II, and the concentration of dodecane in the reactor outlet was followed as a function of time. When a new steady state was reached, the feed was changed back to feed I, and the change in the dodecane concentration was measured.

Table 9.3: Hydrocarbon concentration in wt % in Feed I and Feed II

Component	Feed I	Feed II
decane	9.4	4.7
undecane	36.8	18.4
dodecane	33.5	66.8
tridecane	20.1	10.1
Various hydrocarbons	~	~

As catalyst was present in the reactor during the step-response experiment a small amount of cracking took place (the conversion was less than < 8 %).

9.3 Robinson-Mahoney Reactor Model

This section is concerned with the setting up of a steady-state model for a Robinson-Mahoney reactor. It is assumed that the stirring in the reactor is so effective, that there are no concentration gradients in the bulk gas and liquid phases, and also that the temperature of the two phases is the same. Furthermore it is assumed, that the catalyst pellets are completely wetted, and reaction can only take place in the liquid phase. Any concentration gradient between the bulk liquid and the surface of the catalyst is neglected, but the possibility of a mass transfer resistance at the gas-liquid interface is taken into account. Because of the high conversions obtained, internal mass transport limitations are also considered. Before entering the reactor the gas and liquid feeds are mixed, and it is assumed that a gas-liquid equilibrium is established at the reactor temperature and pressure, before the mixture enters the reactor.

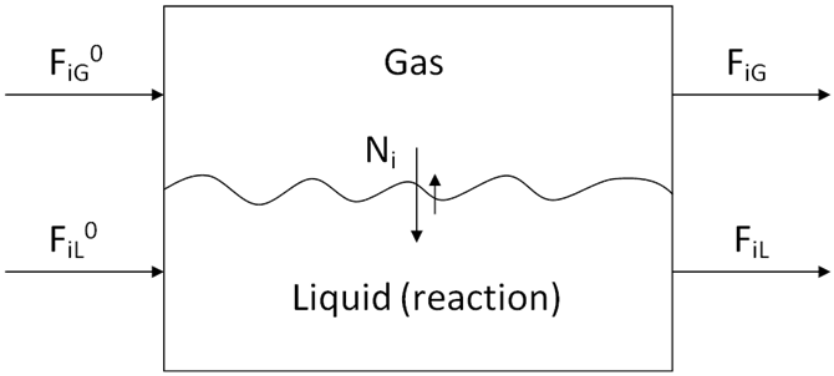

Figure 9.4: Schematics of the different flows used in the Robinson-Mahoney mass-balance

Figure 9.4 shows a diagram of the flows in the reactor. To describe the system a mass balance is set up for the gas and the liquid phase. A steady state mole balance for the gas phase yields:

$$F_{iG} = F_{iG}^{0} - N_i a_v^{'} V_R \epsilon_L \tag{9.5}$$

The mole balance for the liquid phase gives:

$$F_{iL} = F_{iL}^{0} + N_i a_v^{'} V_R \epsilon_L + m_{cat} \sum_{j}^{NR} S_{ij} \eta_j r_j^{'} \tag{9.6}$$

F_i designates the molar flows, N_i the molar flux, $a_v^{'}$ is the gas-liquid interface area per liquid volume, V_R is the total volume of the reactor and ϵ_L is the liquid hold-up. m_{cat} is the total catalyst mass, $r_j^{'}$ is reaction rate in $\frac{mol}{kg\ cat.\ \cdot s}$ for reaction j, η_j is effectiveness factor for reaction j and S_{ij} is the stoichiometric coefficient for component i in reaction j.

The effectiveness factor is determined by solving the diffusion-reaction problem for a spher-

ical catalyst particle:

$$\frac{D_{ie}}{\zeta}\frac{d}{d\zeta}\left(\zeta^2\frac{dC_{is}}{d\zeta}\right) = \rho_s\sum_j^{NR} S_{ij}r_j'\left(C_{is}^s,...,T_s\right) \tag{9.7}$$

ζ is the distance from the center of the pellet, D_{ie} is the effective diffusion coefficient of component i, T is temperature and s denotes surface conditions. The equation is solved using an orthogonal spline collocation method described in [62].

The mass flux from the gas phase to the liquid phase is described by the two-film theory

$$N_i = K_i\left(\frac{C_{iG}}{H_i} - C_{iL}\right) \tag{9.8}$$

C_{iG} and C_{iL} are the gas and liquid concentrations respectively, and H_i is the Henrys law constant calculated from the Peng-Robinson equation of state. The overall mass transfer coefficient, K_i, is calculated from the gas side mass transfer coefficient, k_{Gi}, and the liquid side mass transfer coefficient, k_{Li}, as:

$$\frac{1}{K_i} = \frac{1}{H_i k_{Gi}} + \frac{1}{k_{Li}} \tag{9.9}$$

No correlations have been developed specifically for the gas-liquid mass transfer coefficient in Robinson-Mahoney reactors, but according to Pitault et al. [71] correlations for classical stirred tanks can be used in some cases. The liquid side mass transfer coefficient for hydrogen, is therefore estimated using the following correlation by Bern et al. [81] developed for fat hydrogenation in a slurry reactor:

$$k_{L,H_2}a_v^{'} = 0.326\cdot\left[\frac{N_{stirring}^{3.15}d_{impeller}}{V_{liq}^{1.41}}\right]^{0.37}\cdot u_g^{0.32}\left[s^{-1}\right] \tag{9.10}$$

The liquid volume is given a constant value of 70 % of the total reactor volume. According to the penetration theory, the transport coefficient is proportional to the square root of the diffusion coefficient [82]. In this way all other liquid side coefficients can be estimated as [82]:

$$k_{Li}a_v^{'} = k_{L,H_2}a_v^{'}\cdot\sqrt{\frac{D_{Li}}{D_{L,H_2}}} \tag{9.11}$$

The penetration theory is valid if the gas bubbles are not too small. For very small bubbles the transport coefficient is directly proportional to the diffusion coefficient [83]. Since hydrogen is the component with the highest diffusion coefficient, there is a risk, that the predicted transport coefficient for all other components are too high. As it is most likely that hydrogen is the limiting gas reactant, this will probably have very little significance.

For most practical situations the resistance at the gas side of the gas-liquid interface is negligible. In this work, the gas side mass transfer coefficient is given a constant value of 0.35

s^{-1} as suggested by van Engelandt for laboratory reactors [84].

The steady-state model is solved using a C implementation of Powell's Hybrid Method.

9.4 Results and Discussion

9.4.1 Experimental Results

9.4.1.1 Step-response experiment

The liquid hold-up in the reactor is defined as the volume of liquid in the reactor per total reactor volume. It can be determined by making a step-change in an input to the reactor, and measure the response in the reactor outlet.

If a non-volatile compound is considered, a non-steady state mass balance can be written as:

$$V_L \frac{dC}{dt} = Q_f \cdot C_f - Q \cdot C \tag{9.12}$$

V_L is the volume of liquid in the reactor, C and C_f are the molar concentration in the reactor and the feed respectively, and Q_f and Q are the in- and outlet volumetric flow. If vaporization of the liquid in the reactor can be neglected, the inlet and outlet volumetric flow rates will be equal, i.e., $Q = Q_f$. Defining a liquid residence time as $\tau_L = \frac{V_L}{Q}$, the mass balance can be rewritten as:

$$\tau_L \frac{dC}{dt} = C_f - C \tag{9.13}$$

Solving for the outlet concentration, C, gives the following:

$$C = C_f + (C_0 - C_f) \cdot \exp\left(-\frac{t}{\tau}\right) \tag{9.14}$$

C_0 is the concentration in the reactor at $t = 0$. Rearranging the expression gives:

$$\ln\left(\frac{C - C_f}{C_0 - C_f}\right) = -\frac{t}{\tau} \tag{9.15}$$

By plotting the known quantity, $\ln\left(\frac{C-C_f}{C_0-C_f}\right)$, as a function of time a straight line should be obtained, and the residence time can be determined from the slope. The liquid hold-up, ϵ_L, is related to τ_L as follows:

$$\epsilon_L = \frac{\tau_L \cdot Q}{V_R} \tag{9.16}$$

V_R is the total volume of the reactor.

Figure 9.5 and 9.6 show the plots used to determine residence times based on the 2 different step-responses. It is assumed that there is plug-flow in the pipes before and after the reactor, which gives a small delay in the response.

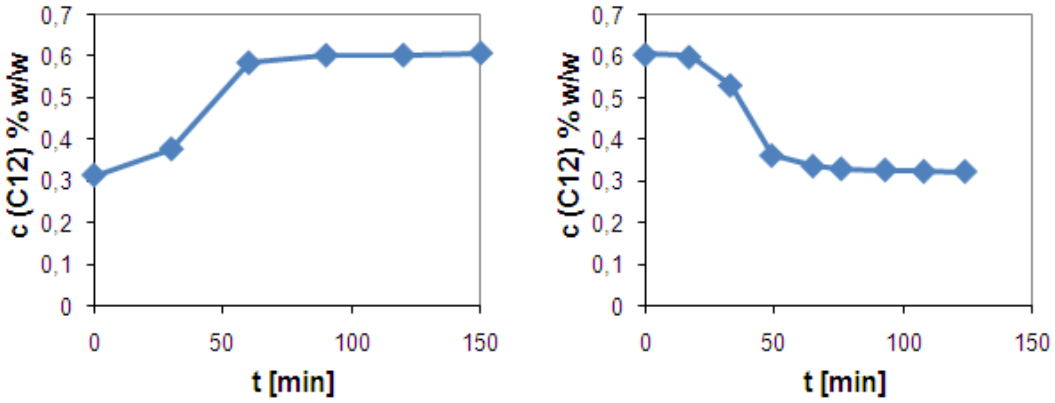

Figure 9.5: Concentration of n-C12 as function of time after a step-changes in the feed concentration

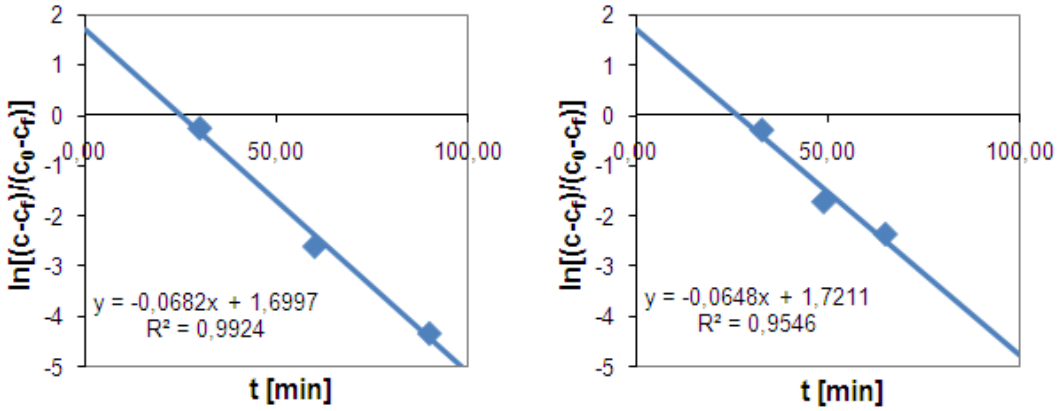

Figure 9.6: Linear plots used to determine the residence time

The calculated values of the residence time and hold-up for the reactor is given in table 9.4. A very similar value is obtained for the 2 experiments, and an average value of 0.1 is obtained. This value of the liquid hold-up, is so low, that this would most likely correspond to a situation where the two phases in the reactor consist of a mist of liquid droplets in a continuous gas phase.

The purpose of the experiment was to illustrate how the residence time is different for the gas and the liquid phase, or in other words that the ratio between the gas and the liquid phase in the reactor is different than in the feed/product mixture. Due to the stronger gravitational forces it is most likely that the liquid fraction in the reactor will be higher than the total liquid fraction of the feed mixture. A (Vapor Liquid Equilibrium) VLE calculation has been done based on the composition of the mixture entering the reactor. The flash calculation was done using Aspen

Table 9.4: Liquid residence time and hold-up determined from a step response experiment

Response	$\tau_L[min]$	$V_L[ml]$	ϵ_L
1	14.7	19.4	0.097
2	15.4	20.4	0.102
Average	15.0	19.9	0.099

Plus 12.1, with the Soave-Redlich-Kwong (SRK) equation of state with default values of the interaction parameters. The result of the calculation is that at the reactor temperature and pressure, the vapor fraction is 1. If this is really the case, the assumption that n-dodecane is a non-volatile component clearly is not correct, and the calculated hold-up has no physical meaning. If V_L is replaced with the gas volume, equation 9.12 can be used to describe a reactor with a single gas-phase. The calculated liquid residence times in table 9.4, will in this case be gas phase residence times. The molar volume of the gas has been calculated using the SRK equation of state and is found to be 412 cm^3/mol, which leads to a total volumetric flow rate of 44.8 ml/min. According to Nist Webbook, the molar volume of pure hydrogen at 360 °C and 135 bar is 406 cm^3/mol, which is quite close to the calculated value [85]. Calculating V_G, which is equal to the reactor volume gives:

$$V_G = \tau \cdot Q_G = 15.0\ min \cdot 44.8\ ml/min = 672\ ml \tag{9.17}$$

This value is approximately 3 times larger than the actual reactor volume, which means assuming that it is a single phase system is not correct.

The step-response experiment has not shown clearly what the situation is in the reactor at these conditions. It is most likely that the actual situation is somewhere in between the 2 extremes, a non-volatile liquid and a single gas-phase, so that the residence time that has been determined is an average or combination of a gas and a liquid residence time. Although no clear answer was obtained, the experiment shows, that the liquid content of the reactor is higher than what is calculated based on the total in- or outlet composition.

9.4.1.2 Naphthalene hydrogenation

The experiments with naphthalene hydrogenation provided some experimental points, that can be compared with simulations. The naphthalene conversion increased with temperature and pressure, and at all the investigated conditions, the naphthalene conversion was higher than 90 %. At all the conditions a significant amount of cis- and trans-decalin was formed from the hydrogenation of tetralin. The range of yields in the experiments are shown in table 9.5:

Table 9.5: Approximate range of yields in the naphthalene hydrogenation experiments

Component	Naphthalene	Tetralin	Decalin (cis- and trans-)
Yields	< 10 %	10-60 %	10-60 %

9.4.2 Model Validation

9.4.2.1 Toluene hydrogenation (Literature data)

The model for the Robinson Mahoney reactor has been implemented in a C program. To verify that the implementation of the model behaves correctly an attempt has been made to reproduce data from another source. Rautanen et al. [86] investigated the hydrogenation of toluene to methylcyclohexane on a Ni/Al_2O_3 catalyst at temperatures between 100 and 200 °C and pressures between 20 and 40 bar:

$$toluene + 3H_2 \rightarrow methylcyclohexane \tag{9.18}$$

At these conditions the reaction was significantly limited by internal mass transfer, and therefore the data is suitable to test the program. They fitted several kinetic expressions to their experimental results. All of them were able to describe the experimental data quite well, but the one that gave the best results in our implementation has the following form:

$$-r'_T = \frac{kK_TK_HC_TC_{H_2}}{\left[1 + (K_HC_{H_2})^{\frac{1}{\gamma}}\right]^{\gamma}(1 + 3K_TC_T)} \tag{9.19}$$

The values of the parameters are given in table 9.6.

Table 9.6: Parameters used in equation 9.19

Parameter	Value
k (400 K) $[mol/kg/s]$	$9.5 \cdot 10^{-2}$
E_A $[kJ/mol]$	48.8
K_T $[m^3/mol]$	$1.1 \cdot 10^{-4}$
K_H $[m^3/mol]$	$38.6 \cdot 10^{-4}$
γ	2

First the effect of the particle size on the observed reaction rate was tested. Figure 9.7 shows a comparison between the simulations and the experimental rates at 100 °C and 20 bar as presented by Rautanen et al. [86]. It shows quite a good fit in the entire range of particle sizes, except for the smallest one. The reason that the fit is poorer for the smallest particle size, is that to use this small particle size, it was necessary to use another basket in the reactor, and a problem with liquid-solid mass transfer resistance was introduced. This is not accounted for in the reactor model and the simulation deviates significantly from the experimental rate. In

the simulation, the range of the effectiveness factor is 0.3 to 1.0 corresponding to particle sizes between 0 and 1.1 mm.

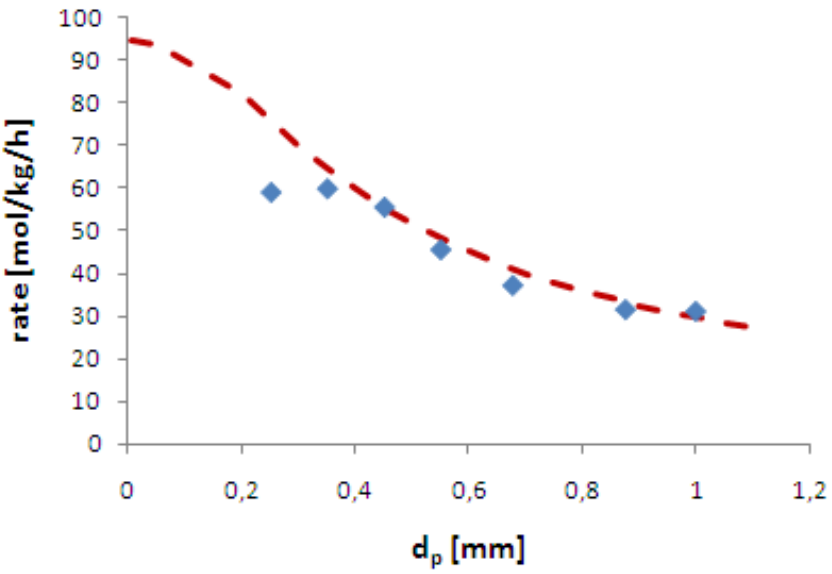

Figure 9.7: Experimental reaction rates as function of particle size for toluene hydrogenation. Dashed line is simulated rates

The effect of temperature and pressure on the rate is shown in figure 9.8. The simulation follows the right trends in that the reaction rate increases with increasing temperature and pressure. At the lowest pressure there is quite good agreement between the experimental rates and the simulation, but as the pressure increases the difference between experiment and simulation becomes larger. Especially at the highest temperature and pressure the difference is significant.

The reason that the simulations in this case underpredict the reaction rate, also when compared to the simulations presented by Rautanen et al. [86], is probably that a significantly smaller value of the gas-liquid mass transfer has been used. Furthermore different equations of state have been used, and there might be a difference in the calculated liquid phase concentrations that become more pronounced at higher temperature and pressure.

Overall, the reactor model has been shown to describe the internal diffusion quite well, and the trends when changing temperature and pressure are also captured.

9.4.2.2 Naphthalene hydrogenation (Literature data)

The rate expressions that were tested against the experimental data were developed by Romero et al. [76, 77]. As a further test of the implementation of the reactor model it was tested whether some of the data from Romero et al. could be reproduced, using equation 9.2 as the rate for naphthalene hydrogenation, and neglecting the hydrogenation of tetralin to decalin. Figure 9.9 shows the experimental results and the simulations. It is clear that the conversion can be described adequately at a large temperature (250-310 °C) interval and space times (1-3.5 $kg{\cdot}s/mmol$). Using the parameters from Romero et al. conversions were too large, and therefore

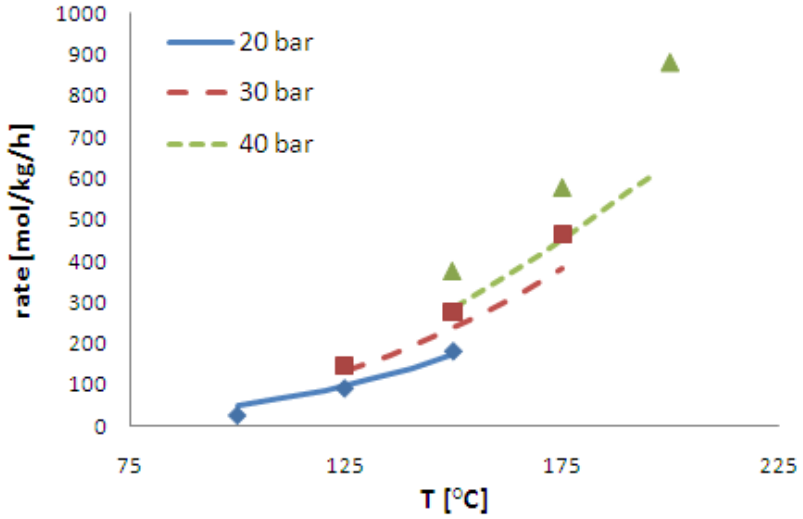

Figure 9.8: Reaction rate for toluene hydrogenation as function of temperature at different pressures. Lines are simulated rates

the rate constant was adjusted to get the simulation results presented in figure 9.9. The reason why it is necessary to adjust the rate constant is not absolutely clear. The rate expressions were developed under the assumption, that there was no internal diffusion resistance. This is in accordance with the simulations at the same conditions where the calculated effectiveness factors in all cases are above 0.98 and therefore practically no diffusion resistance exists.

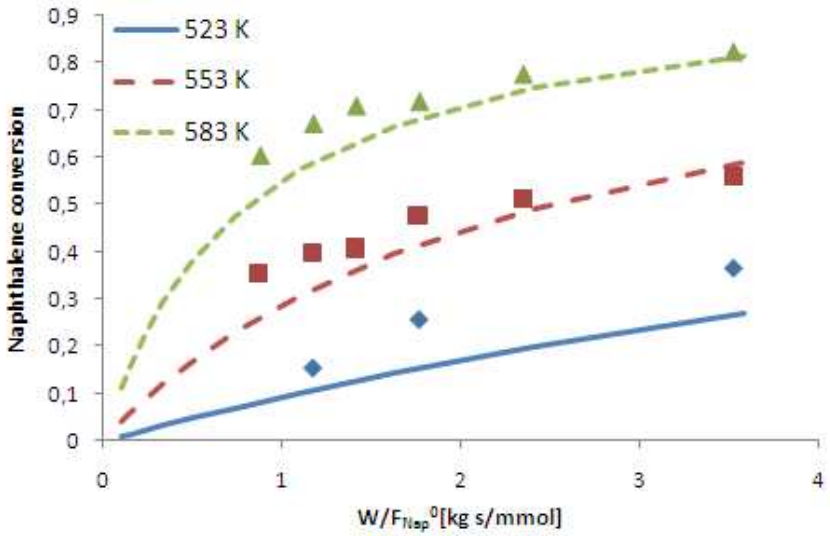

Figure 9.9: Naphthalene conversion as function of the space time. Experimental data from Romero et al. [77]

9.4.3 Test of Kinetic Models

As a reactor model has been implemented and tested, it is now desirable to use it to test existing kinetic models against the new data. The rate expressions, equation 9.2 and 9.3, have

been developed for a NiMo catalyst, while the high conversion experiments in this work were performed using a CoMo catalyst. Due to the different catalysts, parameters such as rate constants, adsorption constants etc. cannot be expected to be the same. As a simplification it will be assumed that all parameters are the same, except the kinetic constants. The ratio between the composite rate constant for naphthalene and tetralin hydrogenation respectively is assumed to be the same as that presented by Romero et al. [76, 77]. The idea was that the simulations would then be fitted to the experimental data by tuning this single constant.

The reactor model has been shown to be able to describe similar data (from Rautanen et al. [86] and Romero et al. [76, 77]) without any problems, but when trying to simulate at these conditions the reactor model fails, and it is not possible to obtain any results. It appears that the reason this happens is due to the very high conversion. In the feed, the molar ratio of hydrogen to naphthalene is close to stoichiometric and at these high conversions up to 83 % of the hydrogen is consumed in the reaction and from a calculation point of view, the gas phase is completely removed. Whether this is the actual situation in the physical experiment is not possible to say. Implicit in the model lies the assumption that the residence time is the same for the gas and the liquid phase, which means that the total (gas + liquid) composition in the reactor is assumed to be the same as the total (gas + liquid) composition at the reactor outlet. By a simple step-response experiment it has been shown previously that this is not necessarily the case.

Normally this assumption is reasonable, since the liquid phase concentration of the main component in the gas phase, hydrogen, is not very sensitive to the total mole fraction of hydrogen. This is illustrated in figure 9.10, which shows the liquid phase hydrogen concentration at equilibrium in the feed as a function of the total hydrogen mole fraction. It illustrates, that above a certain hydrogen mole fraction, the equilibrium liquid concentration is practically the same, and it is not very sensitive to changes in total hydrogen mole fraction. Therefore as long as there is a enough hydrogen, the model will be able to describe the behavior of such a reactor, and this will be the case for most practical applications. The hydrogen mole fraction in the feed for these experiments is approximately 0.3. The vapor fraction becomes 0 when the hydrogen mole fraction becomes lower than approximately 0.1. Thus when more than two thirds of the hydrogen has been consumed, which is the case at many of the experimental points in this work, the calculated amount of gas at equilibrium in the reactor will 0, which is most likely not correct.

In an attempt to do simulations of the experiments with the existing reactor model anyway, it has been necessary to make some assumptions. The calculation problems arise due to a high hydrogen consumption. In order to avoid this, it will be assumed that the molar gas flow of hydrogen does not change in the reactor, i.e. equation 9.5 for hydrogen is replaced by $F_{H_2,G} = F^0_{H_2,G}$. This effectively works as an infinite hydrogen source and the apparent hydrogen depletion is avoided. But it also means that the overall hydrogen mass balance is no longer satisfied. It is likely that the composition of the liquid phase, where the reaction takes place, will still be described quite well. Since the main interest in these experiments, is to describe how much of the aromatics are converted, and the actual hydrogen consumption can be calculated

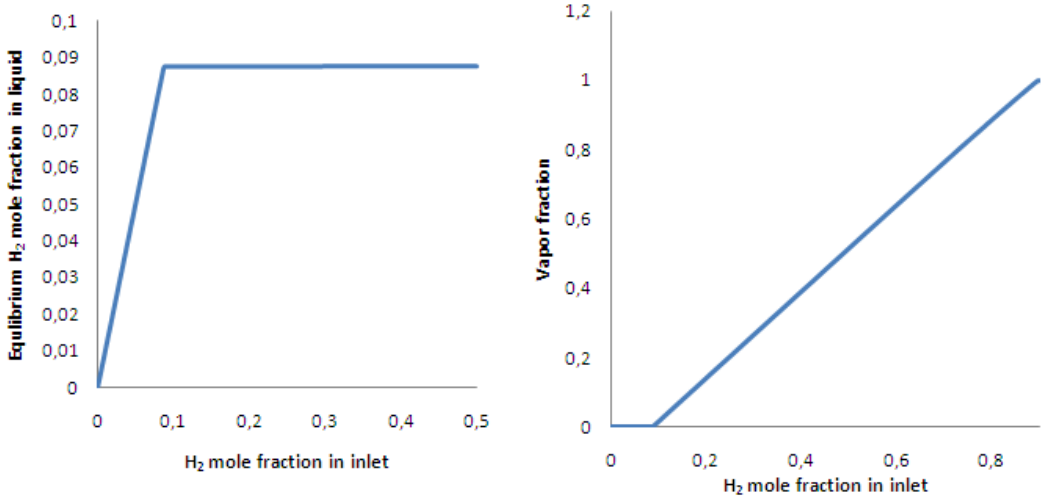

Figure 9.10: Calculated equilibrium concentration of H_2 and the total vapor fraction as function of the total mole fraction of H_2 in the inlet at 280 °C and 50 bar. Calculations have been done in Aspen Plus 12.2 using the Soave-Redlich-Kwong equation of state.

using the yield of the aromatics, the model can still be useful. By assuming that the molar gas hydrogen flow is constant, it is still possible to use the model to estimate the importance of gas-liquid mass transfer and internal diffusion resistance. But in sacrificing the hydrogen balance, the model becomes more empirical.

Using the approach described above it was possible to simulate the conditions used in the experiments. Figure 9.11 shows parity plots of the observed and calculated rates of naphthalene consumption and decalin production. It shows that the rates are described quite well by the model, although there is a little more scattering in the tetralin reaction rate than in the naphthalene reaction rate.

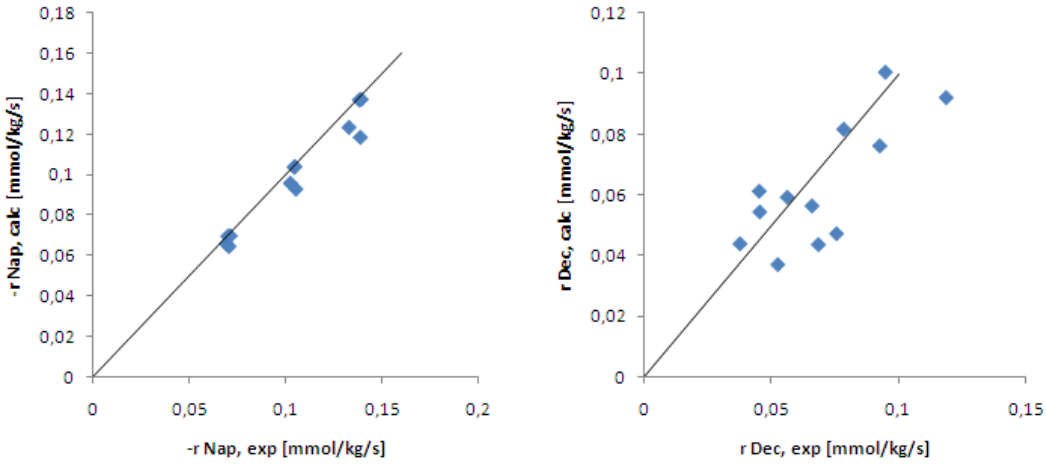

Figure 9.11: Measured and calculated rates for the naphthalene to tetralin reaction and the tetralin to decalin reaction on a CoMo catalyst

As was the case when simulating the toluene hydrogenation data, it appears that the effect

of pressure is under predicted. Increasing the pressure results in a higher reaction rate, but the simulated increase in reaction rate is not as high as what is observed in experiments.

Calculations of the effectiveness factors show that the reactions are not strongly diffusion limited. The effective particle diameter used in the calculations are set to be equal to the diameter of the trilobes, which is a conservative estimate. Of the two reactions, the calculations show that at the investigated conditions the hydrogenation of tetralin is not limited by diffusion, and the effectiveness factor is practically equal to one. The hydrogenation of naphthalene is faster and is more likely to be limited by diffusion. There does not seem to be a large effect of pressure on the effectiveness factor, whereas there is a difference at the two investigated temperatures. At the lowest temperature, 553 K, the effectiveness factor varies between 0.97 and 0.98, which means there are no diffusion resitance. At the highest temperature, 593 K, the calculated effectiveness factor is between 0.90 and 0.92. This is still not strong diffusion limitation, but keeping in mind that a minimum value of the particle sized was used, this shows that at these conditions it should not just be neglected.

The importance of the mass transfer resistance can be determined by comparing the equilibrium liquid concentration with the actual liquid concentration. Hydrogen is the main gaseous compound, and the one that is consumed fastest. The simulations show that mass transfer of hydrogen is not important. At all the experimental conditions the difference between equilibrium concentration and the actual concentration is less than 3 %. The difference is decreasing in the investigated range, as the space time increases.

For the high pressure conditions (100 bar), the liquid concentration of the aromatic and naphthenic compounds are very close to equilibrium, so mass transfer of these reactants will not limit the observed reaction rate. At the low pressure (50 bar) a larger amount of naphthalene, tetralin and decalin is present in the gas phase at equilibrium, and therefore more of the reactant has to be transferred to the liquid phase. At the lowest temperature, 553 K, there is a concentration difference for naphthalene of up to 6 %, which is not a very large difference. At the highest temperature due to a equilibrium concentration in the gas phase, the transport of naphthalene to the liquid phase becomes limiting for the rate, as the liquid concentration becomes as low as 50 % of the equilibrium concentration. It is possible that this is why the effect of pressure on the observed rate is underpredicted, simply because the calculated mass transfer coefficient of naphthalene is too low and becomes rate limiting, when a significant amount of the aromatic reactant is present in the gas phase. A problem may have been introduced when assuming that the gas hydrogen flow is constant, because this inevitably affects the calculated gas phase concentration of naphthalene. The result may have been a too small calculated driving force for gas-liquid mass transfer of naphthalene, which results in reduction of the calculated reaction rate.

9.5 Conclusion

One of the main reasons for using Robinson-Mahoney reactors for measuring kinetics, is to eliminate any mass transfer resistance. But if one is to perform experiments at high temper-

atures and pressures it is not always possible to eliminate this resistance. Therefore models that are able to describe internal and external mass transfer will be useful when developing rate expressions that are to be used in simulation of industrial units.

In this work a steady-state model for a Robinson-Mahoney reactor has been set-up. It includes calculation of the internal effectiveness factor and a possible concentration gradient at the gas-liquid interface. It has been shown that the model to a certain extent can reproduce experimental data from literature, including cases where the internal diffusion resistance is very pronounced.

Although the Robinson-Mahoney reactor has been shown to behave as an ideally mixed reactor in many cases, there are still some situations where the description of the reactor is not so straight forward. First of all, for situations where external mass transfer becomes important, there is a lack of experimental data and therefore correlations for the mass transfer coefficients. Furthermore it has been shown that the description of the equilibrium between gas and liquid phases requires a better understanding of how gas- and liquid hold-ups depend on flow rates and temperature and pressure.

The model had some significant limitations when attempting to simulate the experimental data. Because of the high hydrogen consumption, it led to a calculation error due to the apparent removal of the gas phase. In order to avoid this the hydrogen mass balance was sacrificed, making it a highly empirical model. A possible way to avoid this could be to make a non-steady state model, combining it with a set of controller equations in a way similar to the approach used by Lylykangas [87]. This will allow one to determine the steady state solution, by solving a set of ordinary differential equations. However this method requires knowledge of the actual gas- liquid hold-up.

It is very difficult to make any definitive conclusions regarding the kinetic models. The parity plots show some difference between the calculated and measured reaction rates, but the trends are correct and the fit is reasonably good. It should be noted that the adsorption parameters have been optimized for a different type of catalyst, so it should be possible at least to some extent to improve the fit. One of the reasons that a perfect fit is not achieved is that the effect of the pressure is not fully captured. This might be because the pressure is higher than for the experimental data that is the foundation of the parameters in the rate expressions. This is especially the case for the rate of naphthalene hydrogenation. To provide the best data for testing the rate expressions, these high conversion experiments should have been using the same catalyst as Romero [77].

The model is able to describe diffusion resistance. For the high conversion experiments, where naphthalene is hydrogenated to tetralin and further to decalin, there seems to be a small diffusion resistance at 593 K while at 553 K the reactions are not limited by internal diffusion.

The gas-liquid mass transfer resistance appeared to play a very small role at most of the investigated conditions, with only a difference of 0-6 % between actual concentrations and equilibrium concentrations. At the lowest temperature and pressure a significant amount of naphthalene is present in the gas phase at equilibrium, and transport from gas to liquid was rate limiting. This might be due to an error introduced by assuming a constant hydrogen gas-

flow. Whether the mass transfer coefficients can be predicted with the correlation in equation (9.10) is not possible to say from these experiments.

In this work an attempt has been made at including calculations of mass transfer and diffusion resistance in the simulation of a Robinson-Mahoney reactor. Using the reactor model it has been possible to reproduce data from literature, but calculations have also illustrated the limitations of the model. A better understanding of gas and liquid hold-up and mass transfer correlations which have been developed for this type of reactor is needed in order to improve simulations.

Chapter 10

Conclusions

The purpose of this work has been to study different aspects of the hydrotreating process, and to begin the development of a component based reactor model. The model should consider the kinetics of a set of representative model compounds, and consider mass transfer limitations and the equilibrium between the gas and the liquid phase.

Different aspects of naphthalene to tetralin hydrogenation has been investigated. The reaction can be limited by thermodynamic equilibrium at high temperatures, and experimental results from an equilibrium experiment is presented. The rate can be described by a simple Langmuir-Hinshelwood type rate expression that consideres the adsorption of the reactant. The reaction was found to be first order in the hydrogen concentration. Furthermore it has been shown, that the reaction can be limited by internal diffusion at typical hydrotreating conditions. Experiments with varying sizes of the catalyst particles have shown that for large particles the conversion decreases with increasing particle size. The apparent activation energy was found to decrease with increasing particle size.

The effect of different nitrogen compounds on the hydrodesulfurization of a refractive sulfur compound, 4,6-dimethyldibenzothiophene, has been investigated. It has been been shown, that the strongest inhibitor was the basic nitrogen compound acridine. It was found that the nitrogen compounds had a similar effect on the hydrodesulfization of a real feed as of the model compound. The nitrogen compounds mainly inhibit the hydrogenation pathway which is the main reaction pathway for 4,6-dimethyldibenzothiophene desulfurization. Furthermore it has been shown that acridine can inhibit the hydrodenitrogenation of a non-basic nitrogen compound, 1,4-dimethylcarbazole. This can explain why carbazoles are the main nitrogen compounds left in hydrotreated oils.

A set of experiments with a 13 component model diesel mixture has been carried out, and the behavior of individual compounds in the mixture has been investigated. It was found that increasing the temperature resulted in higher conversions for the sulfur and nitrogen compounds. Increasing the pressure will increase the liquid phase hydrogen concentration and increase the hydrodesulfurization and hydrodenitrogenation rates. Increasing the hydrogen to oil ratio results in an increase in the conversion. This is because the inhibition by hydrogen sulfide and ammonia is reduced, and the vaporization of the lighter oil compounds, and the liquid phase con-

centration of the heavier sulfur and nitrogen compounds becomes larger. At all conditions the most reactive sulfur compound benzothiophene was completely converted. Furthermore it was illustrated, that the reactivity of 4,6-dimethyldibenzothiophene is significantly lower than for dibenzothiophene. For compounds with fused aromatic rings such as naphthalene and phenanthrene, a maximum was observed in the conversion when increasing the temperature. This was due to the reactions being limited by thermodynamic equilibrium. Although a maximum is seen in the total mono-aromatics concentration, the conversion of a single mono-aromatic compound, pentylbenzene, does not go through a maximum, but increases with increasing temperature. A maximum in the total concentration is observed because mono-aromatics are formed through hydrogenation of di- and tri-aromatics, and the conversion of mono-aromatics are limited by the slow kinetics. The conversion of pentylbenzene is low, and the monoaromatic is much less reactive than the di- and tri-aromatics. The dehydrogenation of a mono-naphthene is shown to be negligible. It was shown, that 1,4-dimethylcarbazole was the last nitrogen compound to be removed, which is because the denitrogenation reaction is inhibited by acridine.

A model for a steady-state isothermal trickle-bed reactor has been presented. The model includes equations describing the concentration profiles inside the catalyst pellets, and it considers mass transfer between the gas phase and the liquid phase, and between the liquid phase and the solid phase. Methods for estimating physical properties and equilibrium compositions of the gas and liquid phase has been presented.

A steady state reactor model for a laboratory Robinson-Mahoney reactor has been presented. The model accounts for internal diffusion and mass transfer between the gas and the liquid phase. It was tested against literature data, and was shown to be able to describe the data reasonably well. An attempt was made to use the reactor model to test existing rate expressions against experimental data outside the pressure and temperature range where they were developed. It was found that the reactor model did not work at conditions where a too large fraction of the inlet hydrogen was consumed. In order to test the rate expressions a modification of the model was made, that made it more empirical. The kinetic expressions were shown to be able to capture the right trends, and the calculations showed, that mass transfer did not play a major role, at the investigated conditions.

10.1 Future Work

In terms of understanding and modelling the hydrotreating process, there is a lot of work that can be done. Further experimental studies of the kinetics of model compounds should be done in order to be able to develop reliable rate expressions for a series of key components. Through the studies of model compounds a better understanding of the reaction networks and reactivity of typical diesel components can be obtained. Kinetic models can be implemented in detailed reactor models, such as the one described in this work. This can be a useful tool to understand the effect and importance of the different phenomena controlling the performance of a hydrotreater. Since industrial hydrotreaters are adiabatic, it would be useful to include an energy balance to be able to describe the temperature rise down through the reactor. Other

issues such as pressure drop and partial wetting of the catalyst could also be addressed in a reactor model.

The use of a model diesel mixture consisting of several components can provide useful experimental data to compare with model simulations, as the product analysis will be simplified compared to that of a real gas oil. This can be a good way of testing kinetic models as well as testing the validity of a reactor model. Rate expressions should be able to describe the effect of inhibitors, nitrogen compounds, on the transformation of sulfur compounds. Correlating the reactivity of a given feedstock with the content of the strongest inhibitors can help in the development of more predictive tools.

Experimental studies of the inhibiting effect of polyaromatics on the hydrodesulfurization of different sulfur compounds should be carried out, and the inhibiting effect should be accounted for in the kinetic models. In this work little attention has been given to the effect of hydrogen sulfide and ammonia which is something that should also be accounted for. Hydrogenation of aromatics are important reactions, and since experimental data are quite scarce, more experimental work should be done in order determine equilibrium constants for different types of aromatic compounds at a variety of temperatures and hydrogen partial pressures.

References

[1] C. Schmitz, L. Datsevitch, and A. Jess. Deep desulfurization of diesel oil: kinetic studies and process-improvement by the use of a two-phase reactor with pre-saturator. *Chemical engineering science*, 59(14):2821–2829, 2004.

[2] Dieselnet. *Fuel Regulations, http://www.dieselnet.com/standards/fuels.html*. Ecopoint Incorporated, May 2010.

[3] P. Ghosh and S. B. Jaffe. Detailed composition-based model for predicting the cetane number of diesel fuels. *Ind. Eng. Chem. Res*, 45(1):346–351, 2006.

[4] K. B. Sidhpuria and P. A. Parikh. Aromatic Saturation: A Means to Cleaner Transportation Fuels. *Bull. Catal. Soc. Ind*, 3:67–71, 2004.

[5] K. R. Westerterp and W. J. A. Wammes. *Three-Phase Trickle-Bed Reactors, Ullmann's Encyclopedia of Industrial Chemistry*. John Wiley & Sons, Inc., 2000.

[6] F. S. Mederos, I. Elizalde, and J. Ancheyta. Steady-State and Dynamic Reactor Models for Hydrotreatment of Oil Fractions: A Review. *Catalysis reviews. Science and engineering*, 51(4):485–607, 2009.

[7] G. Hoekstra. The effects of gas-to-oil rate in ultra low sulfur diesel hydrotreating. *Catalysis Today*, 127(1-4):99–102, 2007.

[8] C. Song. An overview of new approaches to deep desulfurization for ultra-clean gasoline, diesel fuel and jet fuel. *Catalysis Today*, 86(1-4):211–263, 2003.

[9] K. G. Knudsen, B. H. Cooper, and H. Topsøe. Catalyst and process technologies for ultra low sulfur diesel. *Applied Catalysis A, General*, 189(2):205–215, 1999.

[10] I. A. Van Parijs, L. H. Hosten, and G. F. Froment. Kinetics of hydrodesulfurization on a CoMo/-Al_2O_3 catalyst. 2. Kinetics of the hydrogeneolysis of benzothiophene. *Ind. Eng. Chem. Prod. Res. Dev*, 25:437–443, 1986.

[11] M. Houalla, N. K. Nag, A. V. Sapre, D. H. Broderick, and B. C. Gates. Hydrodesulfurization of dibenzothiophene catalyzed by sulfided CoO-MoO3γ-Al2O3: The reaction network. *AIChE Journal*, 24(6):1015–1021, 1978.

[12] A. Stanislaus and B. H. Cooper. Aromatic hydrogenation catalysis: a review. *Catalysis Reviews*, 36(1):75–123, 1994.

[13] A. V. Sapre and B. C. Gates. Hydrogenation of aromatic hydrocarbons catalyzed by sulfided CoO-MoO_3/Al_2O_3. Reactivities and reaction networks. *Ind. Eng. Chem. Process Des. Dev.*, 20:68–73, 1981.

[14] S. C. Korre, M. T. Klein, and R. J. Quann. Polynuclear aromatic hydrocarbons hydrogenation. 1. Experimental reaction pathways and kinetics. *Industrial & Engineering Chemistry Research*, 34(1):101–117, 1995.

[15] B. . Cooper and B. B. L. Donnis. Aromatic saturation of distillates: an overview. *Applied Catalysis A: General*, 137(2):203–223, 1996.

[16] P. Wiwel, K. Knudsen, P. Zeuthen, and D. Whitehurst. Assessing Compositional Changes of Nitrogen Compounds during Hydrotreating of Typical Diesel Range Gas Oils Using a Novel Preconcentration Technique Coupled with Gas Chromatography and Atomic Emission Detection. *Industrial and Engineering Chemistry Research*, 39(2):533–540, 2000.

[17] M. J. Girgis and B. C. Gates. Reactivities, reaction networks, and kinetics in high-pressure catalytic hydroprocessing. *Industrial & Engineering Chemistry Research*, 30(9):2021–2058, 1991.

[18] V. Rabarihoela-Rakotovao, S. Brunet, G. Berhault, G. Perot, and F. Diehl. Effect of acridine and of octahydroacridine on the HDS of 4, 6-dimethyldibenzothiophene catalyzed by sulfided $NiMoP/Al_2O_3$. *Applied Catalysis A, General*, 267(1-2):17–25, 2004.

[19] H. Topsøe, B. S. Clausen, and F. E. Massoth. Hydrotreating catalysis. *Science and Technology*, 11, 1996.

[20] H. Topsøe, B. S. Clausen, R. Candia, C. Wivel, and S. Mørup. In situ Mössbauer emission spectroscopy studies of unsupported and supported sulfided Co—Mo hydrodesulfurization catalysts: Evidence for and nature of a Co—Mo—S phase. *Journal of Catalysis*, 68(2):433–452, 1981.

[21] H. Topsøe. The role of Co-Mo-S type structures in hydrotreating catalysts. *Applied Catalysis A: General*, 322:3–8, 2007.

[22] F. Besenbacher, M. Brorson, B. S. Clausen, S. Helveg, B. Hinnemann, J. Kibsgaard, J. V. Lauritsen, P.G. Moses, J. K. Nørskov, and H. Topsøe. Recent STM, DFT and HAADF-STEM studies of sulfide-based hydrotreating catalysts: Insight into mechanistic, structural and particle size effects. *Catalysis Today*, 130(1):86–96, 2008.

[23] H. Topsøe, B. Hinnemann, J. K. Nørskov, J. V. Lauritsen, F. Besenbacher, P. L. Hansen, G. Hytoft, R. G. Egeberg, and K. G. Knudsen. The role of reaction pathways and support interactions in the development of high activity hydrotreating catalysts. *Catalysis Today*, 107:12–22, 2005.

[24] I. Mochida and K. H. Choi. An Overview of Hydrodesulfurization and Hydrodenitrogenation. *J. Jpn. Pet. Inst.*, 47(3):145–163, 2004.

[25] J. V. Lauritsen, J. Kibsgaard, G. H. Olesen, P. G. Moses, B. Hinnemann, S. Helveg, J. K. Nørskov, B. S. Clausen, H. Topsøe, E. Lægsgaard, et al. Location and coordination of promoter atoms in Co-and Ni-promoted MoS_2-based hydrotreating catalysts. *Journal of Catalysis*, 249(2):220–233, 2007.

[26] C. G. Frye. Equilibria in the Hydrogenation of Polycyclic Aromatics. *Journal of Chemical and Engineering Data*, 7(4):592–595, 1962.

[27] C. G. Frye and A. W. Weitkamp. Equilibrium hydrogenations of multi-ring aromatics. *Journal of Chemical and Engineering Data*, 14(3):372–376, 1969.

[28] C. G. Frye and A. W. Weitkamp. Equilibrium hydrogenations of multi-ring aromatics. *Journal of Chemical and Engineering Data*, 14(3):372–376, 1969.

[29] S. Goto and J. M. Smith. Trickle-bed reactor performance. part i. holdup and mass transfer effects. *AIChE Journal*, 21(4):706–713, 1975.

[30] G. F. Froment and K. B. Bischoff. *Chemical reactor analysis and design*. Wiley New York, 1990.

[31] H. S. Fogler. *Elements of Chemical Reaction Engineering*. Prentice-Hall International, Inc., Upper Saddle River, New Jersey 07458, 3rd edition, 1999.

[32] H. G. Rackett. Equation of state for saturated liquids. *J. Chem. Eng. Data*, 15(4):514–517, 1970.

[33] P. B. Weisz and J. S. Hicks. The behaviour of porous catalyst particles in view of internal mass and heat diffusion effects. *Chemical Engineering Science*, 17(4):265–275, 1962.

[34] C. N. Satterfield. *Mass transfer in heterogeneous catalysis*. The MIT Press, 1970.

[35] J. J. Carberry. The micro-macro effectiveness factor for the reversible catalytic reaction. *AIChE Journal*, 8(4):557–558, 2004.

[36] C. I. Chu and I. Wang. Kinetic study on hydrotreating. *Industrial & Engineering Chemistry Process Design and Development*, 21(2):338–344, 1982.

[37] T. C. Ho. Deep HDS of diesel fuel: chemistry and catalysis. *Catalysis Today*, 98(1-2):3–18, 2004.

[38] F. van Looij, P. van der Laan, W. H. J. Stork, D. J. DiCamillo, and J. Swain. Key parameters in deep hydrodesulfurization of diesel fuel. *Applied Catalysis A, General*, 170(1):1–12, 1998.

[39] K. G. Knudsen, D. D. Whitehurst, and P. Zeuthen. A detailed understanding of the inhibition effect of organic nitrogen compounds for ultra deep HDS and the consequences for the choice of catalyst. In *AIChE Spring National Meeting, Atalanta, GA*, March 2000.

[40] G. C. Laredo S., J. A. De los Reyes H., J. Luis Cano D., and J. Jesús Castillo M. Inhibition effects of nitrogen compounds on the hydrodesulfurization of dibenzothiophene. *Applied Catalysis A, General*, 207(1-2):103–112, 2001.

[41] I. V. Babich and J. A. Moulijn. Science and technology of novel processes for deep desulfurization of oil refinery streams: a review. *Fuel*, 82(6):607–631, 2003.

[42] M. Nagai, T. Sato, and A. Aiba. Poisoning effect of nitrogen compounds on dibenzothiophene hydrodesulfurization on sulfided $NiMo/Al_2O_3$ catalysts and relation to gas-phase basicity. *Journal of catalysis(Print)*, 97(1):52–58, 1986.

[43] V. LaVopa and C. N. Satterfield. Poisoning of thiophene hydrodesulfurization by nitrogen compounds. *Journal of catalysis(Print)*, 110(2):375–387, 1988.

[44] A. R. Beltramone, S. Crossley, D. E. Resasco, W. E. Alvarez, and T. V. Choudhary. Inhibition of the Hydrogenation and Hydrodesulfurization Reactions by Nitrogen Compounds over $NiMo/Al_2O_3$. *Catalysis Letters*, 123(3):181–185, 2008.

[45] M. Sun, A. E. Nelson, and J. Adjaye. First principles study of heavy oil organonitrogen adsorption on NiMoS hydrotreating catalysts. *Catalysis Today*, 109(1-4):49–53, 2005.

[46] Á. Logadóttir, P.G. Moses, B. Hinnemann, N. Y. Topsøe, K. G. Knudsen, H. Topsøe, and J. K. Nørskov. A density functional study of inhibition of the HDS hydrogenation pathway by pyridine, benzene, and H2S on MoS2-based catalysts. *Catalysis Today*, 111(1-2):44–51, 2006.

[47] V. Rabarihoela-Rakotovao, F. Diehl, and S. Brunet. Deep HDS of diesel fuel: Inhibiting effect of nitrogen compounds on the transformation of the refractory 4, 6-dimethyldibenzothiophene over a $NiMoP/Al_2O_3$ catalyst. *Catalysis Letters*, 129(1):50–60, 2009.

[48] C. Kwak, J. J. Lee, J. S. Bae, and S. H. Moon. Poisoning effect of nitrogen compounds on the performance of CoMoS/Al2O3 catalyst in the hydrodesulfurization of dibenzothiophene, 4-methyldibenzothiophene, and 4, 6-dimethyldibenzothiophene. *Applied Catalysis B, Environmental*, 35(1):59–68, 2001.

[49] M. Egorova and R. Prins. Competitive hydrodesulfurization of 4, 6-dimethyldibenzothiophene, hydrodenitrogenation of 2-methylpyridine, and hydrogenation of naphthalene over sulfided NiMo/γ-Al2O3. *Journal of Catalysis*, 224(2):278–287, 2004.

[50] T. Koltai, M. Macaud, A. Guevara, E. Schulz, M. Lemaire, R. Bacaud, and M. Vrinat. Comparative inhibiting effect of polycondensed aromatics and nitrogen compounds on

the hydrodesulfurization of alkyldibenzothiophenes. *Applied Catalysis A, General*, 231(1-2):253–261, 2002.

[51] U. T. Turaga, X. Ma, and C. Song. Influence of nitrogen compounds on deep hydrodesulfurization of 4, 6-dimethyldibenzothiophene over Al2O3-and MCM-41-supported Co-Mo sulfide catalysts. *Catalysis Today*, 86(1-4):265–275, 2003.

[52] B.H. Cooper and K.G. Knudsen. Ultra deep desulfurization of diesel: How an understanding of the underlying kinetics can reduce investment costs. *Korea*, 1:297–316, 2005.

[53] P. Zeuthen, K. G. Knudsen, and D. D. Whitehurst. Organic nitrogen compounds in gas oil blends, their hydrotreated products and the importance to hydrotreatment. *Catalysis Today*, 65(2-4):307–314, 2001.

[54] D. Ferdous, A. K. Dalai, and J. Adjaye. Comparison of hydrodenitrogenation of model basic and nonbasic nitrogen species in a trickle bed reactor using commercial $NiMo/Al_2O_3$ Catalyst. *Energy Fuels*, 17(1):164–171, 2003.

[55] T. C. Ho and J. E. Sobel. Kinetics of dibenzothiophene hydrodesulfurization. *J Catal*, 128:581–584, 1991.

[56] T. Takatsuka, S. Inoue, and Y. Wada. Deep hydrodesulfurization process for diesel oil. *Catalysis Today*, 39(1-2):69–75, 1997.

[57] B. E. Poling, J. M. Prausnitz, and J. P. O&Connell. *The properties of gases and liquids*. McGraw-Hill New York, 2001.

[58] C. L. Yaws. *Chemical properties handbook*. McGraw-Hill New York, 1999.

[59] *CRC Handbook of Chemistry and Physics, http://www.hbcponline.com/*. Taylor and Francis, 2010.

[60] J. Marrero and R. Gani. Group-contribution based estimation of pure component properties. *Fluid Phase Equilibria*, 183:183–208, 2001.

[61] ASTM International. *ASTM D6591 - 06, http://www.astm.org/Standards/D6591.htm*. ASTM International, 2010.

[62] J. Villadsen and M. L. Michelsen. *Solution of Differential Equation Models by Polynomial Approximation*. Prentice-Hall, Inc., Englewood Cliffs, New Jersey 07632, 1978.

[63] T. Ahmed. *Reservoir Engineering Handbook (2nd edition)*. Elsevier, ISBN: 0-88415-770-9, 2001.

[64] C. N. Satterfield. Trickle-bed reactors. *AIChE Journal*, 21(2):209–228, 1975.

[65] C. H. Tsai, F. E. Massoth, S. Y. Lee, and J. D. Seader. Effects of solvent and solute configuration on restrictive diffusion in hydrotreating catalysts. *Ind. Eng. Chem. Res.*, 30:22–28, 1991.

[66] H. Korsten and U. Hoffmann. Three-phase reactor model for hydrotreating in pilot trickle-bed reactors. *AIChE Journal*, 42(5):1350–1360, 1996.

[67] G. Soave. Equilibrium constants from a modified Redlich-Kwong equation of state. *Chemical Engineering Science*, 27(6):1197–1203, 1972.

[68] R. D. Gray Jr., J. L. Heidman, S. C. Hwang, and C. Tsonopoulos. Industrial applications of cubic equations of state for vle calculations, with emphasis in H_2 systems. *Fluid Phase Equilibria*, 13:59–76, 1983.

[69] L. Constantinou, R. Gani, and J. P. O'Connell. Estimation of the acentric factor and the liquid molar volume at 298 K using a new group contribution method. *Fluid Phase Equilibria*, 103(1):11–22, 1995.

[70] K. G. Joback and R. C. Reid. Estimation of pure-component properties from group-contributions. *Chemical Engineering Communications*, 57(1):233–243, 1987.

[71] I. Pitault, P. Fongarland, D. Koepke, M. Mitrovic, D. Ronze, and M. Forissier. Gas–liquid and liquid–solid mass transfers in two types of stationary catalytic basket laboratory reactor. *Chemical engineering science*, 60(22):6240–6253, 2005.

[72] J. A. Mahoney. The use of a gradientless reactor in petroleum reaction engineering studies. *Journal of Catalysis*, 32(2):247–253, 1974.

[73] J. M. Schweitzer, P. Galtier, and D. Schweich. A single events kinetic model for the hydrocracking of paraffins in a three-phase reactor. *Chemical Engineering Science*, 54(13-14):2441–2452, 1999.

[74] V. Vanrysselberghe and G. F. Froment. Hydrodesulfurization of dibenzothiophene on a CoMo/Al2O3 catalyst: reaction network and kinetics. *Ind. Eng. Chem. Res*, 35(10):3311–3318, 1996.

[75] V. Vanrysselberghe, R. Le Gall, and G. F. Froment. Hydrodesulfurization of 4-Methyldibenzothiophene and 4, 6-dimethyldibenzothiophene on a $CoMo/Al_2O_3$ catalyst: Reaction network and kinetics. *Ind. Eng. Chem. Res*, 37(4):1235–1242, 1998.

[76] C. M. C. Romero, J. W. Thybaut, and G. B. Marin. Naphthalene hydrogenation over a $NiMo/\gamma$-Al_2O_3 catalyst: Experimental study and kinetic modelling. *Catalysis Today*, 130(1):231–242, 2008.

[77] C. M. C. Romero. *Kinetics of Naphthalene Hydrogenation over a Sulfided NiMo/Alumina Catalyst*. ISBN: 90-8578-046-2, 2006.

[78] M. Mitrovic, I. Pitault, M. Forissier, S. Simoens, and D. Ronze. Liquid-solid mass transfer in a three-phase stationary catalytic basket reactor. *AIChE journal*, 51(6):1747–1757, 2005.

[79] S. W. Benson, F. R. Cruickshank, D. M. Golden, G. R. Haugen, H. E. O'neal, A. S. Rodgers, R. Shaw, and R. Walsh. Additivity rules for the estimation of thermochemical properties. *Chemical Reviews*, 69(3):279–324, 1969.

[80] J. A. M. Arroyo, G. G. Martens, G. F. Froment, G. B. Marin, P. A. Jacobs, and J. A. Martens. Hydrocracking and isomerization of n-paraffin mixtures and a hydrotreated gasoil on Pt/ZSM-22: confirmation of pore mouth and key–lock catalysis in liquid phase. *Applied Catalysis A, General*, 192(1):9–22, 2000.

[81] L. Bern, O. Lidefelt J., and N. Schöön H. Mass transfer and scale-up in fat hydrogenation. *Journal of the American Oil Chemists' Society*, 53(7):463–466, 1976.

[82] P. A. Ramachandran and R. V. Chaudhari. *Three-phase catalytic reactors*. Gordon & Breach Science Pub, 1983.

[83] D. N. Miller. Scale-up of agitated vessels gas-liquid mass transfer. *AIChE Journal*, 20(3):445–453, 1974.

[84] W. van Engelandt. *Reformuleren van Nafta door Selectieve Hydrokraking*. PhD Thesis University of Ghent, 1998.

[85] NIST Chemistry WebBook. *NIST Standard Reference Database Number 69, http://webbook.nist.gov/chemistry/*.

[86] P. A. Rautanen, J. R. Aittamaa, and A. O. I. Krause. Solvent effect in liquid-phase hydrogenation of toluene. *Ind. Eng. Chem. Res*, 39(11):4032–4039, 2000.

[87] M. Lylykangas. *Kinetic Modelling of Liquid-Phase Hydrogenation Reactions*. Helsinki University of Technology, Laboratory of Industrial Chemistry, ISBN: 951-22-6913-9, 2004.

Appendix A

Experimental Results

A.1 Naphthalene hydrogenation: Equilibrium experiments

Table A.1: Experimental results from equilibrium experiments. The feed was a solution of compounds in n-heptane. The experiments was carried out in the set-up described in chapter 2. 2 g of a commercial noble metal catalyst was used for the experiments. w denotes the concentration in weight percent. (NAP: Naphthalene, TET: Tetralin, DEC: Decalin (cis- and trans-).)

			Feed			*Product*					
T [°C]	P [atm]	H_2/oil [Nl/l]	w NAP	w TET	w DEC	w NAP	w TET	w DEC	P_{H_2} [atm]	[TET]/[NAP]	[DEC]/[NAP]
350	31.0	4000	0.0123	0.1156	1.113	0.0069	0.0823	1.1014	29.8	11.50	147.07
350	30.8	250	0.0123	0.1156	1.113	0.0531	0.2330	0.8365	19.1	4.25	14.61
350	31.0	250	0.0123	0.1156	1.113	0.0527	0.2462	0.8923	19.2	4.53	15.70
350	31.0	2000	0.0123	0.1156	1.113	0.0078	0.0901	1.1030	28.8	11.25	131.68
350	31.0	4000	0.0568	0.4226	0.6889	0.0060	0.0775	1.0373	29.8	12.60	161.24
350	31.0	2000	0.0568	0.4226	0.6889	0.0070	0.0849	1.0485	28.8	11.83	139.60
350	31.0	250	0.0568	0.4226	0.6889	0.0503	0.2330	0.8453	19.2	4.49	15.56
350	30.8	250	0.0568	0.4226	0.6889	0.2042	0.4224	0.4927	19.1	2.01	2.24

A.2 Phenanthrene hydrogenation: Equilibrium experiments

Table A.2: Experimental results from equilibrium experiments. The feed was a solution phenanthrene in n-heptane. The experiments was carried out in the set-up described in chapter 2. 2 g of a commercial noble metal catalyst was used for the experiments. w denotes the concentration in weight percent. (PHEN: Phenanthrene, PHP: Perhydrophenanthrene, OHP: Octahydrophananthrene, THP: Tetrahydrophenanthrene, DHP: Dihydrophenanthrene.)

			Feed	*Product*									
T [°C]	P [atm]	H_2/oil [Nl/l]	w PHEN	w PHEN	w PHP	w OHP	w THP	w DHP	P_{H_2} [atm]	[PHP] / [PHEN]	[OHP] / [PHEN]	[THP] / [PHEN]	[DHP] / [PHEN]
350	30.8	4000	0.3327	0.0054	0.1850	0.0488	0.0157	0	29.7	31.83	8.66	2.84	0
350	30.8	2000	0.3327	0.0076	0.2039	0.0543	0.0206	0.0020	28.6	24.73	6.79	2.64	0.26
350	30.5	250	0.3327	0.0938	0.0455	0.0668	0.0767	0.0174	18.9	0.45	0.68	0.80	0.18
350	30.8	250	0.3327	0.0736	0.0772	0.0778	0.0764	0.0143	19.1	0.97	1.01	1.01	0.19

A.3 Naphthalene hydrogenation: Particle size effects

Table A.3: Experimental results from the investigation of the effect of the catalyst particle size on the hydrogenation of naphthalene. The experiments were conducted using the set-up described in chapter 5. The liquid feed was a solution of 2 % (w/w) of naphthalene in n-tetradecane. The liquid flow in each reactor was 3.7 ml/ hr and the H_2/oil was 250 Nl/l. The catalyst was a commercial CoMo catalyst. (NAP: Naphthalene)

Size fraction	**d_p [μm]**	**Cat. Mass [g]**	**T [°C]**	**P [barg]**	**WHSV [hr^{-1}]**	**Conversion NAP**	**k_1 NAP**	**k_{1f} NAP (eq.)**	η
63-105μm	84	0.0501	339.7	29.4	55.2	0.84	102.59	136.11	1.00
150-212μm (1)	181	0.0499	339.7	29.4	61.3	0.85	117.74	160.81	0.98
150-212μm (2)	181	0.05	340.0	29.4	56.0	0.87	116.31	175.01	0.98
300-425μm	362.5	0.05	340.2	29.4	56.8	0.89	123.34	204.13	0.89
600-850μm	725	0.0501	339.6	29.4	57.3	0.78	86.91	103.37	0.79
850-1000μm (1)	925	0.0499	340.2	29.4	55.9	0.73	73.50	83.83	0.73
850-1000μm (2)	925	0.0499	340.1	29.4	56.1	0.80	91.52	112.20	0.66
1270+μm	1413	0.0499	339.8	29.4	56.1	0.71	68.59	77.02	0.53
63-105μm	84	0.0251	341.1	29.4	112.0	0.78	170.28	202.72	0.99
150-212μm	181	0.025	340.2	29.3	112.4	0.66	121.06	132.97	0.98
300-425μm	362.5	0.025	340.4	29.4	114.4	0.83	203.28	260.99	0.86
600-850μm	725	0.025	340.2	29.4	111.9	0.60	103.71	111.75	0.77
850-1000μm	925	0.0251	340.2	29.4	110.9	0.56	90.43	96.22	0.70
1270+μm	1485	0.0252	340.4	29.4	112.3	0.44	64.59	67.17	0.54
-	0	-	339.9	29.4	-	0.01	-	-	-
-	0	-	340.4	29.4	-	0.00	-	-	-

Table A.4: Experimental results from the investigation of the effect of the catalyst particle size on the hydrogenation of naphthalene. The experiments were conducted using the set-up described in chapter 5. The liquid feed was a solution of 2 % (w/w) of naphthalene in n-tetradecane. The liquid flow in each reactor was 1.9 ml/ hr and the H_2/oil was 250 Nl/l. The catalyst was a commercial CoMo catalyst. (NAP: Naphthalene)

Size fraction	**d_p [μm]**	**Cat. Mass [g]**	**T [°C]**	**P [barg]**	**WHSV [hr^{-1}]**	**Conversion NAP**	**k_1 NAP**	**k_{1f} NAP (eq.)**
63-105μm	84	0.0501	340.1	29.4	27.8	0.88	59.23	93.54
150-212μm (1)	181	0.0499	340.2	29.4	31.2	0.89	69.01	121.04
150-212μm (2)	181	0.05	340.6	29.4	28.4	0.89	62.95	111.35
300-425μm	362.5	0.05	340.5	29.4	28.8	0.90	65.40	128.70
600-850μm	725	0.0501	340.1	29.4	29.0	0.87	60.11	90.42
850-1000μm (1)	925	0.0499	340.5	29.4	28.2	0.85	52.92	70.67
850-1000μm (2)	925	0.0499	340.5	29.4	28.3	0.88	59.49	91.55
1270+μm	1413	0.0499	340.2	29.4	28.1	0.83	50.54	65.36
63-105μm	84	0.0251	341.7	29.4	56.3	0.87	115.46	170.31
150-212μm	181	0.025	340.5	29.4	57.0	0.82	96.45	120.36
300-425μm	362.5	0.025	340.9	29.4	58.0	0.89	127.33	216.75
600-850μm	725	0.025	340.6	29.4	56.9	0.77	83.66	98.45
850-1000μm	925	0.0251	340.7	29.4	55.9	0.73	73.17	83.40
1270+μm	1485	0.0252	340.7	29.4	56.8	0.62	54.28	58.69
-	0	-	340.2	29.4	-	0.00		
-	0	-	340.9	29.4	-	0.00		

Table A.5: Experimental results from the investigation of the effect of the catalyst particle size on the hydrogenation of naphthalene. The experiments were conducted using the set-up described in chapter 5. The liquid feed was a solution of 2 % (w/w) of naphthalene in n-tetradecane. The liquid flow in each reactor was 3.7 ml/ hr and the H_2/oil was 250 Nl/l. The catalyst was a commercial CoMo catalyst. (NAP: Naphthalene)

Size fraction	**d_p [μm]**	**Cat. Mass [g]**	**T [°C]**	**P [barg]**	**WHSV [hr^{-1}]**	**Conversion NAP**	**k_1 NAP**	**k_{1f} NAP (eq.)**	η
63-105μm	84	0.0501	300.9	29.4	54.9	0.75	76.16	77.55	1.00
150-212μm	181	0.025	301.2	29.4	111.8	0.45	67.36	67.74	0.99
300-425μm	362.5	0.05	301.3	29.4	56.5	0.85	106.68	110.04	0.94
600-850μm	725	0.025	301.3	29.4	111.6	0.45	65.90	66.26	0.86
850-1000μm (1)	925	0.0499	301.1	29.4	55.6	0.63	55.46	56.08	0.81
850-1000μm (2)	925	0.0499	301.0	29.4	56.0	0.71	69.58	70.65	0.77
1270+μm	1485	0.0252	300.9	29.4	112.3	0.32	43.70	43.85	0.66
-	0	-	300.8	29.4	-	-	0.00	0.00	-
63-105μm	84	0.0251	321.8	29.4	112.2	0.75	154.13	161.65	1.00
150-212μm (1)	181	0.0499	320.4	29.4	61.5	0.85	116.39	120.07	0.98
150-212μm (2)	181	0.05	320.7	29.4	56.1	0.89	124.63	130.16	0.98
300-425μm	362.5	0.025	321.1	29.4	114.6	0.81	190.83	204.02	0.89
600-850μm	725	0.0501	320.2	29.4	57.6	0.77	84.86	89.53	0.82
850-1000μm	925	0.0251	320.8	29.4	111.2	0.50	78.00	79.41	0.75
1270+μm	1413	0.0499	320.4	29.4	56.2	0.69	66.68	69.24	0.57
-	0	-	321.0	29.4	-	0.00	0.00	0.00	-

Table A.6: Experimental results from the investigation of the effect of the catalyst particle size on the hydrogenation of naphthalene. The experiments were conducted using the set-up described in chapter 5. The liquid feed was a solution of 2 % (w/w) of naphthalene in n-tetradecane. The liquid flow in each reactor was 3.7 ml/ hr and the H_2/oil was 250 Nl/l. The catalyst was a commercial CoMo catalyst. (NAP: Naphthalene)

Size fraction	**d_p [μm]**	**Cat. Mass [g]**	**T [°C]**	**P [barg]**	**WHSV [hr^{-1}]**	**Conversion NAP**	**k_1 NAP**	**k_{1f} NAP (eq.)**	η
63-105μm	84	0.0501	320.2	29.4	54.8	0.86	106.06	116.10	1.00
150-212μm	181	0.025	320.5	29.4	112.3	0.60	102.77	105.45	0.99
300-425μm	362.5	0.05	320.6	29.4	56.7	0.91	137.71	161.17	0.91
600-850μm	725	0.025	320.7	29.4	111.9	0.57	93.26	95.40	0.81
850-1000μm (1)	925	0.0499	320.4	29.4	55.8	0.73	72.26	75.46	0.76
850-1000μm (2)	925	0.0499	320.4	29.4	56.0	0.80	90.25	96.11	0.71
1270+μm	1485	0.0252	320.4	29.4	112.1	0.39	56.28	56.95	0.60
-	0	-	320.2	29.4	-	-	-	-	-
63-105μm	84	0.0251	362.0	29.4	112.1	0.73	145.43	213.64	0.99
150-212μm (1)	181	0.0499	360.5	29.4	61.7	0.77	90.07	157.12	0.98
150-212μm (2)	181	0.05	360.8	29.4	56.1	0.78	84.94	164.05	0.98
300-425μm	362.5	0.025	361.1	29.4	115.0	0.75	159.76	255.08	0.87
600-850μm	725	0.0501	360.3	29.4	57.5	0.72	74.23	108.42	0.80
850-1000μm	925	0.0251	360.8	29.4	110.9	0.53	84.13	96.82	0.72
1270+μm	1413	0.0499	360.4	29.4	56.1	0.67	62.81	82.60	0.54
-	0	-	361.1	29.4	-	0.00	0.00	0.00	-

A.4 4,6-dimethyldibenzothiophene desulfurization: Effect of nitrogen inhibitors

Table A.7: Experimental results from the investigation of the effect of nitrogen inhibitors on the hydrodesulfurization of 4,6-dimethyldibenzothophene. The experiments were carried out in the set-up described in chapter 2. The liquid feed was a solution of reactants in n-dodecane. The temperature was 350 °C, the pressure 50 barg and H_2/oil was 125 Nl/l. The catalyst was a commercial NiMo catalyst crushed to a 600-850 μm size fraction. (46DMDBT: 4,6-dimethyldibenzothiophene, ACR: Acridine, 14DMCBZ: 1,4-dimethylcarbazole, 3MEIN: 3-methylindole)

	Feed concentration [% (w/w)]				*Product concentration [% (w/w)]*				46DMDBT	
WHSV [hr^{-1}]	46DMDBT	ACR	14DMCBZ	3MEIN	46DMDBT	ACR	14DMCBZ	3MEIN	Conversion	MCHT/DM-BP
25.6	0.612	-	-	-	0.142	-	-	-	0.77	2.3
51.2	0.612	-	-	-	0.167	-	-	-	0.73	2.0
109.6	0.682	-	-	-	0.332	-	-	-	0.51	1.8
165.6	0.682	-	-	-	0.385	-	-	-	0.43	1.7
9.0	0.631	0.379	-	-	0.408	0.0014	-	-	0.35	2.0
13.5	0.631	0.379	-	-	0.460	0.0020	-	-	0.27	1.7
24.0	0.759	0.470	-	-	0.634	0.0002	-	-	0.16	1.5
9.0	0.625	-	0.415	-	0.173	-	0.046	-	0.72	2.8
12.8	0.625	-	0.415	-	0.277	-	0.096	-	0.56	2.3
25.6	0.625	-	0.415	-	0.358	-	0.162	-	0.43	1.9
8.2	0.737	-	-	0.277	0.102	-	-	0.007	0.86	2.9
12.8	0.647	-	-	0.389	0.271	-	-	0.030	0.58	2.3
25.7	0.647	-	-	0.389	0.377	-	-	0.010	0.42	2.0
9.0	0.594	0.202	0.214	-	0.339	0.0007	0.128	-	0.43	2.4
12.8	0.594	0.202	0.214	-	0.428	0.0006	0.155	-	0.28	2.0
25.7	0.594	0.202	0.214	-	0.478	0.0014	0.165	-	0.19	1.5

A.5 Hydrotreating of model diesel

Table A.8: Conditions and product concentrations after hydrotreating of Feed A in table 7.5. The experiments were carried out using the set-up described in chapter 2 loaded with a commercial NiMo catalyst.

								Aromatics [% (w/w)]		
Exp. No	Cat. Mass [g]	T [°C]	P [barg]	WHSV [hr^{-1}]	H_2 / oil [Nl/l]	ppm S	ppm N	Mono	Di	Tri+
A.1	1.00	331.0	29.8	10.1	483	736	141	20.23	5.32	0.86
A.2	1.00	358.7	29.6	25.2	196	2230	190	19.06	6.46	1.03
A.3	1.00	357.1	29.5	10.1	490	40	112	20.92	4.55	0.75
A.4	1.00	336.1	29.0	10.1	130	2550	150	19.82	5.39	1.11
A.5	1.00	336.7	48.9	10.1	130	2230	97	20.71	4.27	1.02
A.6	1.00	304.9	29.1	10.1	490	4564	206	17.5	7.99	1.24
A.7	1.00	337.2	49.4	10.1	490	610	70	21.92	3.9	0.62
A.8	1.00	346.8	29.7	10.1	490	234	123	21.04	4.72	0.67
A.9	1.00	338.3	81.4	10.1	490	169	3	22.59	2.33	0.07
A.10	1.00	358.6	49.5	10.1	490	3	1	22.05	2.69	0.07
A.11	1.00	357.0	29.8	10.1	490	34	104	20.83	4.23	0.61
A.12	1.00	377.1	30.7	10.1	490	4	89	20	4.81	0.79
A.13	1.00	357.1	30.7	10.1	490	40	113	21.13	4.42	0.62
A.14	2.00	357.0	48.5	5.0	130	219	2	20.34	2.33	0.12

Table A.9: Product concentrations (% (w/w)) of selected compounds after hydrotreating of Feed A in table 7.5. The conditions can be found in table A.8. ((PB: Pentyll-benzene, TET: Tetralin, NAP: Naphthalene, PHE: Phenanthrene, BC: Butyl-cyclohexane, DEC: Decalin(cis- and trans-), BT: Benzothiophene, DBT: Dibenzothiophene, 46DMDBT: 4,6-dimethyldibenzothiophene, ACR: Acridine, 3MEIN: 3-methylindole, 14DMCBZ: 1,4-dimethylcarbazole)

Exp. No	PB	TET	NAP	PHE	BC	DEC	BT	DBT	46DMDBT	ACR	3MEIN	14DMCBZ
Feed	8.528	6.560	5.197	1.725	18.312	12.743	1.745	3.345	0.000	0.056	0.061	0.178
A.1	0.084	9.244	2.400	0.591	18.492	12.782	0.000	0.762	0.000	0.002	0.000	0.137
A.2	0.063	8.202	3.313	0.935	18.260	12.595	0.000	1.449	0.000	0.006	0.000	0.155
A.3	0.198	9.561	1.766	0.453	18.320	12.737	0.000	0.469	0.000	0.002	0.000	0.115
A.4	0.114	9.256	2.098	0.821	18.133	12.672	0.000	1.570	0.000	0.004	0.000	0.142
A.5	0.242	10.058	0.997	0.564	18.214	12.959	0.000	1.352	0.000	0.002	0.000	0.093
A.6	0.021	7.305	4.313	1.218	18.355	12.605	0.000	2.633	0.000	0.006	0.000	0.151
A.7	0.165	10.187	1.123	0.323	18.481	12.986	0.000	0.555	0.000	0.000	0.000	0.063
A.8	0.116	9.561	1.948	0.441	18.415	12.782	0.000	0.518	0.000	0.002	0.000	0.125
A.9	0.638	9.747	0.127	0.071	18.196	14.153	0.000	0.156	0.000	0.000	0.000	0.002
A.10	0.516	9.789	0.539	0.088	18.105	13.472	0.000	0.251	0.000	0.000	0.000	0.000
A.11	0.226	9.752	1.606	0.422	18.307	12.813	0.000	0.468	0.000	0.000	0.000	0.105
A.12	0.350	9.065	2.427	0.723	18.174	12.671	0.000	0.455	0.000	0.000	0.000	0.067
A.13	0.193	9.616	1.707	0.444	18.179	12.753	0.000	0.468	0.000	0.000	0.000	0.116
A.14	1.204	8.321	0.550	0.126	18.354	15.116	0.000	0.300	0.000	0.000	0.000	0.002

Table A.10: Conditions and product concentrations after hydrotreating of Feed B in table 7.5. The experiments were carried out using the set-up described in chapter 2 loaded with a commercial NiMo catalyst.

						Aromatics [% (w/w)]		
Exp. No	Cat. Mass [g]	T [°C]	P [barg]	WHSV [hr^{-1}]	H_2 / oil [Nl/l]	Mono	Di	Tri+
B.1	2.00	351.4	79.4	5.1	1229	20.54	1.46	0.05
B.2	2.00	350.9	49.4	5.1	319	22.13	3.16	0.19
B.3	2.00	350.7	47.3	5.1	483	22.09	2.42	0.08
B.4	2.00	329.8	47.2	5.1	120	22.02	4.62	0.58
B.5	2.00	330.9	48.5	5.1	483	22.57	2.85	0.13
B.6	2.00	330.1	78.7	5.1	126	22.05	4.34	0.39
B.7	2.00	350.0	48.0	5.1	120	21.54	4.49	0.56
B.8	2.00	356.2	28.9	5.0	130	21.48	4.72	0.65
B.9	2.00	358.5	80.7	5.0	124	18.75	1.63	0.05
B.10	2.00	339.0	80.8	5.0	490	18.52	1.34	0.05

Table A.11: Product concentrations (% (w/w)) of selected compounds after hydrotreating of Feed B in table 7.5. The conditions can be found in table A.10. (PB: Pentyll-benzene, TET: Tetralin, NAP: Naphthalene, PHE: Phenanthrene, BC: Butyl-cyclohexane, DEC: Decalin(cis- and trans-), BT: Benzothiophene, DBT: Dibenzothiophene, 46DMDBT: 4,6-dimethyldibenzothiophene, ACR: Acridine, 3MEIN: 3-methylindole, 14DMCBZ: 1,4-dimethylcarbazole)

Exp. No	PB	TET	NAP	PHE	BC	DEC	BT	DBT	46DMDBT	ACR	3MEIN	14DMCBZ
Feed	9.151	7.541	5.583	1.928	19.308	13.457	1.889	3.797	0.681	0.040	0.083	0.199
B.1	1.167	9.141	0.168	0.005	19.160	16.521	0.000	0.047	0.000	0.000	0.000	0.001
B.2	0.725	10.458	0.645	0.153	19.159	15.062	0.000	0.357	0.172	0.000	0.000	0.007
B.3	0.886	10.379	0.654	0.090	19.307	15.563	0.000	0.251	0.014	0.000	0.000	0.000
B.4	0.272	11.429	0.978	0.650	19.300	14.157	0.000	1.854	0.552	0.000	0.000	0.087
B.5	0.558	11.036	0.336	0.163	19.243	14.917	0.004	0.358	0.269	0.000	0.000	0.029
B.6	0.391	11.037	0.777	0.491	19.241	14.540	0.003	0.058	0.489	0.000	0.000	0.052
B.7	0.528	10.430	1.202	0.536	19.094	14.388	0.000	0.056	0.429	0.000	0.000	0.084
B.8	0.473	9.956	1.889	0.593	18.612	13.274	0.000	0.512	0.350	0.005	0.000	0.074
B.9	1.678	7.276	0.173	0.032	18.431	16.999	0.000	0.140	0.057	0.000	0.000	0.001
B.10	1.585	7.639	0.066	0.007	18.621	17.097	0.000	0.042	0.025	0.000	0.000	0.000

Appendix B

Physical Properties of Model Compounds

Table B.1: Properties of selected compounds

Compound	Short name	M_w [g/mol]	T_b [°C]	T_c [°C]	P_c [bar]	V_c [cm^3/mol]	ω
Hydrogen	H2	2.02	-252.8	-240.0	13.0	65.1	-0.218
n-nonane	NON	128.26	150.9	321.5	22.9	548.0	0.445
n-hexadecane	HEX	226.45	286.9	448.9	14.1	930.0	0.742
Pentylbenzene	PB	148.25	205.5	401.9	25.8	550.0	0.439
Tetralin	TET	132.21	207.6	445.9	35.1	408.0	0.303
Naphthalene	NAP	128.17	218.0	475.3	40.5	413.0	0.302
Phenanthrene	PHE	178.23	339.9	599.9	29.0	554.0	0.495
Butylcyclohexane	BC	140.26	181.0	393.9	25.7	534.0	0.274
Decalin (cis-)	DEC	138.25	195.8	429.2	32.0	486.3	0.286
Benzothiophene	BT	134.20	219.9	480.9	41.4	349.0	0.296
Dibenzothiophene	DBT	184.26	332.6	623.9	38.6	512.0	0.484
4,6-dimethyldibenzothiophene	46DMDBT	212.31	327.9	634.8	34.6	627.0	0.584
Acridine	ACR	179.22	344.9	618.0	32.1	548.0	0.548
3-methylindole	3MEIN	131.17	257.3	496.5	32.9	436.3	0.450
1,4-dimethylcarbazole	14DMCBZ	196.26	326.4	565.1	27.3	638.5	0.660

Appendix C

Solution of the Diffusion-reaction Problem

The numerical solution of diffusion reaction problem in a spherical catalyst pellet is described in this section. The equations are solved using an optimal collocation method given by Villadsen and Michelsen [62].The dimensionless equation, (8.6), for reactions taking place in a single spherical catalyst pellet has the following form, as described in chapter 8:

$$x^2\frac{d^2y_k}{dx^2} + 2x\frac{dy_k}{dx} - \phi_k^2 x^2 \cdot \rho_k(\underline{y}) = 0$$

The boundary conditions are as follows:

$$B.C.\ \ 1 : x = 0 \qquad \frac{dy_k}{dx} = 0 \tag{C.1}$$

$$B.C.\ \ 2 : x = 1 \qquad y_k = y_{k,0} \tag{C.2}$$

Because of the symmetry around $x = 0$ the first boundary condition can be eliminated by using the variable $u = x^2$. The equation then becomes:

$$4u\frac{d^2y_k}{du^2} + 6\frac{dy_k}{dx} - \phi_k^2 \cdot \rho_k(\underline{y}) = 0 \tag{C.3}$$

with the boundary condition:

$$B.C. : u = 1 \qquad y_k = y_{k,0} \tag{C.4}$$

The equations are solved using an optimal collocation method. In this method the real solution are approximated with a polynomium of degree N. Expressed in terms of Lagrange polynomiums, $l_i(u)$, the approximate solution will have the form:

$$y_{kN}(u) = \sum_{i=1}^{N+1} l_i(u) y_{ki} \tag{C.5}$$

y_{ki} are the unknown function values of the i*th* collocation point. The Lagrange polynomium, $l_i(u)$, has the characteristic of having the value 1 in the i*th* collocation point but being 0 in all of the other collocation points. The first and the second derivatives of the approximate solution in the collocation points, u_j,are given by can be expressed as:

$$\left.\frac{dy_{kN}}{du}\right|_{u=u_j} = \sum_{i=1}^{N+1} l_i'(u_j) y_{ki} = \sum_{i=1}^{N+1} A_{ji} y_{ki} \tag{C.6}$$

$$\left.\frac{d^2 y_{kN}}{du^2}\right|_{u=u_j} = \sum_{i=1}^{N+1} l_i''(u_j) y_{ki} = \sum_{i=1}^{N+1} B_{ji} y_{ki} \tag{C.7}$$

The residual function can be expressed in terms of the discretization matrices A and B:

$$R_{kN}(u_j) = 4u_j \sum_{i=1}^{N+1} B_{ji} y_{ki} + 6 \sum_{i=1}^{N+1} A_{ji} y_{ki} - \phi_k^2 \cdot \rho_k(\underline{y}) \tag{C.8}$$

It is desired to determine the function values in the collocation points. This is done by setting the residual equal to zero in the collocation points:

$$4u_j \sum_{i=1}^{N+1} B_{ji} y_{ki} + 6 \sum_{i=1}^{N+1} A_{ji} y_{ki} - \phi_k^2 \cdot \rho_k(\underline{y}) = 0 \tag{C.9}$$

As collocation points are used N interior points, and the end point $u_{N+1} = 1$. The collocation points are determined as the zeroes of the orthogonal polynomium $P_N^{\alpha,\beta}$ with $\alpha = 0$ and $\beta = 0$. By using the boundary conditions $y_{k,N+1} = y_{k,0}$ the system of equations can be written as:

$$4u_j \sum_{i=1}^{N} B_{ji} y_{ki} + 6 \sum_{i=1}^{N} A_{ji} y_{ki} - \phi_k^2 \cdot \rho_k(\underline{y}) + 4B_{j,N+1} y_{k,0} + 6A_{j,N+1} y_{ki} = 0 \tag{C.10}$$

This is in general a system of kN non-linear equations with kN unknowns. The system can be solved using Newtons method.

C.1 Calculation of apparent rate

Based on the solution to the diffusion reaction problem, the apparent reaction rate can be calculated by evaluating the following integral:

$$R_{k,app} = \frac{3}{2} R_k(\underline{c}_0) \int_0^1 \rho_k(y(u)) \cdot u^{0.5} du \tag{C.11}$$

By reusing the collocation points as quadrature points, the value of the integral can be calculated using a Gauss-Jacobi quadrature formula. If w_j denote the gaussian weights, the apparent

reaction rate can be calculated by:

$$R_{k,app} = \frac{3}{2} R_k(\underline{c}_0) \sum_{j=1}^{N} w_j \cdot \rho_k(\underline{y}_j) \cdot u_j^{0.5} \tag{C.12}$$